GENERATION OF A REPORTER-RETINITIS PIGMENTOSA MOUSE MODEL FOR RETINAL REGENERATION STUDIES USING CRISPR/dCAS9-BASED ARTIFICIAL TRANSCRIPTION FACTORS

By

YEŞİM TÜTÜNCÜ

Submitted to the Graduate School of Engineering and Natural Science

In partial fulfillment of the requirements for the degree of

Master of Science

Sabanci University

July 2022

ABSTRACT

GENERATION OF A REPORTER-RETINITIS PIGMENTOSA MOUSE MODEL FOR RETINAL REGENERATION STUDIES USING CRISPR/dCAS9-BASED ARTIFICIAL TRANSCRIPTION FACTORS

Many blinding diseases of the retina involve neurodegeneration, including age-related macular degeneration, diabetic retinopathy, glaucoma, and inherited retinal diseases (IRDs). Inherited retinal diseases are one of the most common causes of blindness with the major subtype retinitis pigmentosa (RP) occurring with a worldwide prevalence of 1:4000. More than 200 genes are linked to inherited retinal diseases, which complicates approaches to target all individual blinding conditions. Furthermore, more than 150 mutations have been identified solely in the rod visual pigment, rhodopsin, that causes RP. In the majority of RP cases, the ongoing photoreceptor degeneration cannot be stopped, or the disease is diagnosed at a very late stage. Therefore, in addition to the therapies that will stop the ongoing degeneration, there is also a demanding need for restorative therapies to regain vision in patients that already have a severe neuronal loss. Mammalians have very limited retinal regeneration capacity. However, in zebrafish, the Muller glia has an extraordinary regenerative capacity, which opens up the possibility of Muller glia reprogramming for compensating the neuronal loss in IRDs. To mimic this feature of teleost fish, several studies have been performed in mammalian models to reprogram Muller glia. Here, we established a reporter mouse model for RP using one of the very-well studied rd1 mouse models and the rhodopsin reporter system that labels the newly regenerated rods *in vivo* which will allow us to elucidate the regenerative potential of candidate drugs. Furthermore, the RP-reporter model was combined with the novel dCas9-SPH system for multiplex gene regulation and to establish synthetic gene regulatory networks using artificial transcription factors for the treatment of neurodegenerative retinal diseases. This system already allowed us to robustly label retinal cells *in vivo* using our AAVShH10-Cre vectors that mainly target Muller glia. We have also generated and tested stable Muller glia cell lines expressing CRISPR-dCas9 activators for the establishment of artificial transcription factors. These transgenic mice and cell lines will be valuable tools for combining the gene therapy approach with potential candidate drugs.

YEŞİM TÜTÜNCÜ

Molecular Biology, Genetics and Bioengineering, MSc Thesis, July 2022

Thesis Supervisor: Asst.Prof. Cavit Agca

Keywords: Retinal Regeneration, Retinitis Pigmentosa, Müller glia, Artificial Transcription Factors, Transgenic Mouse Models

ÖZET

CRISPR/dCAS9-TEMELLİ YAPAY TRANSKRİPSİYON FAKTÖRLERİ KULLANARAK RETİNAL REJENERASYON ÇALIŞMALARI İÇİN BİR RAPORTÖR-RETİNİTİS PİGMENTOZA FARE MODELİNİN OLUŞTURULMASI

Retinada körlüğe sebep olan birçok hastalık, örneğin yaşa bağlı makula dejenerasyonu, diyabetik retinopati, glokom ve diğer kalıtsal retina hastalıkları (KRH'ler) dahil olmak üzere önemli bir kısmı nörodejenerasyon temellidir. Kalıtsal retina hastalıkları, dünya çapında her 4000 kişiden birinde ortaya çıkan görülme sıklığına sahiptir ve bunların başlıcalarından olan retinitis pigmentoza (RP) körlüğün en yaygın nedenlerinden biridir. 200'den fazla gen, kalıtsal retina hastalıklarıyla bağlantılıdır ve bu, tüm körlüğe sebep olan koşulların hedeflenmesini karmaşıklaştırır. Ayrıca, yalnızca RP'ye neden olan çubuk görsel pigmenti olan rodopsin'de 150'den fazla mutasyon tanımlanmıştır. RP vakalarının çoğunda devam eden fotoreseptör dejenerasyonu durdurulamaz veya hastalık çok geç bir aşamada teşhis edilir. Bu nedenle, devam eden dejenerasyonu durduracak tedavilere ek olarak, halihazırda ciddi bir nöron kaybı olan hastalarda görmenin yeniden kazanılması için restoratif tedavilere de ihtiyaç duyulmaktadır. Memelilerin retina rejenerasyon kapasitesi çok sınırlıdır. Bununla birlikte, zebra balıklarında Müller glia, KRH'lerdeki nöronal kaybı telafi etmek için Müller glia'nın yeniden programlanması olasılığını açan olağanüstü bir rejeneratif kapasiteye sahiptir. Teleost balıkların bu özelliğini taklit etmek için memeli modellerinde Müller glia'yı yeniden programlamak için çeşitli çalışmalar yapılmıştır. Bu tezde ise, önceden karakterizasyonu yapılmış olan rd1 fare modellerinden birini ve yeni rejenere edilmiş çubukları in vivo olarak etiketleyen rodopsin raportör sistemini kullanarak RP için bir raportör fare modeli oluşturulmuştur. Bu oluşturulan yeni model ise aday ilaçların rejeneratif potansiyelini açıklamamız için bir araç olacaktır. Ayrıca, RP raportör modeli, multipleks gen

regülasyonu için yeni dCas9-SPH sistemi ile birleştirilmiş ve nörodejeneratif retina hastalıklarının tedavisi için yapay transkripsiyon faktörleri kullanılarak sentetik gen düzenleyici ağlar kurulmuştur. Bu sistem, esas olarak Müller glia'yı hedefleyen AAVShH10-Cre vektörlerimizi kullanarak retina hücrelerini in vivo olarak etkili bir şekilde etiketlememize olanak sağlamıştır. Ayrıca yapay transkripsiyon faktörlerinin oluşturulması için CRISPR-dCas9 aktivatörlerini eksprese eden stabil Müller glia hücre dizileri üretilerek test edilmiştir. Bu transgenik fareler ve hücre dizileri, gen terapisi yaklaşımını potansiyel aday ilaçlarla birleştirmek için değerli araçlar olacaktır.

YEŞİM TÜTÜNCÜ

Moleküler Biyoloji, Genetik ve Biyomühendislik, Yüksek Lisans Tezi, Temmuz 2022

Tez Danışmanı: Dr. Öğretim Üyesi Cavit Ağca

Anahtar Kelimeler: Retinal Rejenerasyon, Retinitis Pigmentoza, Müller Glia, Yapay Transkripsiyon Faktörleri, Transgenik Fare Modelleri

ACKNOWLEDGEMENTS

I would like to thank Assistant Professor Cavit Ağca, my principal investigator, who always gives me endless scientific guidance and always supports me as a master student during my whole master process. He was not only a PI, but also a role model for my future career path.

I would like to thank to my family for always loving and supporting me unconditionally in every stage of my life.

I would like to thank my lab members İskalen Cansu Okan, Halit Yusuf Altay, Mehri Ahmadian, Ferdows Afghah and Fatma Özdemir for making all the times we worked in the lab unforgettable and being my second family in Sabanci University. I will never forget our trips to Gebze, full of laughter, and your support, which always lifted me up when I was about to give up.

I would like to thank our previous intern students and scientists at FENS 2100 Cemre Memiş, Büşra Kuloğlu, Emircan Ülkü and Melike Çokol Çakmak for their friendships.

I would like to thank also Şevin, Nilay, Oya and Efsun in the SUNUM G168 for their support and friendly attitudes during the long cell culture experiments.

I would like to thank Dr. Ahsen Morva Yılmaz who always supports us during our long FACS experiments in TUBITAK and make us feel like at home.

I would like to thank Asst. Prof. Stuart James Lucas for being one of my jury members and his support.

I would like to thank Gebze Technical University Animal Facility workers for giving us opportunity to complete our mice experiments in there.

I would like to express my gratitude to the Scientific and Technological Research Council of Turkey (TUBITAK), who provided financing under project number 118C226.

This master thesis is dedicated to my beloved family..

LIST OF FIGURES

LIST OF TABLES

LIST OF ABBREVIATIONS

AAV: Adeno-associated Virus

AMD: Age-related Macular Degeneration

arRP: Autosomal Reccessive Retinitis Pigmentosa

Ascl1: Achaete-Scute Family Basic Helix Loop Helix Transcription Factor 1

ATF: Artificial Transcription Factor

BP: Base Pair

CBA: Chicken Beta Actin Promoter

cDNA: Complementary DNA

cGMP: Cyclic Guanosine Monophosphate

c-Myc: Cellular Proto-oncogene Myc

CNS: Central Nervous System

CO_2: Carbon dioxide

CRISPR: Clustered Regularly Interspaced Short Palindromic Repeats

dCas9: Dead Caspase 9

ddH_2O: Double Distilled Water

ddPCR: Digital Droplet Polymerase Chain Reaction

DMEM: Dulbecco's Modified Eagle Medium

DNA: Deoxyribonucleic Acid

dNTP: Deoxynucleoside triphosphate

FACS: Fluorescence-Activated Cell Sorting

FBS: Fetal Bovine Serum

FDA: Food and Drug Administration

FGF2: Fibroblast Growth Factor 2

FSC: Forward Scatter

FSK: Forskolin

GCL: Ganglion Cell Layer

GDP: Guanosine Diphosphate

GFAP: Glial Fibrillary Acidic Protein

GFP: Green Fluorescence Protein

GPCR: G-Protein Coupled Receptor

gRNA: Guide RNA

GS: Glutamine Synthetase

GTP: Guanosine Triphosphate

HEK293T: Human Embryonic Kidney 293 T

ILM: Inner Limiting Membrane

INL: Inner Nuclear Layer

IPL: Inner Plexiform Layer

IPM: Interphotoreceptor Matrix

IRD: Inherited Retinal Disorders

iPSC: Induced-Pluripotent Stem Cell

KCl: Potassium Chloride

Klf4: Krüppel-like Factor 4

LB: Lysogeny Broth

LCA: Leber's Congenital Amaurosis

MAPK: Mitogen-Activated Protein Kinase

$MgCl_2$: Magnesium Chloride

NaCl: Sodium Chloride

NaOH: Sodium Hydroxide

Nrl1: Neural Retina Leucine Zipper 1

O/N: Overnight

OCT: Optical Coherence Tomography

Oct4: Octamer-binding Transcription Factor 4

OLM: Outer Limiting Membrane

ONL: Outer Nuclear Layer

OPA: Optic Atrophy 1

OPL: Outer Plexiform Layer

PAM: Pharmacologically Active Molecule

PBS: Phosphate Buffer Serum

PCR: Polymerase Chain Reaction

PDE: Phosphodiesterase

PDE6B: Phosphodiesterase 6B

PEI: Polyethyleneimine

PL: Photoreceptor Layer

PN: Post Natal Day

Rd: Retinal Degeneration

RGC: Retinal Ganglion Cell

RHO: Rhodopsin

RNA: Ribonucleic Acid

RP: Retinitis Pigmentosa

RPE: Retinal Pigment Epithelium

Sox2: SRY-Box Transcription Factor 2

SPH: SunTag-p65-HSF1

SSC: Side Scatter

TAE: Tris Acetic Acid EDTA

TALE: Transcription Activator-like Effectors

TGFß: Transforming Growth Factor Beta

VEGF: Vascular Endothelial Growth Factor

1. INTRODUCTION

1.1. Degenerative Eye Diseases

The eye diseases causing blindness are significant health issues all over the world. In 2020, 295 million people were diagnosed with moderate to severe levels of impaired vision and 43 million people detected as blind, globally [1]. It also put a huge economic burden on the society, for instance the healthcare cost of people suffering from vision loss was over 34 billion dollars in the USA [2]. Main retinal disorders that cause vision loss are age-related macular degeneration (AMD), inherited retinal disorders (IRDs), diabetic retinopathy and glaucoma. Death of the photoreceptors (rods and cones) and retinal pigment epithelium (RPE) cells in AMD and retinitis pigmentosa (RP), are the main outcome for these degenerative retinal disorders. Retinal ganglion cell (RGC) loss in glaucoma is another leading cause of blindness. Despite the tremendous advancements in medicine, both AMD and IRDs still have very few treatment options. AMD causes pathologic alterations in the macula, which is responsible for central vision, and the surrounding vascular system, which impairs central vision. There are two different forms of AMD in terms of disease initiation: dry and wet AMD. Retinal deposit formations known as drusen are crucial symptoms of the dry AMD and it causes atrophic scars in the macula. Dry AMD is considered as the most frequent one which may cause the wet AMD, resulting abnormal neovascularization that led to bleeding and leakage in the eye. Intravitreal injection of the anti-vascular endothelial growth factor (anti-VEGF) is a preferred method for the treatment of these abnormalities. However, dry AMD cannot be treated with the intravitreal anti-VEGF injections [3].

The most common inherited retinal degenerative disease, RP, is caused by several mutations and it affects 1 in 3000 people in the USA [4, 5]. When the disease is developed, the ongoing degeneration causes the progressive photoreceptor loss. The condition is first distinguished by night blindness, and early loss of the peripheral vision due to the rod photoreceptor degeneration. This is followed by cone photoreceptor degradation which results in central vision loss in the late phase of the disease [6]. According to the studies, individuals may not notice any visual changes until the 90 percent loss of their rod photoreceptors. In other words,

it is mostly discovered when it already progressed to an advanced level [7]. Furthermore, retinitis pigmentosa is a disorder with a wide range of symptoms; some people experience significant visual loss in childhood while others don't exhibit any symptoms until they are in their mid-twenties. RP is caused by more than 70 genes with over 3000 mutations and in most of the cases, genetic changes occurs on rod photoreceptors [8]. Patients with retinitis pigmentosa have significantly diminished rod and cone photoreceptor nuclei, which make up the outer nuclear layer of the retina [9]. There are three possible inheritance patterns for RP: autosomal recessive (50–60%), autosomal dominant (about 30–40% of cases), and X-linked (5–15%) [6, 10-12]. First gene mutation which is associated with RP was found on rhodopsin gene [13]. This 6.7 kb sized rhodopsin gene is located on long arm of the chromosome 3 with a total 5 exons. Gene therapy approaches are served as a treatment option for the people who suffer from RP. It helps to remove/fix mutated gene or substitute with a functional copy [14]. There are recent advancements in gene therapy such as the treatment of Leber's Congenital Amaurosis (LCA) type 2 (LCA2; NCT00999609). In the LCA2 patients, they have null mutation or biallelic loss of function in the RPE65 gene. The treatment ensures the substitution of null mutation on RPE65 gene with a functional one by using intravitreal AAV vector carrying human RPE65 gene. This let to the development of the only retinal gene therapy which is FDA approved for retinal degeneration called Luxturna (voretigene neparvovecrzyl) [15]. These advances in the gene therapy provide a glimmer of hope for treating other retinitis pigmentosa mutations.

1.2. Vertebrate Eye and its Basic Anatomy

Eyes of the vertebrates are complex sensory organs, and they are made to improve eyesight under the different ranges of lighting conditions. Eyes are responsible to sense light, transform it into neuronal electro-chemical signals and process the visual information. When we compare the basic elements of the eye and video camera, they are quite similar. Focusing of the light is the main function of the eye. Cornea is the translucent portion of the mammalian eye that protects the iris and pupil while allowing the light to pass through. The colored-part of the eye which is placed behind the cornea named iris. The one’s eye color is determined via quantity of the pigments located in the iris. For example, brown-eyed people have more pigments on their iris than blue-eyed people. The iris also has muscles that react to changes

in light exposure by expanding and contracting the pupil. This feature is quite similar with the camera aperture. Entered light moves through the eye lens where the light is precisely focused and is placed on retina, which is the light sensitive neuronal layer of the eye. Clear vision can only be attained if light from an object is accurately focused onto the retina. The image you see is distorted if the light focuses either in front of or behind the retina. If the light focusing procedure is distorted, the perceived image will be fuzzy. A refractive mistake occurs when the structure of the eye does not appropriately bend the light to focus on retina.

The mammalian retina has mainly three layers of nerve cell bodies and two layers of synapses as illustrated in **figure 1**. Cell bodies of rods and cones are found in the outer nuclear layer (ONL), cell bodies of bipolar, horizontal, and amacrine cells are found in the inner nuclear layer (INL), and cell bodies of ganglion cells and displaced amacrine cells are found in the ganglion cell layer (GCL). There are two neuropils, which means the space between neuronal and glial cell bodies and filled with dendrites, axons and synapses separate these nerve cell layers, where synaptic connections take place. The outer plexiform layer (OPL) is the first layer of neuropils, and it states here to process connections between rod and cones, as well as vertically running bipolar cells and horizontally oriented horizontal cells. The inner plexiform layer (IPL) is the retina's second neuropil, and it serves as a transfer point for perpendicular-information-carrying nerve cells, known as bipolar cells, to link to ganglion cells. Furthermore, the central retina, near to the fovea, is significantly thicker than the peripheral retina due to the compact photoreceptor density, especially cones.

There are also three distinct glial cell type in retina involving Muller glia, astrocytes and Microglia. Muller glia and astrocytes are responsible for regulating local blood flow, triggering the blood-retinal barrier, participating in retinal glucose metabolism, and maintaining the stability of extracellular ions and neurotransmitters [16]. They are also crucial for information processing in neuronal circuits. Muller glia cells are the most important glial components for the retina repertoire regarding their distribution. The blood-retina barrier is also formed in vascularized retinas by Muller glia. Müller glia cells also regulate neurovascular linkage and create a close metabolic alliance with photoreceptors and other retinal neurons [17, 18]. Microglia also play important roles in retinal homeostasis, recovery from injury and progression of disease [19]. Muller and photoreceptor cells' inner

segment constitute the outer limiting membrane (OLM) of the retina. Inner limiting membrane (ILM) is also made up of laterally contacting Müller cell terminal foot and related basement membrane elements. The ILM is the retina's inner surface that borders the vitreous fluid, establishing a diffusion barrier between the neuronal retina and the vitreous humor.

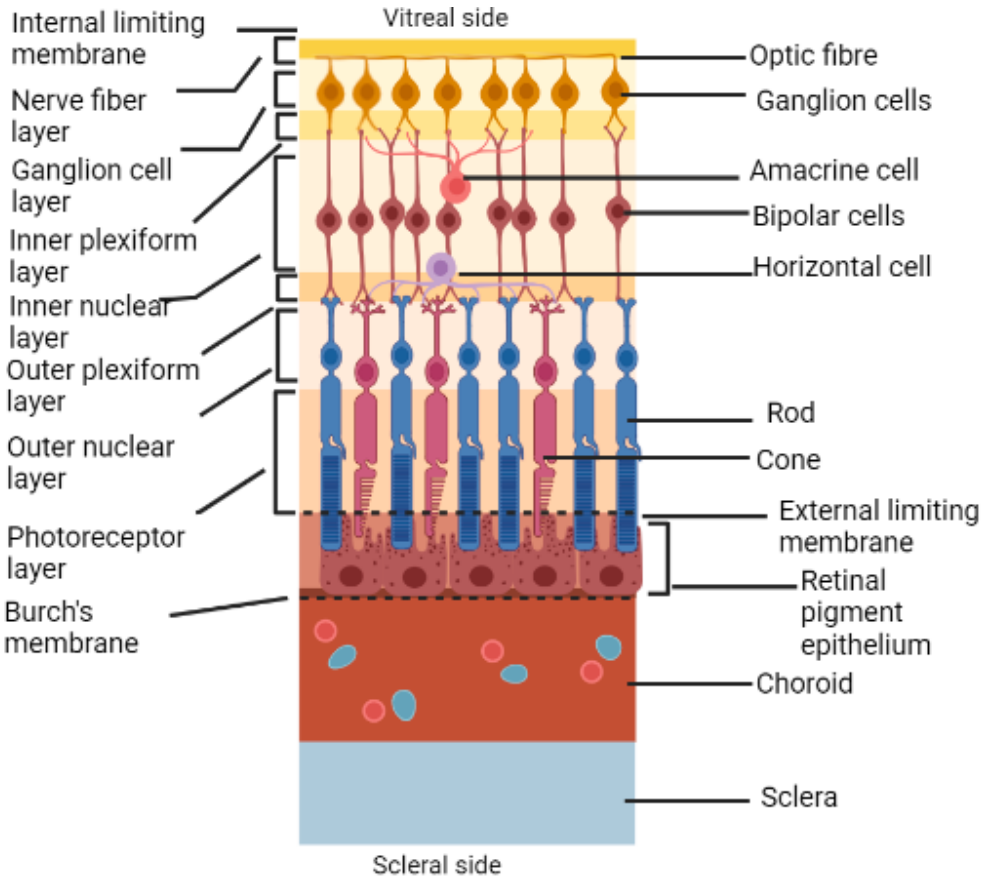

Figure 1. ***Retinal cells and layers***. *Illustration of the retina organization. The mammalian retina layers are named as inner limiting membrane (ILM); nerve fiber layer (NFL); ganglion cell layer (GCL); inner plexiform layer (IPL); inner nuclear layer (INL); the outer plexiform layer (OPL); the outer nuclear layer (ONL); the outer limiting membrane (OLM); the photoreceptor layer (PL), and retinal pigment epithelium (RPE). It is created by using BioRender software. Adapted from "Retina", by BioRender.com (2022)*

1.3. Photoreceptors and Their Role on Vision

In the mammalian retina there are two types of photoreceptors called as rods and cones as illustrated in **figure 2.** These photoreceptors are the specialized cell structures placed in the retina. For vision in bright light (daylight), cones, which are cone-shaped structures, are

necessary. For vision in low light (darkness or twilight), rods—rod-like structures scattered throughout the retina, aside from the fovea—are necessary. Both of these two visual elements have light-sensitive pigments [20]. Perceiving light, which is the role of rods, is by far the most fundamental and important role of photoreceptors. Except the fovea which is the central part of the retina and lack off rods but enriched with cone photoreceptors, rods can be found throughout the retina. The human eye roughly contains 120 million rods and 6 million cone cells [21]. Rods are thousand times more sensitive than every individual cones. The cone and rod photoreceptors perform many functions quite differently. Due to their high sensitivity, rods can be activated by a single photon [22, 23]. Rods gather impulses from all angles, enhancing our perception of depth, movement sensitivity, and peripheral vision. Nonetheless, rods only detect light and dark; they do not perceive color. Visual perception at dim light conditions relies on only the rod signal. Cone photoreceptors require day light conditions to initiate signaling. In humans, there are 3 different types of cone photoreceptors: L type, S type, and M type. All these three types of cones contain separate opsins that are responsible for their capacity to recognize various light wavelengths and provide color vision. Red-sensing cones (L-cones) with 564 nm wavelength, blue-sensing cones (S-cones) with 437 nm wavelength, and green-sensing cones (M-cones) with 533 nm wavelength are categorized in three different groups according to their response to the light. In basic terms, the ratio of each color detected by each type of cone to the other determines the exact color that we see. This phenomenon is known as trichromatic vision theory [24].

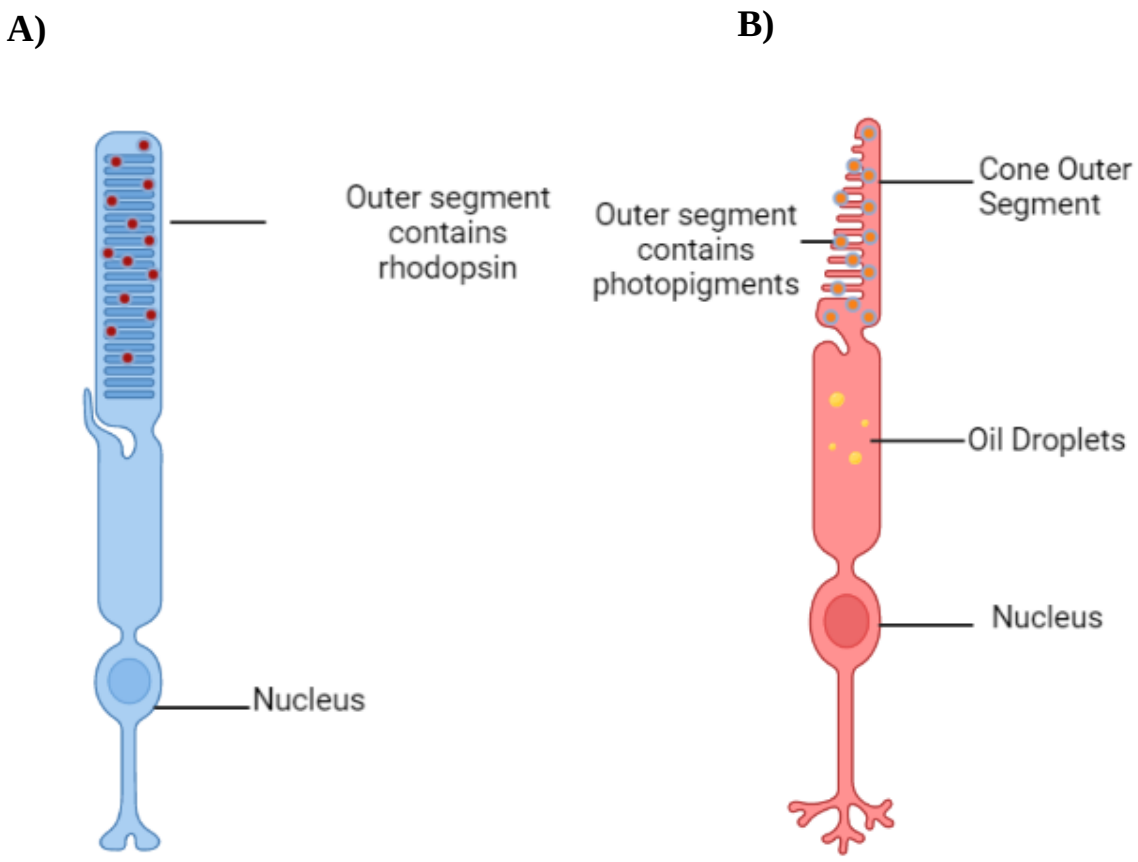

Figure 2. ***Illustration of Rod and Cone Photoreceptors***. *It represents the Rod* ***(A)*** *and Cone* ***(B)*** *photoreceptors and their structures. Rod photoreceptors have rhodopsin known as a light-sensitive G-protein-coupled receptor and it is functional under the dim light especially for night vision. Cone photoreceptors are responsible for the color vision and their photopigments are located in the outer segment of the cell body. Oil droplets in the cone photoreceptors improve the light capture especially in nocturnal animals.*

Vision is initiated by the isomerization of the visual pigment called chromophore by a captured photon. The process of phototransduction changes the electrical potential of the cell membrane in response to light. An array of signaling proteins is sequentially activated during the process, which ultimately results in the opening or closure of ion channels in the membrane of the photoreceptor cell [25]. A membrane protein known as an opsin which belongs the family of GPCRs and a chromophore are the two main components of a visual pigment (photopigment). The chromophore is the molecule that absorbs the photon. All photoreceptors contain the chromophore 11-cis-retinal, a vitamin A derivative [26]. The wavelength absorbed by photoreceptor is determined by the rhodopsin protein that compose

the photopigment formation in rods, and organized in the disc membranes [27]. Photoreceptor discs, which are flattened membrane organelles, are located within the cylindrical or conical outer segments of rod and cone photoreceptors. Discs structures continuously renew themselves during life by adding new membranes to the outer segment and removing the old membranes [28].

When the photoreceptor is not activated by light, it is in the depolarized state. In this state, the photoreceptor secretes its neurotransmitter, as neurons often do when they are depolarized. Depolarization causes voltage-gated Ca^{+2} channels to open, which allows calcium ions to let glutamate-containing vesicles fuse with the cell membrane, releasing the neurotransmitter into the synaptic cleft. As a result, the photoreceptor terminal continuously releases glutamate while it is dark. A photoreceptor's internal ion circuit causes the depolarized state to exist. Na^{+} ions can pass through the channels, and a high concentration level of cytoplasmic cGMP keeps the cGMP-gated cationic channels open.

Phototransduction in the rods is initiated when a photon is absorbed by visual pigment 11-cis retinal, shattering a double bond in 11-cis-retinal creates the activated isomer all-trans-retinal as represented in **figure 3**. As soon as all-trans-retinal is formed, rhodopsin protein undergoes a series of structural modifications. These structural changes are resulted the production of some mediators. Transducin ,which is a G-protein and main mediator in the phototransduction, is stimulated by activated-metarhodopsin II and changes into inactive metarhodopsin III before all-trans-retinal separates from the photopigment [29]. Exhibited sensitivity of rhodopsin photopigment after their exposure to bright light is called as bleaching [30]. Once activated, transducin attaches to and turns on a different peripheral protein that is a precursor to phosphodiesterase (PDE). This activated phosphodiesterase causes the hydrolysis of cGMP [31]. PDE is a crucial component of the phototransduction cascade because it contributes to the hydrolysis of the second messenger cGMP, which causes channels to close in response to light [32]. Autosomal recessive RP (arRP) patients have been shown to have mutations in the phosphodiesterase 6B, cyclic guanosine monophosphate-specific, rod, beta (PDE6B) gene in humans [33]. Mutations in the PDE6B gene cause retinitis pigmentosa, one of the most severe and quickly progressing types of retinal diseases [34]. PDEs with Pde6b mutations become inactive, which leads to cGMP

accumulation [35, 36]. Increased amounts of cGMP causes the death of photoreceptors in the cells lacking a functional PDE6B enzyme [37]. Mutations in Pde6b produce severe, early-onset, fast retinal degeneration in the rd1 mouse model and it is served as a great disease model for arRP [38]. Activation of phototransduction process reduces cGMP, which causes the photoreceptor to become hyperpolarized, the disc channel located in the photoreceptors releases all-trans-retinal, which travels into the cytoplasm where it is converted to all-trans-retinol. The molecule needs to be delivered by certain carrier proteins from the interphotoreceptor matrix (IPM) to the RPE because the photoreceptor is unable to re-isomerize it [39].

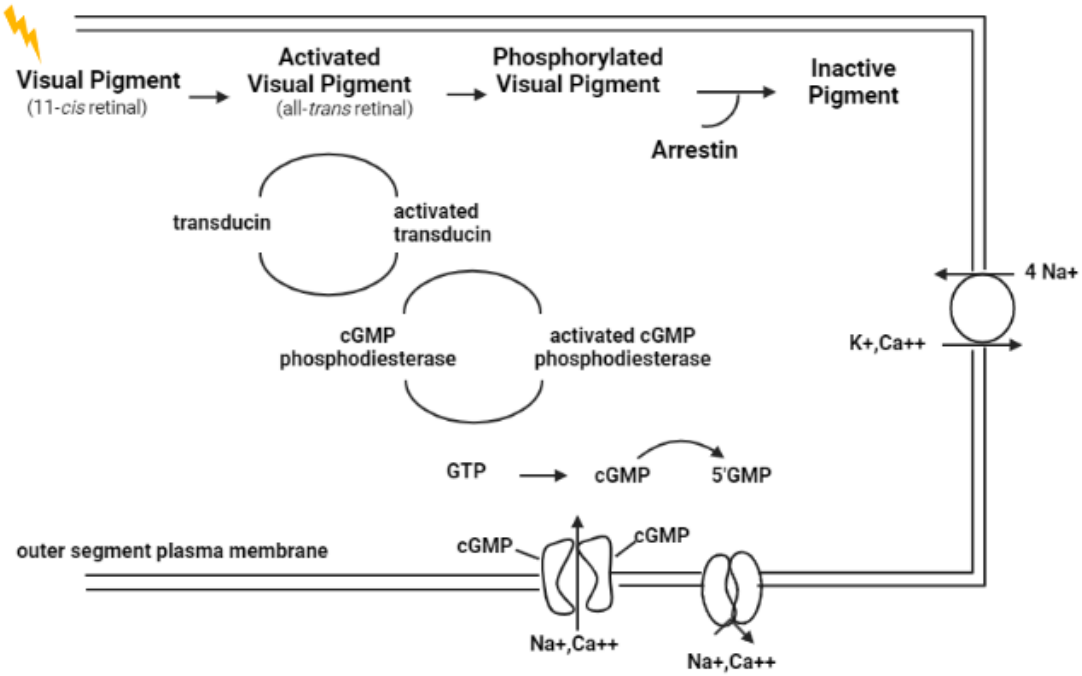

Figure 3. ***Schematic Representation of the Basic Phototransduction Signaling*** *Following photon absorption, the activated rhodopsin activates the heterotrimeric G protein, catalyzing the exchange of GDP to GTP activating the transducin. Transducin binds to the PDE and activates the PDE which catalyzes the hydrolysis of cGMP. Decrease in the cytoplasmic cGMP concentration leads to closure of the cGMP-gated channels on the plasma membrane and blocks the cation flux into the outer segment.*

1.4. Retinal Degeneration and Disease Models

Retinal degenerative disorders affect millions of people who suffer from vision loss in all around the world. RP, Age-related macular degeneration (AMD) and retinal ganglion cell (RGC) loss in glaucoma, and diabetic retinopathy are the most important degenerative retinal diseases regarding their distribution on world population. One of the leading causes of blindness in elderly people is AMD and generally develops in people aged 60-years or older. According to the recent cases in the world, it affects 8.7% of the global population [40]. In the early stages of AMD, atrophy or hypertrophy conditions are observed in the retinal pigment epithelium (RPE). This condition brings along the drusen deposits with them. In the late stages of AMD, central vision is affected. This is a devastating situation for the AMD patients, since central vision is necessary for performing daily tasks, such as face recognition, reading a book, cooking and many others.

RGC loss in glaucoma causes another common type of blindness. Since RGCs process the whole visual information from light entrance to the eyeball and transmit them to the brain, they are the corner stones of the mammalian visual system. Once RGCs die because of glaucoma, they cannot replace. RGCs are the part of the central nervous system, and they cannot regenerate when there is any damage. RP is an inherited retinal dystrophy and characterized by rod and cone (photoreceptor) loss and visible pigment deposits on fundus. Both drusen formation, and photoreceptor degeneration are ended up with retinal detachment, night blindness, light sensitivity, tunnel vision and peripheral or total vision loss during the progression of disease. There are many forms of RP known as autosomal dominant, autosomal recessive, X-linked and digenic forms [41]. Retinitis pigmentosa has been associated with mutations in more than 70 genes [42]. The autosomal dominant RP is linked to more than 20 of these genes. Autosomal dominant retinitis pigmentosa is caused by mutations in the RHO gene in twenty to thirty percent of cases, making it the most frequent genetic disease [42]. Moreover, the autosomal recessive version of the RP has linked at least 35 genes [43]. The most prevalent gene among the 35 gene is USH2A and between 10–15% of all instances of autosomal recessive retinitis pigmentosa are caused by mutations in USH2A gene. The X-linked type of the illness is considered to be brought on by changes in

at least six genes. The majority of cases of X-linked retinitis pigmentosa are caused by mutations in the RPGR and RP2 genes together [44].

Due to its monogenic nature, RP is also an attractive target for gene therapy applications. Moreover, eye has a number of characteristics that make it an excellent candidate as a target organ for gene therapy applications in vertebrates, like minimal systemic affects and vector amount. Eye is also readily available for treatment, and a gene can be delivered via intravitreal or subretinal injections [45].

There are also several animal models that mimic RP conditions such as rd1, rd2, rd10 and P23H. Rd1 mouse model is also known as rodless mouse model for the autosomal recessive form of Retinitis Pigmentosa. Keeler and his colleagues first identified the rd1 mice in 1924 and reported it as an autosomal recessive disorder resulting to the absence of the rod photoreceptor and it is characterized with thinner ONL [46, 47]. The insertion of murine leukemia provirus in intron1 and a point mutation in exon7 are the mutations on *Pde6b* gene which is located on chromosome 5 and the mutation on exon7 introduces a stop codon. This mutation causes severe, early onset and fast retinal degeneration [35, 38].

However, rd2 mouse model is a slower recessive RP model and there is a functional impairment on gene which encodes *Peripherin2*. Since Peripherin2 is a membrane protein and it is required for the photoreceptor outer segment disc formation, *Peripherin2* knockout mice are unable to produce photoreceptor outer segment [48]. In rd2 model, retinal degeneration starts two weeks later after the birth and reaches the peak at post-natal day 18 (PN18) together with apoptotic photoreceptor cell death [49, 50].

Another mouse model known as Rd10 has an autosomal missense R560C mutation of the *Pde6b* gene that causes recessively inherited retinal degeneration [51]. The phosphodiesterase 6 (PDE6) protein ß component, which is encoded by *Pde6b* gene, is necessary for the photoreceptors to work in an efficient way. The effector enzyme of rod phototransduction is made up of this catalytic ß subunit and two inhibitory gamma subunits. Due to the alterations on ß subunit of the PDE6 protein, phototransduction of the rod photoreceptors has some abnormalities and causes degeneration [52, 53].

There are more than 150 rhodopsins mutations that cause RP including P23H mutation. P23H autosomal dominant retinitis pigmentosa (adRP) model mouse has a mutation on the Rho (rhodopsin) gene and causes progressive degeneration of the retina. In the presence of this mutation, substitution was observed from proline amino to histidine at codon 23 from CCC to CAC by changing the single nucleotide. Since this changing occurs P to H on the 23rd codon of the *Rho* gene, this model is named as P23H [54].

These models have been very-well studied and several therapeutic applications are tested. Since, there are still limited treatment options for degenerative retinal diseases, the ongoing degeneration cannot be stopped, and patients usually end up with severe visual loss. One of the most promising approaches to treat retinal degeneration causing vision loss is inducing regeneration and reprogramming of the damaged area together with a gene therapy that targets the mutant gene. For the development of retinal regeneration therapy strategies, understanding vertebrate retinal regeneration is also essential to find a candidate therapy.

1.5. Regeneration Capacity of Vertebrate retina

Regeneration process takes places in all organisms to sustain their tissue and organ maintenance. However, retinal regeneration varies among vertebrates. While organisms like axolotl [55], zebrafish [56], xenopus and chicken have substantial retinal regeneration capacities, their mammalian counterparts have lost or did not develop. The regenerative properties of these retinas have attracted a lot of attention in the scientific community so that researchers have tried to mimic these features to organisms with less regenerative capacity.

In that sense zebrafish retinal regeneration have been studied extensively [57]. Retinal regeneration in zebrafish occurs in three distinct steps. Müller glia cells undergo reactivation in degenerative conditions and then they start to proliferate, afterwards reprogramming occurs [58, 59]. Müller glia cells in adult zebrafish is examined as multipotent stem cells, since they do not need reprogramming in the classical manner [60]. Induced Müller cells in response to damage, reprogramming factors are activated [61-63]. Müller glia starts to proliferate and, reprogramming occurs after expression of factors such as Ascl1 [64], Lin28 [63] , Stat3 [65], and Oct4 [66]. It has been shown that Ascl1 (Achaete-Scute Family BHLH Transcription Factor 1) impacts Müller glia reprogramming by re-adjusting the Wnt signaling pathway [67]. Lin28 is an RNA-binding protein and expressed in stem cells. Furthermore, it

has a role in mammalian regeneration [68]. Let-7 is a small administrative RNA-associated miRNA molecule and acts on cellular differentiation [69]. Both Lin28 and Let-7 antagonistically regulate each other's expression. Immediately after retinal injury, Müller glia cells re-enter the cell cycle, de-differentiate into neuronal progenitor cells which are capable of rebuilding retinal neurons (only in lower vertebrates), releasing neuroprotective substances, and removing degenerated cells debris by phagocytosis. Although innate immune system has a vital role in the regeneration procedure in fish and birds, recent findings reported that microglia lessened the neurogenic ability of Müller glia cells during Ascl1-associated regeneration in adult mice retina [70]. Another interesting study reported that lin28a is also regulated by Myc which is crucial for retinal regeneration in zebrafish [71]. As soon as reprogramming is achieved, regeneration of the photoreceptors has been observed within roughly 14 days. Similar regeneration steps are followed in chicken retina as well. However, endpoint of regeneration is distinctively different. Müller glia cells also enters the cell cycle like in zebrafish however only random neuronal regeneration is observed which is an undesirable outcome for retinal regeneration [72].

Müller cells are also primary cell types that control retinal homeostasis and tissue integrity in mammals. In the presence of retinal damage, different vertebrates have different responses Mammalian Müller glia exhibit tremendous cellular and molecular alterations in almost all of the types of retinal disorders, which are characterized as reactive gliosis, which can have both supportive and harmful impacts on functions of neurons and survival [73]. In the retinal disease conditions depending on the damage, overgrowth of Müller cells and GFAP upregulation is observed. These outputs are the markers of reactivity and retinal stress [74, 75]. Interestingly, some neurotrophic factors are observed in mammalian reactive Müller glia such as FGF2 [76]. Even though reactive gliosis has neuroprotective effect in the beginning, neuronal cell death is slowing down and constant gliosis causes the destruction of ordinary action of Müller cells [17, 77]. Retinal gliosis can also be triggered by other stimulant factor such as retinal degeneration [78], mechanical trauma [79], inflammation [80], light-induced damage [61], or aging [81].

There are two types of persistent reactive gliosis: proliferative and non-proliferative. In the non-proliferative version of reactive gliosis, there is no severe damage but some alterations

are observed such as GFAP upregulation and glutamine synthetase (GS) downregulation [76]. Uncontrollable Müller glia proliferation serves as a sign of the proliferative reactive gliosis. [82, 83]. In the serious retinal damage conditions, Müller cells undergo proliferation which may result in glial scar formation. Glial scar formation can eventually encompass the complete retina in the final phases of degeneration [81, 84]. This permanent glial scar formation is only observed in mammalians, there is no such an event in lower vertebrates. This gives hope that the mammalian glial scar formation may be preventable by using highly regenerative features of vertebrates such as zebrafish.

In mammalians like mice, Müller glia cells are usually arrested in the G1 phase and cannot get into the S phase following the retinal damage, therefore the first step of regeneration - proliferation - is hampered [85]. If Müller glia proliferation occurs in certain degenerative conditions, the resulting outcome will not be regeneration but an unfavorable disease-like condition; gliosis/scar formation in the mammalian retina. To activate regeneration in the mammalian retina, first of all proliferation capacity of the Müller glia should be induced. Neuronal fate induction is also needed following the proliferation. In mammals, not only transition of the proliferated cells into the specific subtypes but also their integration to the visual circuitry is required to make them functional. All these processes occur in zebrafish which provides a very suitable model to study all aspects of regeneration. As the non-mammalian vertebrate's Müller glia regeneration is better understood, these properties may be combined with mammal regeneration models to enhance our current knowledge of the mammalian Müller glia gliosis/regeneration.

We have already mentioned that non-mammalian vertebrates, like zebrafish [86], have exceptional regeneration capacity in the presence of a retinal damage. However, in mammals, regeneration capacity is quite restricted [87]. Instead, retinal damage triggers more elaborate neuroprotective pathways in mammalians. Discovering why retinal self-repair differs tremendously between different species is crucial for understanding and improving the regeneration capacity of mammalian Müller glia cells [88]. Therefore, one strategy to improve mammalian regenerative capacity would be to elucidate and mimic regenerative properties of non-mammalian vertebrates. Nowadays, regenerative medicine also gives valuable opportunities using stem cells and their features to find new approaches for retinal

diseases. Here, we generated novel animal models that will enhance understanding of retinal regeneration in mammals.

1.6. Rod Fate Induction by Using Stem Cell- and Rod-Specific Transcription Factors

One intriguing way to control gene regulation is artificial transcription factors (ATFs). ATFs are synthetic transcription factors that can either enhance or suppress the gene expression [89]. ATFs can be generated by using the sequence specific DNA binding activity of novel proteins including Zinc-Fingers, Transcription activator-like effectors (TALEs), and Clustered regularly interspaced short palindromic repeats - Cas (CRISPR-Cas). In the latter case, DNA editing properties of CRISPP-Cas9 is eliminated, and named as dCas9. These proteins are fused with gene activators or inhibitors to generate ATFs to alter the gene expression.

Yamanaka factors are a family of transcription factors that are essential for the development of induced pluripotent stem cells (iPSC) [90, 91] **(Fig. 4).** The Yamanaka factors accurately controlled with well-established embryonic stem cell pluripotency-associated pathways through cooperative and distinct combinations. *Oct4*, *Sox2*, *Klf4* and c-*Myc* were found to regulate the p53 signaling pathway, whereas *Oct4*, *Sox2*, and *c-Myc* had role on the regulation of the Wnt and TGF-ß signaling pathways. Moreover, *Oct4* and *Klf4* were found to regulate the Hedgehog signaling pathway, while *Oct4* was found to regulate the MAPK signaling pathway [90, 92] **(Fig. 5)**.

In non-degenerative mammalian retina, there is a strong *Sox2* and weak *Klf4* expression. However, there is no c-*Myc* and *Oct4* expression under normal conditions. In the presence of a degenerative condition, c-*Myc* expression is turned on, but no *Oct4* activity was observed **(unpublished data)**. Therefore, we anticipate that it should be feasible to induce pluripotency in degenerating mouse retina by overexpressing the missing Yamanaka factors. Artificial transcription factors (ATFs) could be the appropriate tool for this approach.

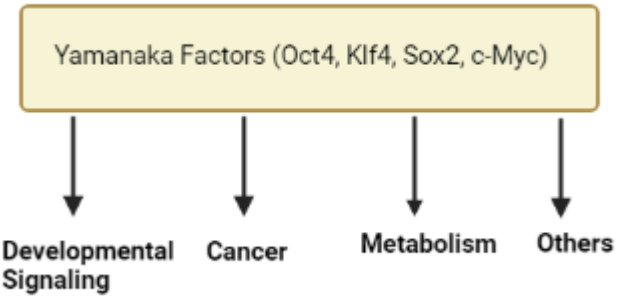

Figure 4. ***Pathway Classification of Yamanaka Factors.*** Main target of Yamanaka Factors are Developmental, Cancer and Metabolic pathways.

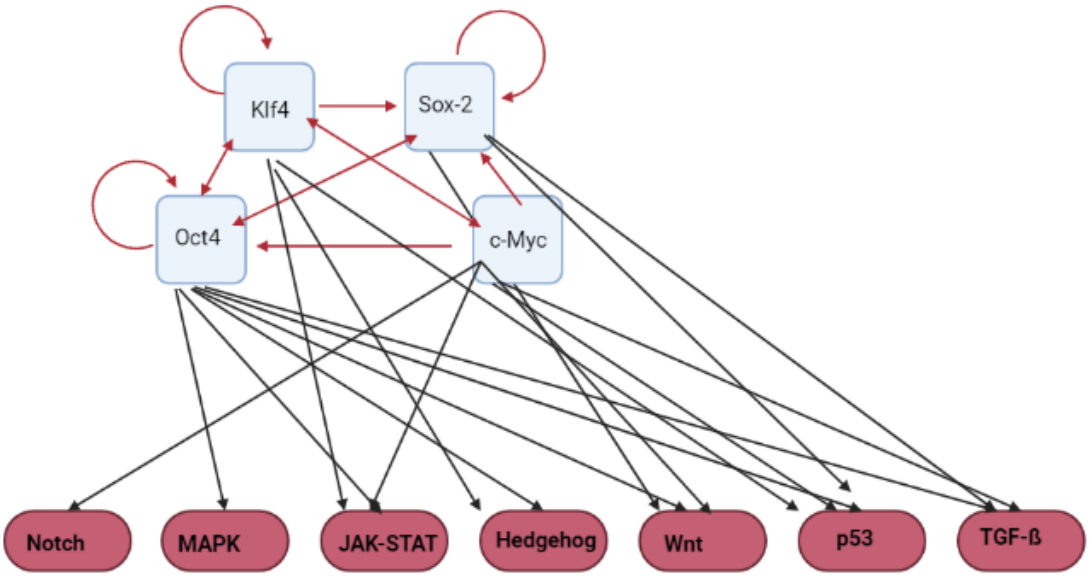

Figure 5. ***Yamanaka Factors and Downstream Signaling Pathways****. Self-regulation, interconnection and feedforward control mechanisms of Yamanaka factors are shown. Pink arrows represent the endogenous Yamanaka signaling network and long arrows shows the pluripotency-related pathways.*

Regulation and combinations of these factors may trigger the induction of pluripotency and may remove regeneration block in mammalian retina. Furthermore, overexpression of the

missing Yamanaka factors in mammalian retina may remove this block and potentiates the rod induction.

It is also feasible to further dedifferentiate proliferating Muller glia by expressing rod-specific transcription factors. It was previously shown that it is feasible to force proliferate Müller glia by ß-*catenin* overexpression and further overexpression of *Nrl1* induced Muller glia dedifferentiation into rod fate [93]. This study also showed that regeneration can be induced by using gene therapy approaches.

In order to generate ATFs that target and upregulate rod-fate in Müller glia, gRNAs are needed which is expressed under the human U6 promoter together with its complement dCas9-Activator. For this aim, we have generated approximately 15 gRNA clones for efficient upregulation of *Nrl*, *Klf4* and *Oct4* genes. In this thesis, we established stable Muller glia cell lines expressing different dCas9 activators such as VP64 and SPH and tested the gRNA constructs in *vitro*, which will be later used for *in vivo* approaches to accelerate the process of dedifferentiation and perhaps compensate the loss of rods in the mammalian retina.

1.7.Chemical Induction of the Rod Fate

In the groundbreaking research of Yamanaka and his co-workers, it was found that reprogramming the somatic cell into pluripotent stem cells is feasible just by overexpression of four key pluripotency genes *Oct4*, *Klf4*, *c-Myc* and *Sox2* in specific culture conditions [91]. After the establishment of Yamanaka's pluripotency induction method, several research groups successfully converted the somatic cells into different cell types such as neurons [94, 95], cardiomyocytes [96], oligodendrocytes [97, 98], and hepatocytes [99] by using lentiviruses or retroviruses as a delivery vector. However, there are legitimate worries about the security of using the patient cells in clinics due to the use of viral vectors and induction of oncogenes. Recently, the focus of the field has been extended toward faster methodologies and new chemical/small molecule-based reprogramming techniques. In 2013, Hou and his colleagues was the first scientists, to generate mouse induced pluripotent cells (iPSC) from mouse embryonic fibroblasts just by using 7 different small molecules which are designated as VC6TFZ: VPA, CHIR99021 (CHIR), 616452, tranylcypromine, forskolin (FSK), 2-methyl-5-hydroxytryptamine (2-Me-5HT), and D4476 [100]. When compared to Yamanaka's iPSC procedure, this chemical induction approach showed an 0.01% to 0.1% greater efficiency and similar gene expression profile. This study established the general

principle that small molecules can be used for cell fate reprogramming without the need for exogenous expression of *Oct4*, *Klf4*, *c-Myc* and *Sox2*. This idea opens the door to an all-chemical reprogramming approach that may be used to produce cell types that are functionally desirable for cell therapy.

Since reprogramming with drugs is feasible, our group previously did a pharmacologically active molecules (PAMs) screen that identified the several drugs that can reactivate the Müller glia cells to induce the rod fate. This was achieved by triple transgenic Tg(Rlbp1-GFP);Tg(Rho-Cre);ROSA26-LSL-tdTomato mouse cell line by immortalizing the retinal primary cells coming from these triple transgenic animals. The screen works activation of rhodopsin and thus Cre expression. This removed the stop codon flanked by flox sites and activated tdTomato expression as a read out for rod fate. According to results of this screen which was performed by using 1280 drugs, top ten drugs regarding the tdTomato positive cell numbers belonged to three different pathways: (1) ion channels, (2) glutamate and (3) prostaglandin. Ion channels are the common membrane proteins in mammals. They have crucial roles on physiological functions such as modulation of the electrical potential, signal and transduction [101]. Since the vertebrate central nervous system (CNS) relies heavily on glutamate which is an important neurotransmitter, it has a main role on retinal synaptic circuitry [102]. Prostaglandins are acidic lipid compounds that can be generated enzymatically by most mammalian cell types in response to different stimulations such as mechanical, chemical, or immunological and they have a role on blood-retina barrier [103, 104].

We have also used two of these candidate drugs to evaluate whether our new screen platform is successful for rod fate induction on the primary Müller glia cells coming from Tg(Rho-Cre)-ROSA26-LSL-tdTomato animals. In this strategy, primary cells were not immortalized. Instead, direct seeding of dissociated retina was performed and a selection procedure for Muller glia was applied which was successful in terms rod fate induction with the selected candidate drugs.

2.AIM

In this master thesis, we aimed to establish a reporter mouse line for Retinitis Pigmentosa disease and primary cell culture lines from both reporter and dCas9-SPH transgenic mouse lines for the regeneration studies using CRISPR-dCas9 based Artificial Transcription Factors (ATFs). For this purpose, rd1 fast degeneration Retinitis Pigmentosa reporter mouse model was established to be used in rod-fate induction studies. Furthermore, crossing of dCas9-SPH animals with Retinitis Pigmentosa reporter model was done to generate a novel animal model to test ATFs targeting *Oct4*, *Nrl1* and *Klf4*.

3.MATERİALS AND METHODS

3.1.Animal Breeding

Sabanci University and Gebze Technical University Ethics Committees approved all experimental methods, and studies were carried out in conformity with the Association for Research in Vision and Ophthalmology's statement on the use of animals in research. Maintenance and breedings of the mice were performed in Gebze Technical University and records are kept with the help of the PyRat software. Transgenic mice were originally provided from JaksonsLaboratory and kept in regular 12h: 12h light-dark cycle and exposed with 60 lux led for their light cycle. Food was provided as *ad libitum*.

3.2. Genotyping

3.2.1.PCR Genotyping

3.2.1.1. Rd1 PCR

21 µL GoTaq Green Master Mix (Promega, M7123), 1 µL Forward and 1 µL Reverse primers, 0.15 µL 5000U/mL Taq DNA polymerase (NEB, Cat#M0267S) and 2 µL of homogenized DNA sample was distributed to PCR reaction tubes. When tubes were ready for PCR amplification, they were vortexed, spun down and placed on the PCR machine to run reaction. Reaction steps and cycles were set up as mentioned below **(Table 1)**

Steps	Temperature	Time
1	94 ºC	5 min
2	94 ºC	30 sec
3	62 ºC	45 sec
4	72 ºC	45 sec
5	Go to Step 2	35X
6	72 ºC	10 min
7	4 ºC	∞

Table 1. ***Time and temperature intervals of the Rd1 Genotyping PCR amplification.*** *Time intervals, temperate and cycle repeats for rd1 genotyping PCR reaction are shown.*

After PCR reaction was completed, DdeI digestion of the amplified PCR products was performed. If there is a mutation in *Pde6b* gene, mutated ones (T→C), PCR amplicon is digested by DdeI restriction digestion enzyme and the genotype was recorded according to the results of agarose gel electrophoresis **(Fig. 6)**. For this purpose, 8 µL of non-purified PCR product, 9.5 µL nuclease free H_2O (Wisent Multicell, Cat#809-115) and 0.5 µL 28U DdeI enzyme (NEB, Cat#R0175S) mixed and incubated at 37ºC for 3 hours. When the incubation is finished, samples were used for the gel electrophoresis.

A)

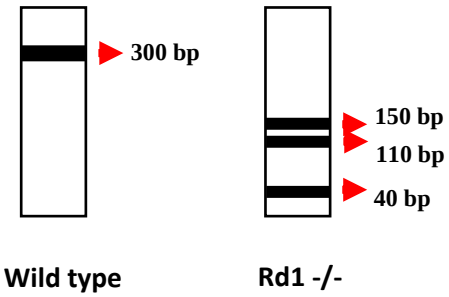

B)

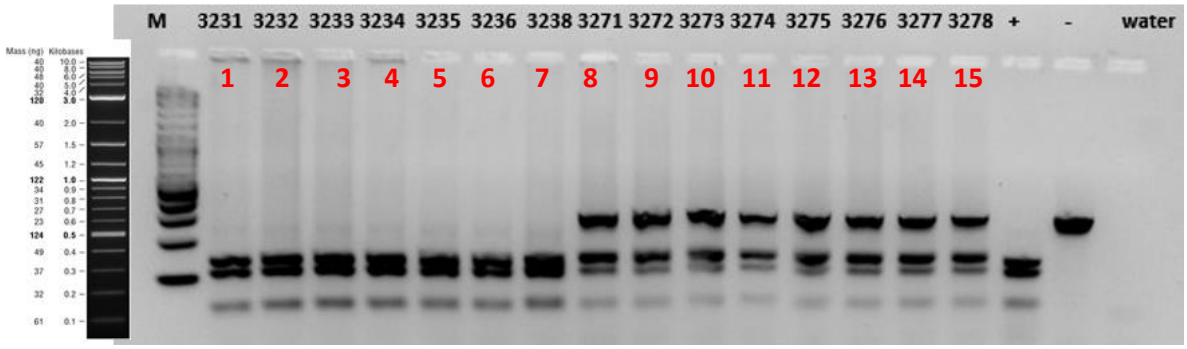

Figure 6. ***Representative Gel Image of Rd1 PCR***

Expected wild-type and mutant Rd1-/- bands were shown as 300 bp for wild-type and 150 bp, 110 bp and 40 bp three different bands were observed after the DdeI digestion for the rd1-/- mutant mice, respectively ***(A)****. Negative (-) control represents the wt mouse which has no mutation in Pde6b gene and thus not digested. The band size of the positive control is 300 bp. Positive (+) control represents that there is a mutation in Pde6b gene and triple band size is observed from top to bottom 150 bp, 110 bp and 40 bp, respectively. It is also clearly seen that first 7 samples are rd1-/- and other samples are rd1wt/-* ***(B)****.*

3.2.1.2. dCas9-SPH PCR

dCas9-SPH PCR reaction mix was prepared as 10.5 µL GoTaq Green Master Mix (Promega, M7123), 0.5 µL Forward and 0.5 µL Reverse primers, 0.075 µL 5000U/mL Taq DNA polymerase (NEB, Cat#M0267S) and 2 µL of homogenized DNA sample was distributed to PCR reaction tubes. When tubes were ready for PCR amplification, they were vortexed, spun down and placed on the PCR machine to run reaction. Touchdown PCR protocol was used for the amplification. Touchdown is a technique to reduce off-target priming and boost the specificity. Reaction steps and cycles were set up as mentioned below **(Table 2)**.

Steps	Temperature	Time	Note
1	94 ºC	-	
2	94 ºC	-	
3	65 ºC	-	-0.5 ºC per cycle decrease
4	68 ºC	-	
5			Repeat steps 2-4 for 10 cycles (Touchdown)
6	94 ºC	-	
7	60 ºC	-	
8	72 ºC	-	
9			Repeat steps 6-8 for 28 cycles
10	72 ºC	-	
11	10 ºC	-	∞

Table 2. ***Dcas9-SPH Touchdown PCR Amplification****. Time intervals, temperate and cycle repeats for dCas9-SPH genotyping PCR reaction are shown.*

After amplification was done, agarose gel electrophoresis was performed **(Fig.7).**

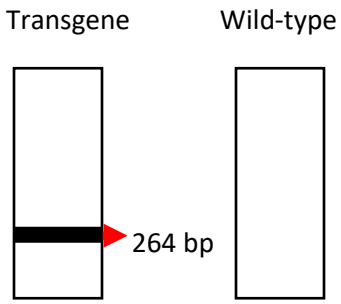

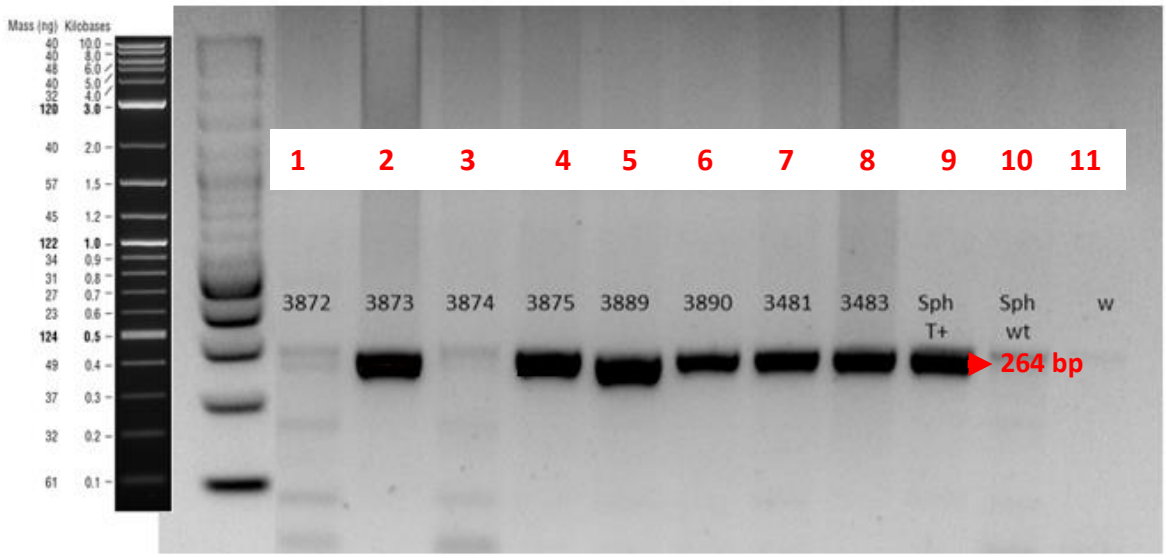

Figure 7. ***Representative Gel Image of dCas9-SPH PCR*** *Gel image shows that out of first and third sample, all samples are dCas9-SPH positive regarding the 264 bp transgene band. As a negative control which does not include transgene, C57BL/6 Control mouse was used.*

3.2.1.3. GFAP-Cre PCR

GFAP-Cre PCR reaction mix was as 10.5 µL GoTaq Green Master Mix (Promega, M7123), 0.5 µL Forward and 0.5 µL Reverse primers, 0.075 µL 5000U/mL Taq DNA polymerase (NEB, Cat#M0267S) and 2 µL of homogenized DNA sample was distributed to PCR reaction tubes. When tubes were ready for PCR amplification, they were vortexed, spined down and placed on the PCR machine to run reaction. Touchdown PCR protocol was used for the amplification. Touchdown is a technique to reduce off-target priming and boost the specificity. Reaction steps and cycles were set up as mentioned below **(Table 3).**

After amplification was done, agarose gel electrophoresis was performed **(Fig. 8).**

Steps	Temperature	Time	Note
1	94 ºC	-	
2	94 ºC	-	
3	65 ºC	-	-0.5 ºC per cycle decrease
4	68 ºC	-	
5			Repeat steps 2-4 for 10 cycles (Touchdown)
6	94 ºC	-	
7	60 ºC	-	
8	72 ºC	-	
9			Repeat steps 6-8 for 28 cycles
10	72 ºC	-	
11	10 ºC	-	∞

Table 3. ***GFAP-Cre Touchdown PCR Amplification***. *Time intervals, temperature, and cycle repeats for GFAP-Cre genotyping PCR reaction are shown.*

Expected bands:

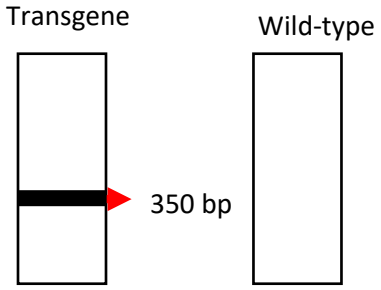

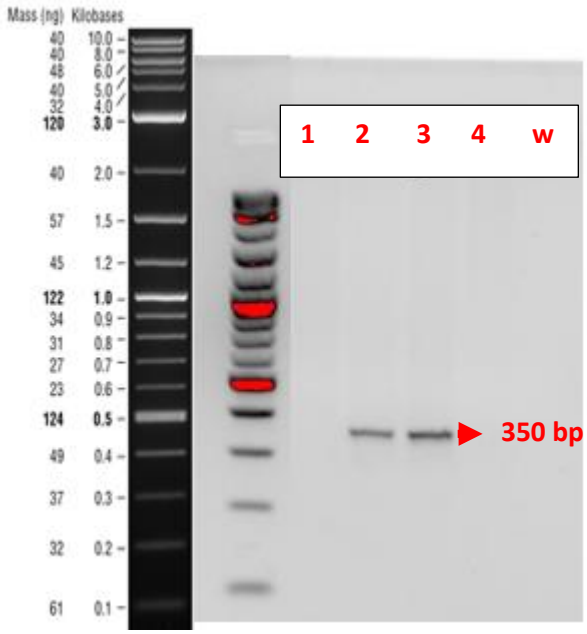

Figure 8. ***Representative Gel Image of dCas9-SPH PCR.*** *Gel image shows that first sample is wild-type, and second and third samples are dCas9-SPH positive regarding the 350 bp transgene band. As a negative control which does not include transgene, wild-type C57BL/6 control mouse sample was used (sample 4).*

3.2.1.4.ROSA26-Ai14-tdTomato PCR

The loxP-flanked STOP cassette in the Cre reporter allele Ai14, which was introduced into the Gt(ROSA)26Sor locus, prevents transcription of a tdTomato, known as red fluorescent protein variant, driven by the CAG promoter . tdTomato fluorescence is strongly expressed in Ai14 mice after Cre-mediated recombination. 21 µL GoTaq Green Master Mix (Promega, M7123), 1 µL 10 µM Forward and 1 µL 10 µM Reverse primers, 0.15 µL 5000U/mL Taq DNA polymerase (NEB, Cat#M0267S) and 2 µL of homogenized DNA sample was distributed to PCR reaction tubes. When tubes were ready for PCR amplification, they were vortexed, spun down and placed on the PCR machine to run reaction **(Fig. 9)**. Reaction steps and cycles were set up as mentioned below **(Table 4)**.

Steps		Temperature	Time	Note
1	Denaturation	94 ºC	2 min	
2	Denaturation	94 ºC	20 sec	
3	Annealing	65 ºC	15 sec	-0.5 ºC per cycle decrease
4	Synthesis	68 ºC	10 sec	
5	Go back to step 2 for 9 times			
6	Denaturation	94 ºC	15 sec	
7	Annealing	60 ºC	15 sec	
8	Synthesis	72 ºC	10 sec	
9	Go back to step 6 for 27 times			
10	Elongation	72 ºC	2 min	
11	Cool down	10 ºC	hold	∞

Table 4. ***Time And Temperature Intervals of ROSA26-Ai14-tdTomato Touchdown PCR Amplification*** *Time intervals, temperature, and cycle repeats for GFAP-Cre genotyping PCR reaction are shown.*

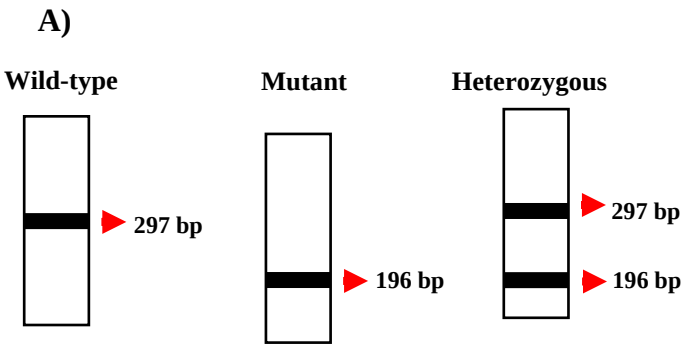

B)

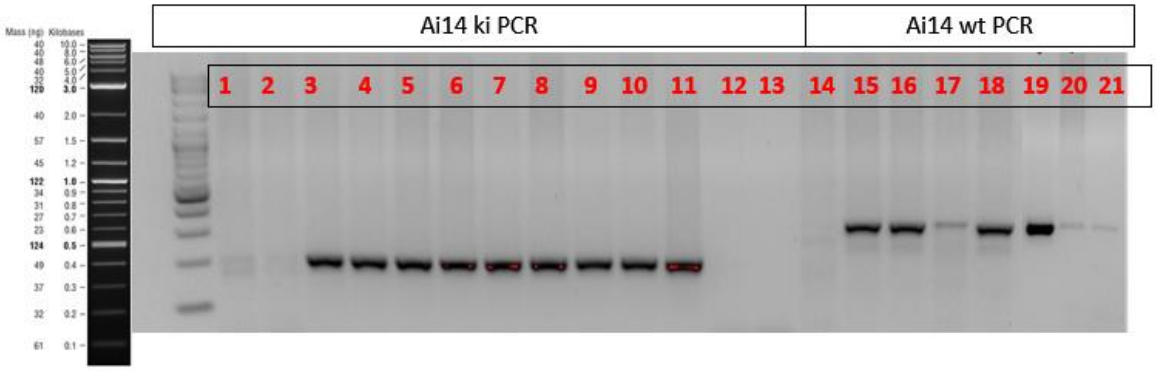

Figure 9. ***Representative Gel Image of Ai14 ki and wt PCR***. *Illustration of expected band sizes represent the wild-type, mutant and heterozygous band locations in the Ai14 PCR* ***(A)***. *In this Ai14 ki and Ai14 wt PCR agarose gel image, bands #11 and #19 represents the positive controls (representing presence of Ai14 allele or wildtype allele, respectively) while bands #12 and #20 negative controls (representing absence of Ai14 allele or wildtype allele, respectively), and #13 and #14 water controls, respectively* ***(B)***.

3.2.2. Agarose Gel Electrophoresis

50X TAE stock solution was prepared using 242 g Tris-base (Merck, Cat# 77861), 57.1 mL glacial acetic acid (Merck, Cat# 64197) and 100 mL 500 mM EDTA (Merck, Cat#60004) and filling up to 1 L with ddH20. Agarose gels were prepared by using 1X TAE solution and appropriate amount of agarose (GeneON BioScience, Cat#604001). PCR samples for genotyping were loaded into 2% (w/v) agarose-TAE gel and run at 100V for 1 hour. DNA samples for gel extraction and DNA samples treated with restriction digestion enzyme were loaded into 0.8% (w/v) TAE agarose gel and run at 100V for 1 hour.

3.2.3. MicronIV Genotyping

Genotyping of the mice were not only determined by polymerase chain reaction (PCR) but also with MicronIV fundus imaging technique. MicronIV genotyping provides to double check the PCR genotyping results and decreases the PCR genotyping workload. In the dCas9-SPH, if we observe the GFP expression we could say that it is transgenic (T+) mouse due to the GFP expression leakage in this model. On the other hand, we can check Rho-Cre and ROSA26-Ai14-tdTomato phenotype just by checking the fundus image with tdTomato filter.

If there was a Ai14 phenotype either ki/wt or ki/ki, we will be able to observe crescent-like tdTomato expression around the optic nerve. For the Rho-Cre assessment, Rho-Cre T+ mice will be expressing tdTomato in the fundus imaging.

3.3. Retina Isolation[105]

Rd1 mutant and wild-type animals were humanely sacrificed by using CO_2 inhalation. The eyeball was shifted to forward by placing a forceps around the eyeball. The lens and left over vitreous homour are removed by gentle pressure. Furthermore, connection of the retina and the optic nerve is interrupted with a curved forceps to cut the connection to the eyeball. This step is followed by gentle squeeze of the retina. Dissected retinas are transferred to the 1.5 mL Eppendorf tube. Retinas were subject to several different protocols including establishment of primary glia cell line, retinal gene expression by direct total RNA isolation or after FACS sorted.

3.4. Primary Cell Line Strategies

3.4.1. Establishment of Primary Müller Glia Cell Line for 10-mL Plate

400 µL dissociation mix was added onto the isolated retinas. Dissociation mix includes 100 mM 320 µL HEPES (Sigma Aldrich), 40 µL Papain (Roche) and 40 µL L-cysteine/EDTA (Merck Millipore). L-cysteine/EDTA, 50mM 20 µL L-cysteine and 10 mM 20 µL EDTA pH:7 and added to each sample tube. Also, all mixture is activated at 37ºC for 15 min. When dissociation mix become activated, mixture color was expected to turn clear. After addition of 400 µL dissociation mix, retina samples were incubated at 37ºC for 7 minutes. Supernatant part was discarded as much as possible. Then, trituration was performed with normal media containing 25 µl 1% (w/v) Kolliphor P 188 (Sigma, Cat#K4894) by using fire-polished glass Pasteur pipettes. After dissociation was completed, 10-mL plates which were pre-coated with 20µg/mL Fibronectin (Sigma Aldrich, Cat#F2006) were used. Fibronectin-coating strategy was used for better cell attachment to the wells. As soon as fibronectin was dried out within 2 hours, plates were washed with PBS three times to make them ready for usage. 39 mL DMEM media containing no glucose and no pyruvate (Gibco, Cat#11966025), 25 mM D-sorbitol (AppliChem, Dresden, Germany, Cat#50704), 1% Penicillin/Streptomycin (Gibco, Cat#15140122), 10% FBS (Gibco, Cat#10500064) and 40ng/mL of EGF (Cayman, Cat#32025) was distributed to 10 mL and 96-well plates. 25 mM D-sorbitol (AppliChem,

Dresden, Germany, Cat#50704) was used for Müller cell selection for 7 days. After the trituration step, cell mixture was transferred into directly to the fibronectin-coated plates and moved directly to the 37ºC incubator. During the selection procedure, media was changed in every 2 days for 1 week. When the selection was done, normal media containing 10% FBS, 1% Penicillin/streptomycin and 1% L-glutamine was used. Cells were incubated at 37ºC until they reach 70%-80% confluency.

3.4.2.96-well strategy for drug test

For the 96-well plates, same strategy for retinal dissociation was used **(3.4.1).** 30µL of the dissociated retina mix were distributed directly to the plate containing 200 µL of the selection media. During the selection procedure, media was changed in every 2 days for 1 week. When the selection was done, normal media containing 10% FBS, 1% Penicillin/streptomycin and 1% L-glutamine was used for further steps. Cells were incubated at 37ºC until they reach 70%-80% confluency.

3.5. Total RNA Isolation from Retina

Animals were sacrificed by using CO_2. Retinas were isolated according to the protocol mentioned above (part 2.3.) and transferred to 1.5 mL Eppendorf tubes and they are placed in liquid nitrogen. For these protocol, Roche High Pure RNA Isolation Kit and manufacturer's protocol is used with some optimizations. 400 µl Lysis/Binding buffer is added to the samples. Since Lysis/Binding buffer is viscous, this step should be performed carefully. Retinas are homogenized with a 1 ml syringe and 21G needle. 190 µl 100% ethanol is added and mixed well. Vortex usage is not recommended in this step. Lysate is transferred into the Roche Spin Column. 1 minute centrifuge is performed at 14000 rpm. Flow-through after centrifuge is discarded and column is put back into the same collection tube. 100 µL Dnase-mix is added directly to the membrane. DNase mix includes 80 µL DNase incubation buffer and 20 µL DNase as total of 181U of DNase. In this step, trying not to touch the membrane is important. After addition of DNase mix, 15 minutes at room temperature incubation is required. After incubation is over, 500 µL Wash Buffer I is added to the column. 1 minute centrifuge is performed at 14000 rpm. Flow-through is discarded and column is put back in same collection tube. As a second wash, 200 µL Wash Buffer II is added and then 1 minute centrifuge is performed at full speed. After centrifuge, flow-through is discarded and

column is put back into the same collection tube. Additional 2 minutes centrifuge at full speed is performed to avoid any Wash Buffer carryover and column should be put in fresh 1.5 mL DNase/RNase free Eppendorf tube. 50 µl sterile water is added directly on membrane without touching the membrane and incubated for 1 minute at room temperature. By following incubation, 1 minute centrifuge at 10.000 rpm is performed. Lastly, column is discarded. RNA concentration is measured by using Nanodrop machine and stored at -80ºC for further usage.

3.6.Cloning strategy

3.6.1. Establishment of gRNA vectors

Designing gRNA vector strategy was started by selection of candidate genomic regions for the *Oct4, Nrl1* and *Klf4* genes and their DNA sequences were downloaded as FASTA format to target their coding regions which are selected as first 1000 bp in the first exon. This 1000 bp sequence was copied and pasted to the Benchling software as raw bases to create SpCRISPR-Cas9 guides. Guide length was selected as 20 bp, PAM sequence as NGG Spcas9 3' side and genome type as *mus musculus* GRCm38 which is an updated version of mouse genome. Top-scored gRNAs were chosen according to their off target and on target scores. gRNA selection strategy based on the location of the primers which were nearly located or located in the coding region. Due to the gRNA which are close to the coding region have better efficiency, but we also tried to take gRNAs from different distances from the coding promoters, as well while staying within a 1 kb area. Lastly, selected clones that have were sent to company for synthesis.

3.6.2. Oligonucleotide Annealing

Forward and reverse primers were prepared with DNase-RNase free sterile water according to the instructions from provider. Stock solutions were 100 µM for each primer. 1µl of primer from stock, 5 µl 10X Annealing Buffer (Addgene) and 43 µl sterile water are combined. Final primer concentration for each primer was 2 µM. Below protocol for oligonucleotide annealing was run **(Table 5).**

Steps	Temperature	Time
1	95 ºC	5 min
2	94 ºC – 57 ºC	-1ºC per min
3	57 ºC – 30 ºC	-3ºC per 3 min
4	30 ºC – 27 ºC	-3ºC per 2min
5	27 ºC – 25 ºC	-2ºC per 2min
6	25 ºC	∞

Table 5. ***Time and temperature intervals of the oligonucleotide annealing protocol*** *Time intervals and temperatures for oligonucleotide annealing are shown.*

3.6.3. Restriction Digestion of the Plasmid

11-6 plasmid was used as a backbone in all cloning procedure for *Oct4*, *Klf4* and *Nrl1* genes **(Fig. 10).** 11-6 plasmid consists of functional sequences including U6 promoter, gRNA scaffold region, CBA promoter, hybrid intronic region, EGFP, polyA signal and origin of replication, ampicillin resistance gene. With the aim of inserting the gene of interest into the gRNA scaffold region, BbsI (NEB #R0539) digestion enzyme which has two cutting site inside of this gRNA scaffold region is used. BbsI enzyme was used to make plasmid linearization according to its sticky end restriction feature to insert the vector which has BbsI sequences on their 3’ and 5’ ends.

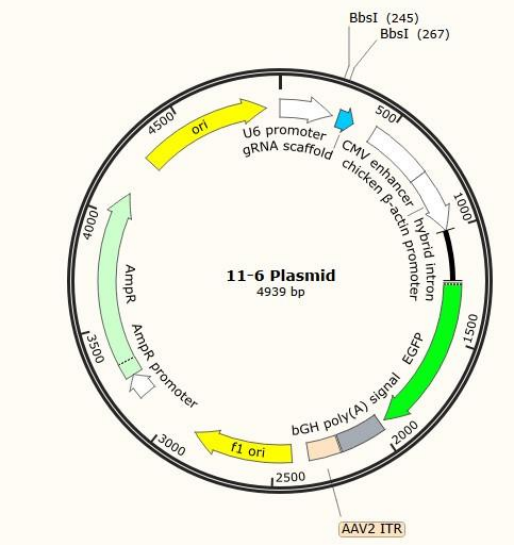

Figure 10. ***11-6 Plasmid Map and BbsI Restriction Digestion Sites.*** *BbsI enzyme site was used for insertion of specific gRNA sequences. EGFP expression is regulated by CBA promoter.*

10 µg 11-6 plasmid, 0.5 µL 300U BbsI restriction digestion enzyme (NEB, Cat#R0539), 5 µL 10X CutSmart Buffer and water added to generate 50 µL total restriction digestion reaction mix. Reaction is performed at 37ºC for 1 hour.

3.6.4. Gel Extraction

10 µg digested 4939 bp 11-6 plasmid is run on 0.8% (w/v) agarose gel to extract linearized dsDNA for further cloning steps. NEB GeneRuler 10kb marker is used to assess appropirate DNA band and digested plasmid are extracted using QIAquick Gel Extraction Kit (QIAGEN, Cat# 28704). Steps were followed according to the manufacturer's protocol. Firstly, DNA fragment from the agarose gel was cut out properly with a sharp and sterile scalpel. Gel slice was placed in a clear tube and weighed. For the 1 volume of gel, volumes of buffer QG was added (e.g., 200 mg gel ~200 µL). Tubes were incubated at 50°C water bath until the gels were completely dissolved. Then, DNA-binding QIAquick spin column was places into the 2 ml of collection tube. Dissolved DNA was poured onto the QIAquick spin column and 1 minute centrifuge at high-speed (16900 rcf). For the wash step, to wash, add 750 µL of Buffer PE was added onto QIAquick column carefully and centrifuge for 1 minute at high-speed. Additional 2 minutes centrifuge step was performed to remove residual wash buffer.

QIAquick column was placed into a clean 1.5 mL microcentrifuge tube and labeled. DNA was eluted using RNase/DNase free water (Wisent Multicell, Cat#809-115) to the center of the QIAquick membrane and centrifuged for 1 minutes at high-speed. Lastly, DNA concentration and purity was measured using NanoDrop™ 2000/2000c Spectrophotometer (Thermo Scientific™, Cat#ND-2000).

3.6.5. Ligation

To ligate vector DNA and plasmid, 4 µL of the annealed oligoduplex, 200 ng 11-6 digested plasmid, 1 µL 10X T4 DNA Ligase Buffer (BioLabs, Cat#B0202), 0.5 µL 400.000 U/mL T4 DNA Ligase (BioLabs, Cat#M0202S) and appropriate amount of volume for nuclease-free water (Wisent Multicell, Cat#809-115) were used to reach 10 µL total volume. All samples are incubated at 16ºC for O/N.

3.6.6. Competent Cell Preparation

For the whole steps to produce competent cell, Zymo Mix&Go (Cat# T3001) manufacturer's protocol was followed.

3.6.7. Transformation

Stbl3 E. coli strain (Invitrogen, Cat#C737303) was used as competent cell for the bacterial transformation. Competent cells were thawed on ice before the ligation procedure. Ligated plasmids were added into competent cells and incubated on ice for 30 minutes. Heat shock is followed this procedure at 42ºC for 30 seconds. Another incubation is performed on ice for 5 minutes and 1 ml LB broth is added to each microcentrifuge tubes. All samples are incubated at 37ºC for 1 hour.

3.6.8. Agar and Liquid Bacterial Culture for Colony Selection

Transformed bacteria were inoculated on ampicillin agar plate and incubated at 37ºC O/N. After the O/N incubation, ampicillin resistant colonies were picked up and they were growth in 3mL liquid Luria-Bertani (LB) broth containing 1:1000 ratio ampicillin again at 37ºC O/N.

3.6.9. Colony PCR

When bacterial colony numbers were reached to the log phase, colony PCR was run to be sure vector is successfully inserted. 1 µl 10µM U6 forward primer, 1 µl 10µM guide reverse

primer, 1 µl bacterial sample, 1 µl nuclease-free water, 0.15 µL 5000 U/mL *taq* polymerase (NEB) and 21 µL no enyme PCR master mix (NEB GoTaq) were prepared to run colony PCR reaction **(Fig. 11 and Table 6)**.

Steps	**Temperature**	**Time**
1	95 ºC	5 min
2	95 ºC	30 sec
3	51 ºC	1 min
4	68 ºC	1.5 min
5	Go to Step 2	34X
6	68 ºC	5 min
7	4 ºC	∞

Table 6. ***Colony PCR Steps.*** *Time intervals, temperate and cycle repeats for rd1 genotyping PCR reaction are shown*

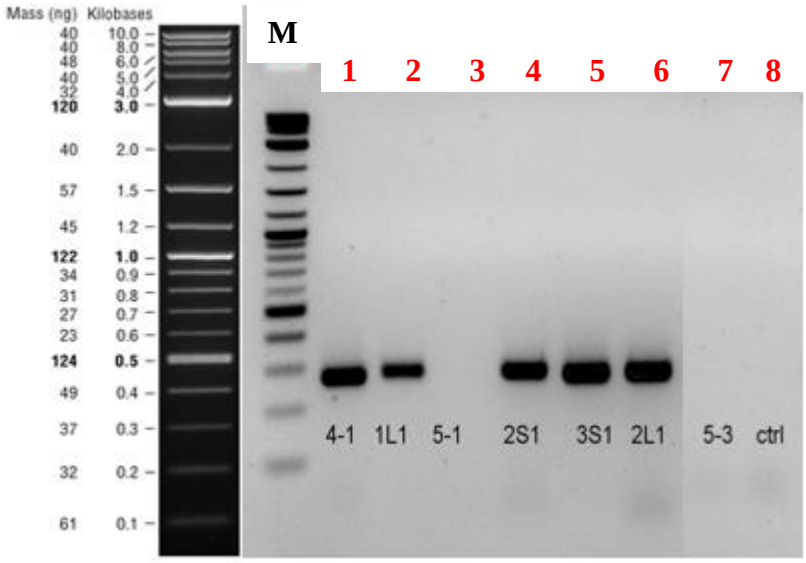

Figure 11. ***Representative Gel Image of OCT4 Colony PCR.*** *Gel image shows that all colonies have the insert in the bacterial genome which means that they were cloned*

accordingly with the expected sequences except 3rd and 7th wells. 8th well is the water control to distinguish whether there is a contamination or primer dimer. Sample names are simplified for interpretation.

3.6.10. Glycerol Stock and DNA Isolation (mini-prep)

500 µL of sterile 80% (v/v) glycerol solution and 200 µL bacterial culture were mixed and stored at -80ºC for further usage. Rest of the bacterial culture was used for DNA isolation using plasmid miniprep kit (Zymo Research, Cat # D4019).

3.6.11. Sequencing

Sanger sequencing is performed by Medsantek company for all samples. 15 µL 100 ng/µL sample and for each and 2 µL of 10 µM U6 forward primer were provided for each sample tube. In this step it was crucial to provide 100 ng/µL sample amount. Sequences were confirmed by aligning expected gRNA sequences.

3.7. Large Scale Endotoxin-Free DNA Isolation

3.7.1. Starter Culture for Large Scale Endotoxin-Free DNA Isolation

LB Broth was prepared containing 1:1000 ratio ampicillin. 3 mL ampicillin selective LB broth and 10 µL 50% (w/v) glycerol stock of the plasmid of interest inoculated with bacterial farms and incubated at 37ºC 200 rpm shaker for overnight. After the overnight incubation, 100 mL fresh ampicillin-selective LB broth containing ampicillin was poured into autoclaved-sterile 1L erlenmeyer together with 100 µL bacterial culture to obtain large amount of plasmid and incubated at 37ºC 200 rpm shaker for overnight.

3.7.2. Large Scale Endotoxin Free DNA Isolation

An endotoxin-free commercial kit (NucleoBond Xtra Midi EF, Macherey-Nagel, Cat# 740420.50) was used for large scale plasmid isolation. The cultured bacteria were centrifuged at 6000g, 4°C for 15 minutes. Supernatant was removed and the pellet was resuspended in 8mL resuspension buffer. 8mL lysis buffer was added and the mixture was incubated at room temperature for 5 minutes. Lysate was neutralized by adding 8mL neutralization buffer and incubated at 4°C for 5 minutes. The lysate was added into a column pre-wetted with 15mL equilibration buffer. Column together with filter was washed using 5mL buffer FIL-EF. The

filter was discarded, and the column was washed with 35mL buffer ENDO-EF. Column was washed again with buffer WASH-EF. The plasmid DNA was eluted using 5mL buffer ELU-EF. Following elution, plasmid DNA was precipitated by adding 3.5mL room temperature isopropanol to the elute. The elute was centrifuged at 15000g 4°C for 30 minutes. Supernatant was discarded and room-temperature 70% endotoxin-free ethanol was added to the pellet. This mixture was centrifuged at 15000g 22°C for 5 minutes. Ethanol was removed and the pellet was dried for 15 minutes. Pellet was resuspended in 200 mL H_2O-EF and plasmid DNA concentration was determined using a UV-Vis spectrophotometer**.**

3.8. Assessment of the gRNAs *in vitro*

3.8.1. Transfection

3.8.1.1. Preparation of Polyethyleneimine (PEI)

450 mL of the ddH_2O was added into the 500 mL glass beaker. 500 mg of the PEI (Polyscience, Inc.) was added into the beaker and stirred with a magnetic fish. 12M HCl solution was added drop by drop until pH reaches the 2. Solution was stirred until PEI completely dissolved and this procedure take nearly 3 hours. Later on, 10 M NaOH was added onto the solution to make pH:7 and poured into the 500 mL glass cylinder to adjust the volume to 500 mL by adding ddH_2O. As a last step, solution was filter-sterilized through a 0.22 um membrane and aliquoted into the falcon tubes to store at -20ºC.

3.8.1.2. Polyethyleneimine (PEI) Transfection

Cells were seeded as 150.000/well for the 6-well plates. The day after the seeding, all transfection reagents were prepared for each wells as 100 µL Optimem (Gibco, Cat#31985070), 6 µL Polyethyleneimine (PEI) 1 mg/mL and 2 µg plasmid of interest.

3.8.1.3. FuGENE Transfection

Cells were seeded as 150.000/well for the 6-well plates. The day after the seeding, all transfection reagents were prepared for each wells as 100 µL reduced-serum medium Opti-MEM (Gibco, Cat#31985070), 9 µL transfection reagent FuGENE (Promega, Cat#E2311) and 3 µg plasmid of interest.

3.8.1.4. Immortalization of Müller Glia Cell Lines

In order to increase proliferation capacity of isolated primary Müller glia cells, SV40 transfection was performed in 10-ml culture dishes using 500 µL Opti-MEM, 45 µL FuGENE and 15 µg SV40 plasmid.

3.8.2. FACS Sorting

Fluorescent-activated Cell Sorting (FACS) strategy is a sophisticated form of the flow cytometry. Specific cell types can be identified using fluorescent labeling to separate a population of cells into sub-populations. All FACS experiments in this master thesis was performed by BD FACSAria Fusion Flow Cytometer which has a maximized signal detection system, and it provides more accurate and efficient cell sorting. FACS data was analyzed using the Flowjo software.

3.8.2.1. Preparation of The Cells for FACS

Two types of media were pre-prepared for this procedure. DMEM without phenol red, pyruvate (Thermo, Cat#31053028) containing 2% FBS (Thermo, Cat#10500056) with 1:1000 ratio 300 µM DRAQ7^{TM} (BioLegend, Cat# 424001) as a viability dye and DMEM without phenol red and pyruvate (Thermo, Cat#31053028) containing 2% FBS (Thermo, Cat# 10500056) and without DRAQ7 (BioLegend) were prepared. For the cell harvesting, old media was discarded, and cells were washed with sterile DPBS (Thermo, Cat#14190094) to remove the artifacts. 300 µL no phenol red trypsin was added onto the each well and incubated for 3 minutes in the incubator. After the cells were detached, 700 µL pre-prepared DMEM were added, and cells were collected into the 5 mL Corning Falcon Round-Bottom Polystyrene Test Tubes with Cell Strainer Snap Cap (Cat#352235) collection tubes after filtering with the 40µm cell strainer cap. Then, samples were placed on ice immediately for the further applications.

3.8.2.2. Müller Glia Cell Sorting

Cells were prepared for the FACS Sorting as mentioned above (11.2.1). TM buffer (AMSBIO, Cat#K3011010-1) was distributed as 3µL to 1.5 mL DNA low-binding microcentrifuge tubes (Sarstedt, Cat# 72706700). Cell sorter was set up by selecting appropriate nozzle. Template was created with a multivariate graph that demonstrates the

forward scatter (FSC) and side scatter (SSC). DRAQ7 (BioLegend, Cat# 424001) was used for the live-dead cell segregation while mCherry and GFP channels were the reporter fluorescence for the gRNAs. To locate the target population, negative control sample tube was recorded, and necessary adjustments were done regarding the forward scatter and side scatter. Then, positive control sample was run, and data recorded for each sample tubes. Two interval gates were created for the histogram's negative portion and positive section of the data. To identify the populations of interest, experimental sample that needs to be sorted was kept track and gating tools and sub-setting techniques were engaged. Once the gates are established, the gates were chosen for sorting into external sample collection tubes containing 3µL TM buffer. For each gRNAs will be tested, cells were sorted as 200 cells per sample tube and triplicate for each sample.

3.8.3. cDNA Synthesis

3.8.3.1.cDNA Synthesis from FACS Sorted Muller glia

High-capacity cDNA reverse transcription kit (Thermo, Cat#4368814) was used for the cDNA synthesis from FACS sorted cell. According to the protocol, 2.7µL 10X RT random primers, 2.7µL 10X RT Buffer, 1.35 µL MultiScribe Reverse Transcriptase (50U/µL) enzyme, 1.08 µL 25X 100mM dNTP Mix, 0.675 µL RNasin ribonuclease inhibitor (Promega, Cat#N2515) and 15.495 µL RNase/DNase free water (Wisent Multicell, Cat#809-115) were added onto the FACS sorted cells within 3 µL TM buffer and final volume was adjusted to the 27µL for each sample. Reaction was performed 25ºC for 10 minutes, 37ºC for 2 hours and 85ºC for 5 minutes. Samples were stored at -80ºC until further usage.

3.8.3.2.cDNA Synthesis from Retinal Samples

Same cDNA kit (Thermo, Cat#4368814) with the cDNA synthesis for FACS sorted Müller glia cells was used for the isolated total RNA samples. According to the protocol, 2.7µL 10X RT random primers, 2.7µL 10X RT Buffer, 1.35 µL 50U/µL MultiScribe Reverse Transcriptase enzyme, 1.08 µl 25X 100mM dNTP Mix, 0.675 µL RNasin ribonuclease inhibitor (Promega, Cat#N2515), 500 ng RNA sample and RNase/DNase free water (Wisent Multicell, Cat#809-115) to reach 27µL total volume were used for each sample to run cDNA synthesis reaction. Reaction was performed 25ºC for 10 minutes, 37ºC for 2 hours and 85ºC for 5 minutes. Samples were stored at -20ºC until their usage.

3.8.4. Digital Droplet PCR (ddPCR) [105]

3.8.4.1. ddPCR for gRNA Primer Test

gRNA primers for ddPCR were tested with cDNA synthesized from mouse retina total RNA. cDNAs were diluted as 1:40 and reached the 125 pg/µl with RNase/DNase free water (Wisent Multicell, Cat#809-115) and for each primer testing, 1µL of the diluted retina cDNA were used. Separate reactions were performed for each gRNA primers with a final concentration of 125 nM. Droplet generation was performed in a 20 µL of PCR reaction mix including 1µL 1:40 diluted cDNA, 125 nM primers, and 2x Evagreen supermix via Droplet Generator (Bio -Rad Cat#186-4002). Sample mix was loaded in the middle part of the cartridge for droplet generation. Samples were loaded to cartridge and then 70 µL of the droplet generation oil was added into the bottom row of the cartridge. Gasket was placed on top of the cartridge and inserted into the droplet generator. In this part it is important to note that a space in between gasket and the cartridge must not exist. As soon as the droplets generated, they were taken gently from the top rows as roughly 40 µL and added directly into the semi-skirted 96-well PCR reaction plate. Semi-skirted PCR plate was sealed with aluminum sealing foil by PCR plate sealer. PCR plate was placed into the 96-well heat-sealed thermal cycler. 95 °C for 5 minutes, 95°C for 30 seconds for 40 cycles, 60 °C for 1 minute, 4 °C for 5 minutes, 90 °C for 5 minutes and 4 °C infinite hold PCR protocol was run. 2 °C/s ramp rate was applied during each cycle for PCR amplification to achieve the appropriate temperature for each step during the amplification in order not to harm droplets. After PCR reaction is done, droplets were quantified using ddPCR software named QuantaSoft by inserting PCR plate into droplet reader (Bio -Rad Cat#1700-5228). For Evagreen which is a DNA-binding dye, a template was created utilizing special specifications. 1-D plot chart was utilized to examine the data for fluorescence intensity vs. droplet quantity for each specimen. The threshold point was fixed up so that droplets above the threshold were accepted as a positive value, while those below the threshold were accepted as a negative value. The Poisson distribution probability technique was then used to calculate the initial concentration of the target DNA in units of copies/µL.

3.8.4.2. ddPCR for Evaluation of gRNAs

cDNAs were produced using FACS-sorted cells and diluted as 1:10 with RNase/DNase free water (Wisent Multicell, Cat#809-115) and 1µL of the diluted retina cDNA sample were used. As a control, house-keeping gene GAPDH was used with a 1:40 dilution. For the further steps, same protocol mentioned in the above **(3.8.4.1.)** was performed.

3.9. In vivo Imaging Techniques

3.9.1. MicronIV Fundus Imaging

Phoenix MicronIV is a retinal imaging microscope used for the fluorescence imaging of common reporter molecules including GFP, YFP, and mCherry, as well as fundus images. To enlarge the pupil 0.5% tropicamide and 2.5% phenylephrine hydrochloride drop were applied into each eye of the mouse. The initial induction of anesthesia was performed in a small isoflurane chamber. During the anesthesia, 1.5% isoflurane (1 L/min) was implemented after first step of deep anesthesia of mice with 5% isoflurane (1 L/min). Deep anesthesia was confirmed by checking the key indicators such as loss of the righting reflex, the withdrawal reflex, and the tail pinch reaction. Mouse was placed on the imaging platform and proper pupil dilation was assured with the fundus camera. 0.2 % carbomer 980 topical gel was applied to prevent the surface of the eyes from drying out under anesthesia and as a coupling gel for imaging. Imaging stage was adjusted for alignment with the objective's nosepiece. Stage was aligned to center the mouse eye. Once the eye is in its proper position in the center, objective was moved gently until it makes contact with the pupil.

3.9.2. Optical Coherence Tomography (OCT)

An effective non - invasive imaging technique known as optical coherence tomography (OCT) was used to image the retina at high definition and at micron scales in cross-section. This method was given an opportunity to measure and observe the retinal layer to evaluate the changes regarding retinal thickness. OcuScience OCT was used in our in vivo imaging system. For the imaging procedure of OCT, mice were anesthetized and prepared for imaging with the same procedure mentioned above **(3.9.1.).** Animal was placed on the imaging frame and as same as micronIV fundus imaging, 2 % carbomer 980-containing topical gel was applied to prevent the surface of the eyes from drying out under anesthesia and as a coupling

gel for imaging. When animal was placed properly on the stage and optic nerve monitored on the computer, scanning of the retina was started. Then, average of the scan data was used for the retinal layer assessments.

Primer Name	Sequence
Mus musculus OCT4 ddPCR Forward 1	TTGAGAACCGTGTGAGGTGG
Mus musculus OCT4 ddPCR Forward 2	TGGGCTAGAGAAGGATGTGGTT
Mus musculus OCT4 ddPCR Forward 3	ATTTTGTCCTCAGTGGGGCG
Mus musculus OCT4 ddPCR Reverse 1	ACCATACTCGAACCACATCCT
Mus musculus OCT4 ddPCR Reverse 2	GAAAGGTGTCCCTGTAGCCT
Mus musculus OCT4 ddPCR Reverse 3	GCTGAACACCTTTCCAAAGAGA
Mus musculus KLF4 ddPCR Forward 1	ACTACCGCAAACACACAGGG
Mus musculus KLF4 ddPCR Forward 2	TTACCACTGTGACTGGGACG
Mus musculus KLF4 ddPCR Forward 3	TGTGACTATGCAGGCTGTGG
Mus musculus KLF4 ddPCR Reverse 1	TGTGGGTCACATCCACTACG
Mus musculus KLF4 ddPCR Reverse 2	CCCTGTCACACTTCTGGCAC
Mus musculus KLF4 ddPCR Reverse 3	AGGTTTCTCGCCTGTGTGAG
Mus musculus NRL1 ddPCR Forward 1	CTGGGGTCGGATGAGGTTCT
Mus musculus NRL1 ddPCR Forward 2	ATGAGGTTCTCGGGCTGAGT
Mus musculus NRL1 ddPCR Forward 3	TGGAGGAGCTATATTGGCTGG
Mus musculus NRL1 ddPCR Reverse 1	AAAATCTCTCGGGCAGCTGGA
Mus musculus NRL1 ddPCR Reverse 2	TCCGAAAATCTCTCGGGCAG
Mus musculus NRL1 ddPCR Reverse 3	TTCAACTCGCGCACAGACATC
Mus musculus GAPDH ddPCR Forward	CAGCAATGCATCCTGCACC
Mus musculus GAPDH ddPCR Reverse	TGGACTGTGGTCATGAGCCC

Table 7: List of Primers For ddPCR Gene Expression Analysis of Oct4, Klf4 And Nrl1 Genes. *ddPCR primers were designed by Primer BLAST software. Up to three primer set is designed for each gene*

3.10. Large Scale AAV Production

3.10.1. HEK293T Cell Seeding

20-24 hours before transfection, HEK293T cells were seeded into 10 x 15-cm^2 plates for 1 high-titer viral preparation. Regular DMEM (Thermo, Cat#31053028) containing 10% FBS (Thermo, Cat#10500056) and %1 Penicillin / Streptomycin (Gibco, Cat#15140122) was used. For 1 viral prep, 3 confluent 15cm^2 plates of HEK293T cells were split into 10 x 15cm^2 plates until 70-80 confluency.

3.10.2. PEI (polyethyleneimine) Transfection

Preparation of the PEI (Polysciences, Inc., Cat #23966) solution was performed by adding to de-ionized H_2O and stirred for approximately 1 hour on at low temperatures (30^oC to 50^oC) until all of the particles were dissolved in solution. Molecular weight of the PEI is 40.000 and prepared as a final concentration of 1mg/mL. After the preparation of fresh PEI solution, plasmids for transfection were adjusted. 70µg of the AAV capsid vector, 70µg of the AAV plasmid and 200µg pHGTI-adeno1 plasmid (Plasmid Factory). 70µg of the AAV vector, 70µg of the AAV plasmid and 200µg of the pHGTI-adeno1 adenoplasmid together with 49 mL of DMEM was added into the falcon. Lastly, PEI transfection reagent was added, and solution was mixed by gently inverting the falcon 5-6 times. Then, incubated at room temperature for 15 minutes. As soon as the incubation was completed, 5mL of the transfection mix was added gently per plate.

3.10.3. Harvesting of the Cells

48-60 hours after the PEI transfection supernatant was collected to filter into a 250mL 0.22um stericup (TPP, Cat#99250). Dislodged cells were collected by pipetting up and down with the culture media from the 10 x 15cm^2 plates in two falcon tubes. 20 minutes at 1400 rcf centrifuge was performed and rest of the stericup was filled with the rest of supernatant, roughly 5 mL. 50 mL of the PEG solution was added onto the nearly 250 mL of the supernatant and stored at 4ºC for overnight. Next day, supernatant was spun for 1 hour at 1600 rcf at 4ºC. PEG pellet was re-suspended in Lysis buffer. Lysis buffer contains 150mM NaCl (Thermo, Cat#7647-14-5), 20mM Tris (Invitrogen, Cat#15504020) pH 8.0 and should be filtered with 0.22 um filter (AISIMO, Cat#ASF33PS22S). Freeze-thaw

protocol was performed three times for the cell pellet by using dry ice/ethanol bath and 37ºC water bath. Between the step freeze-thaw, vortex was used. Cell pellet was re-suspended in 15 mL of lysis buffer. 15uL of 1M $MgCl_2$ (Sigma, Cat#7786-30-3) from a stock of 1 mM was added. 15uL of 250,000U/mL stock Turbonuclease (Accelagen, Cat#N0103L) was added as of 250U/ml final concentration. Mix was prepared and incubated at 37ºC for 30 minutes. This step is important to dissolve genomic DNA/protein aggregates that formed from the thaw/freeze cycle. Cell debris were spun down at 1400 rcf 4ºC for 20 minutes. Supernatant containing viruses still contains cellular debris. Iodixanol purification method was performed for the further purification steps.

3.10.4. Iodixanol Concentration and Virus Purification

Optiprep Iodixanol (Sigma, Cat#D1556) was prepared with different concentrations and completed to 200 mL with distilled H_2O. Gradients were added from the bottom to top. Firstly, 5 mL of 60% concentration of iodixanol, secondly 7mL of 40% concentration of iodixanol, then 5 mL of 25% concentration of iodixanol and lastly 5ml of 17% concentration of iodixanol into the Optiseal tubes (Beckmann, Cat#362183). This step is critical, and gradients should not be mixed. The supernatant containing the virus was transferred onto the Optiseal tube. 90 minutes ultracentrifugation was performed at 50.000rpm at 16ºC by using Beckman Vti50 rotor (Beckmann, Cat#362758). Viral fraction located in 40% gradient layer was harvested with 21 gauges needle by inserting the needle 2mm below the intersection area 60% and 40%. Most of the 40% layer should be collected but avoided to collect 25% layer. Virus fraction was added into a 50mL Falcon tube and filled up to 15mL with 1X PBS. Virus cocktail was mixed well and transferred into the pre-wetted Amicon columns (Milipore, Cat#UFC910096). This step was used to remove the Iodixanol and to concentrate the virus. 30 minutes 1400 rcf centrifuge was performed at 4ºC and bottom part of the supernatant was discarded. Amicon column was filled with 1X PBS again and mixed with up and down three times for optimal removal of the Iodixanol. Again, 30 minutes 1400 rcf centrifuge was performed at 4ºC and bottom part of the supernatant was discarded. Screw cap tubes were labeled and placed onto the ice for the virus aliquots. AAVs were aliquoted as 20 µL per screwed cap tubes and 5µL of the virus was used for the titration by using ddPCR.

3.11. Intravitreal Injection of AAV-Cre Vector[105]

3.11.1.1. Equipment Preparation

10 µL Hamilton syringe (nanofil) with a 36 G blunt needle was prepared as an initial step. Then, five times rinsed with ddH_2O, 70% ethanol and 1X PBS, respectively. Hamilton syringe was filled with the AAV or PBS for injection. Surgical needle (suture, silk, 6/0), tape, forceps, and scissors were prepared for ready-to-use.

3.11.1.2. Intravitreal Injection

1 drop of 0.5% tropicamide and 2.5% phenylephrine hydrochloride containing eye drop was applied before anesthesia step to dilate pupils. Same anesthesia conditions and ophthalmic solutions were applied as previously mentioned above **(3.9.1. & 3.9.2.).** Surgical hook was used to stabilize the upper eyelid and pulled back just a little to make the dorsal portion of the eye visible. Tape was used to keep the hook in place on the bench. Conjunctiva was removed not more than 1 mm^2 by using the help of curved iris scissors under the dissecting microscope. 30 G sterile and freshly-opened insulin syringe was used to puncture the sclera part of the eye. Needle of the micro syringe was inserted through the exact same puncture by using a micromanipulator. 1 µL of the 1.88 x 10^{12} gc/ml AAV-Cre vector and 1 µL of the PBS were injected to contralateral eye, respectively. Injection volume of the Hamilton syringe was controlled manually, and needle was withdrawn carefully 1 minute after the injection. Eyelid was released from the hook and anti-inflammatory and anti-bacterial topical gel was applied to whole eyecup. Animals were placed back into the cages after recovery.

3.12. Statistical Analysis

Data analysis was performed using Student's t-test for *Klf* overexpression in dCas9 SPH cell line. ANOVA with Dunnett's Multiple Comparison test was used for comparison *Opa1* overexpression in Cre-induced and un-induced dCas9 SPH muller glia.

4. RESULTS

4.1. Generation of a Novel RP-Reporter Line

4.1.1. Strategy

Previously, our lab has generated a double reporter line by crossing three different transgenic mouse lines, Tg (Rlbp1-GFP), Tg(Rho-Cre) and ROSA26-LSL-tdTomato (Ai14) **(Fig. 12).** Ai14 (IMSR_JAX:007908) is a Cre reporter strain expressing tdTomato fluorescence in response to Cre-associated recombination. Tg (Rho-Cre) breeding strategy was allowed the Cre-mediated specific rod targeting since Cre is activated by the rhodopsin promoter in this line. In the presence of Cre-expressing cells, loxP-flanked STOP cassette is removed (**Fig. 12 B)** by the Cre recombinase and tdTomato expression is monitored due to the red fluorescence protein. **(Fig. 12 C, Unpublished data)**. This was an extremely useful model for both *in vivo* and *in vitro* studies. To be able to generate reporter mouse line for regeneration platform, it was important to have rod-free retina to be able to follow the newly regenerated rod photoreceptors **(Fig. 13)**. Since rd1 mouse model is a very fast rod degeneration model due to the mutation on *Pde6b gene*, these mice were used as a platform for the regenerative studies **(Fig. 13)**. This further allowed us to quickly evaluate the degeneration status of the rod photoreceptor cells without any quantitative analysis.

We have generated the RP-reporter (rd1-tdTomato) mouse line by two consecutive crossings with rd1 -/- mice and the Tg (Rlbp1-GFP);Tg(Rho-Cre);ROSA26-LSL-tdTomato. First the triple transgenic was switched to rd1 wt/- and then to rd1 -/- status together with the Tg (Rho-Cre);ROSA26-LSL-tdTomato **(Fig. 12 A).** Tg (Rlbp1-GFP) was excluded in the process as it was not necessary for rod labeling.

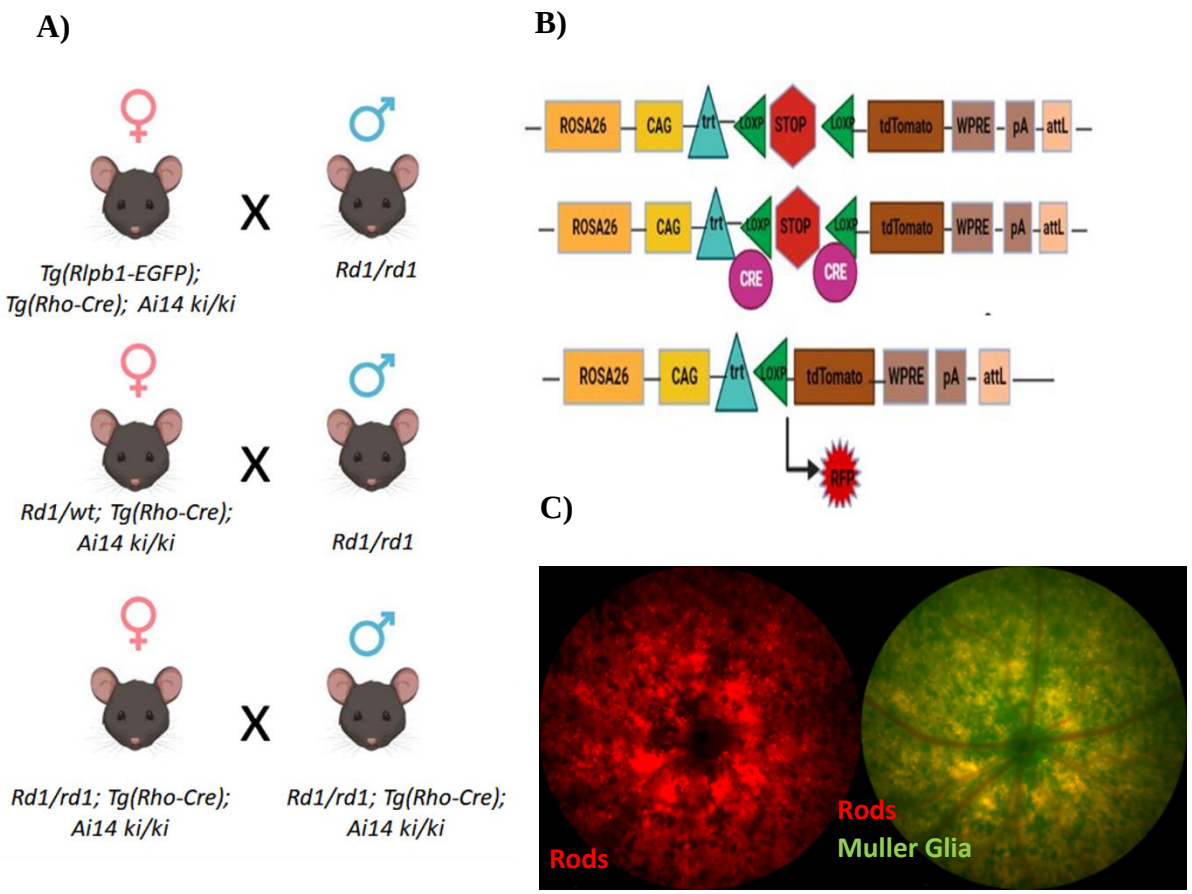

Figure 12. ***Establishment of multiplex regeneration platform by using transgenic mouse lines. (A)*** *Mice were crossed to get homozygous fast retinal degeneration model (rd1 -/-) to detect Müller glia fate alterations into the rod photoreceptor fate induction. As a strategy, the mouse line expressing Cre recombinase is used to remove LSL stop codon to turn on rhodopsin promoter.* ***(B)*** *Cre-Flox removes the stop codon.* ***(C)*** *Colocalization of rods (red) and Müller glia cells (green) in Tg (Rlbp1-Gfp); Tg(Rho-Cre); ROSA26-LSL-tdTomato.*

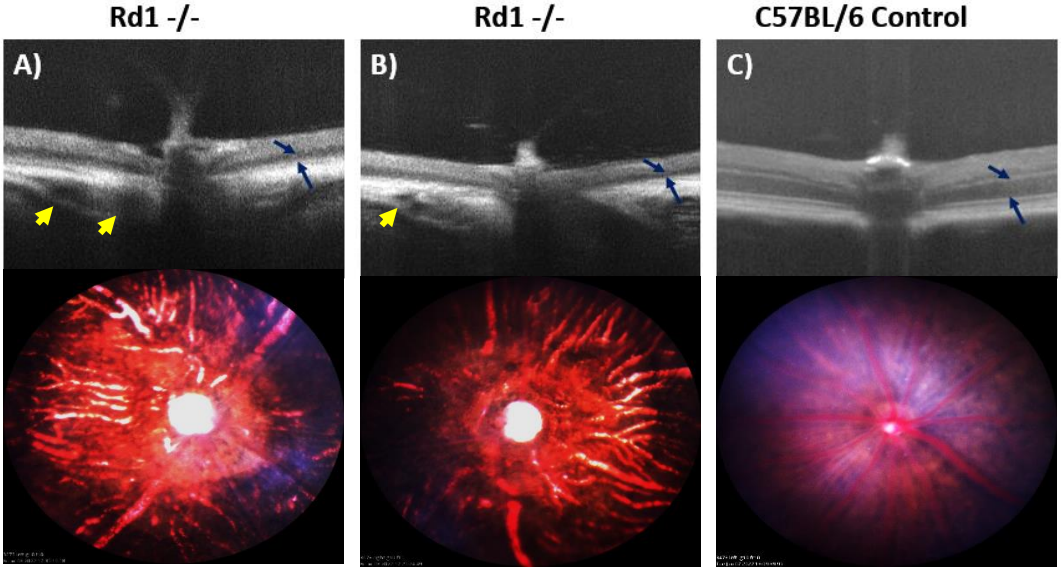

Figure 13. ***OCT and MicronIV Fundus Images of Rd1 Mice***. *5 weeks* ***(A)*** *and 9 weeks* ***(B)*** *animals were imaged to compare changes in ONL compared with C57BL/6 control* ***(C)*** *mouse. Dark blue arrows represent the thickness of outer nuclear layer (ONL). Yellow arrows show the retinal detachment of the retina in Rd1 -/- mice but not in C57BL/6 control mice*

4.1.2. Analysis of rd1-tdTomato mouse line

As it was described previously, we further improve our double reporter model by crossing it to rd1 retinitis pigmentosa model and generated the rd1-tdTomato model. This model is a quadruple transgenic animal and will be extremely beneficial to quickly evaluate regenerated rods by tdTomato follow-ups. The very low levels of tdTomato expression in rd1-tdTomato retina already shows severe rod loss as excepted. (**Fig. 14).** Since rods are almost completely lost, newly formed rods will be easily detected due to tdTomato expression with the help of reference points **(Fig. 14 white arrows).** Conversely, it is feasible to follow up rod degeneration in this model with weekly follow-ups **(Fig. 14 Blue arrows).** All the retinas that were followed showed distinct patterns of tdTomato expression and even digested rods can easily be visualized **(Fig. 14 Yellow arrows).** It is important to mention that we were able to detect same regions with the same quality images week by week which is important for the detection of even small alteration in the follow up experiments on this fast retinal degeneration model animals.

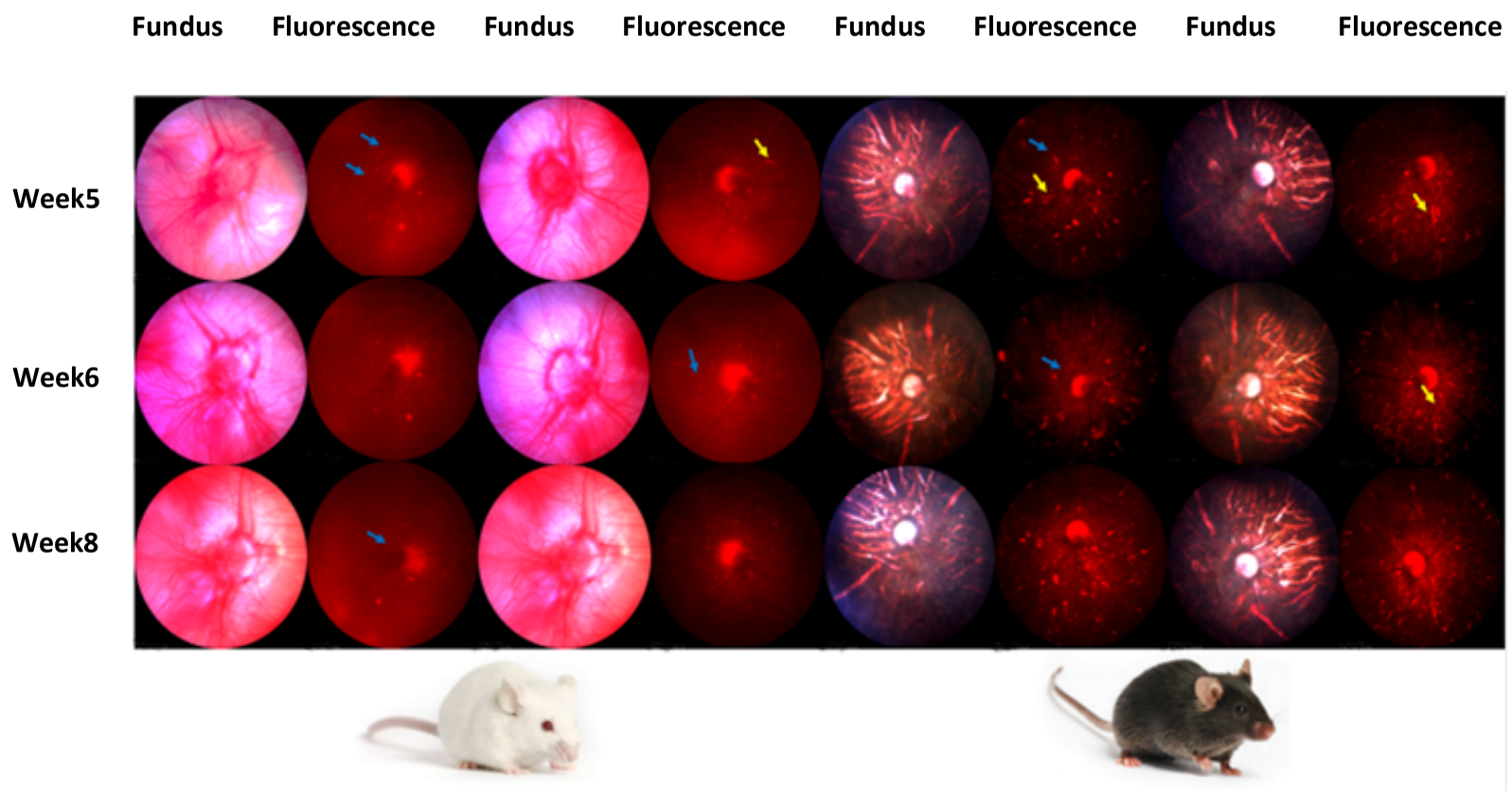
Fundus
Fluorescence
Fundus
Fluorescence
Fundus
Fluorescence
Fundus
Fluorescence
Week5
Week6
Week8

Figure 14. ***MicronIV Follow-up of Albino and Non-Albino Reporter Rd1-tdTomato Mouse****. Fundus and tdTomato fluorescence images represents that there is a severe degeneration and vessel attenuation as well as other pigmented Rd1 pure and reporter mouse eyes. Since animal of intereset in here is albino, it has no retinal pigment epithelium (RPE) cells in it's eyes. Blue and yellow arrows represents the degenerated cells, yellow ones are most likely macrophage or microglia digesting tdTomato positive rod cells. Blue arrows are reference points in the follow up procedure of the retina. Mice may have the two different phenotypes in rd1-/- strain. They might be normal C57BL/6 with a color pigmentation and albino with a white furr and non-pigmented retina* ***(Bottom panel).*** *Representative mice images were provided from Jaksons Laboratory mouse database.*

Optical Coherence Tomography (OCT) was used as a complementary key study for fluorescence fundus imaging to show thinner ONL in comparison with control animal. It is important because it facilitates to follow up regeneration studies due to the alterations on ONL where reporter lines are not available. Both well-established rd1 mouse model and the Rd1-tdTomato mice were shown to have decreased ONL thickness compared with the control animal suggesting that both models have severe rod loss **(Fig. 15)**. Overall, we will benefit from Rd1-tdTomato as a basis for our small molecule therapies to detect rod fate induction from Muller glia **(Fig. 14 & 15)**.

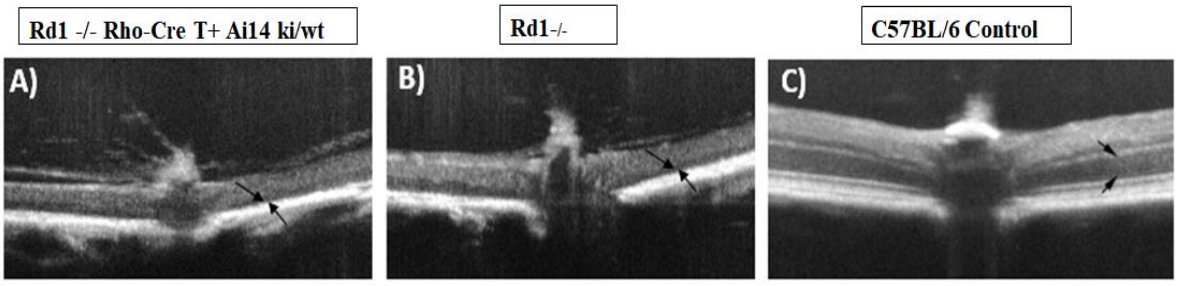

Figure 15. ***OCT Images of Rd1 Mice Lines and C57BL/6 Control Mouse.*** *OCT images of Rd1-tdTomato* ***(A),*** *Rd1 -/-* ***(B)*** *and Black6 control* ***(C)*** *OCT images were taken at 8th to 10th week. The area between two arrows represents the thickness of outer nuclear layer (ONL) where rod and cone photoreceptors located. Both Rd1-tdTomato and Rd1 -/- mice have thinner ONL than control animal due the photoreceptor degeneration.*

4.2. Establishment of the rd1-tdTomato model as rod reporter for regeneration studies

We have further tested rd1-tdTomato model for its *in vivo* reporter capacity. In follow up studies, we have shown rods are almost completely lost, and even it is feasible to follow recently degenerating rods (**Fig. 14**). Therefore, it will also be feasible to follow up on newly formed rods after the Muller glia dedifferentiation approach. We have tested this by using AAV-Cre vectors (**Fig. 16 A**) to show that after Cre recombinase expression, tdTomato expression will be initiated. We have generated large-scale AAV-Cre vectors which targets Müller glia. It is clearly shown that intravitreally injected AAV-Cre vector had activated the tdTomato expression by removing the stop codon from the tdTomato as early as day 4 (**Fig. 16 B-D**). It was quite important because Muller glia will be labeled in Cre-expressing cells which will allow us to follow up Muller glia dedifferentiation into the rod fate. Week 4 follow up images ashow that tdTomato expression was increased as the AAV induced gene expression peaks around 4 week and the intensity of the tdTomato images were reduced due to excessively bright tdTomato signal (**Fig. 16 B-D**). In all cases PBS injected contralateral eyes showed no additional tdTomato expression suggesting that the tdTomato expression is due to Cre recombinase expression (**Fig. 16 B`-D`**). This was a very exciting finding and suggested that upon rod induction, muller glia will be labeled by continuous tdTomato expression which will allow us to follow up Muller glia dedifferentiation in an *in vivo* set up. This will further allow us to test variety of regenerative approaches *in vivo* with a very simple readout and will accelerate our reseach.

A)

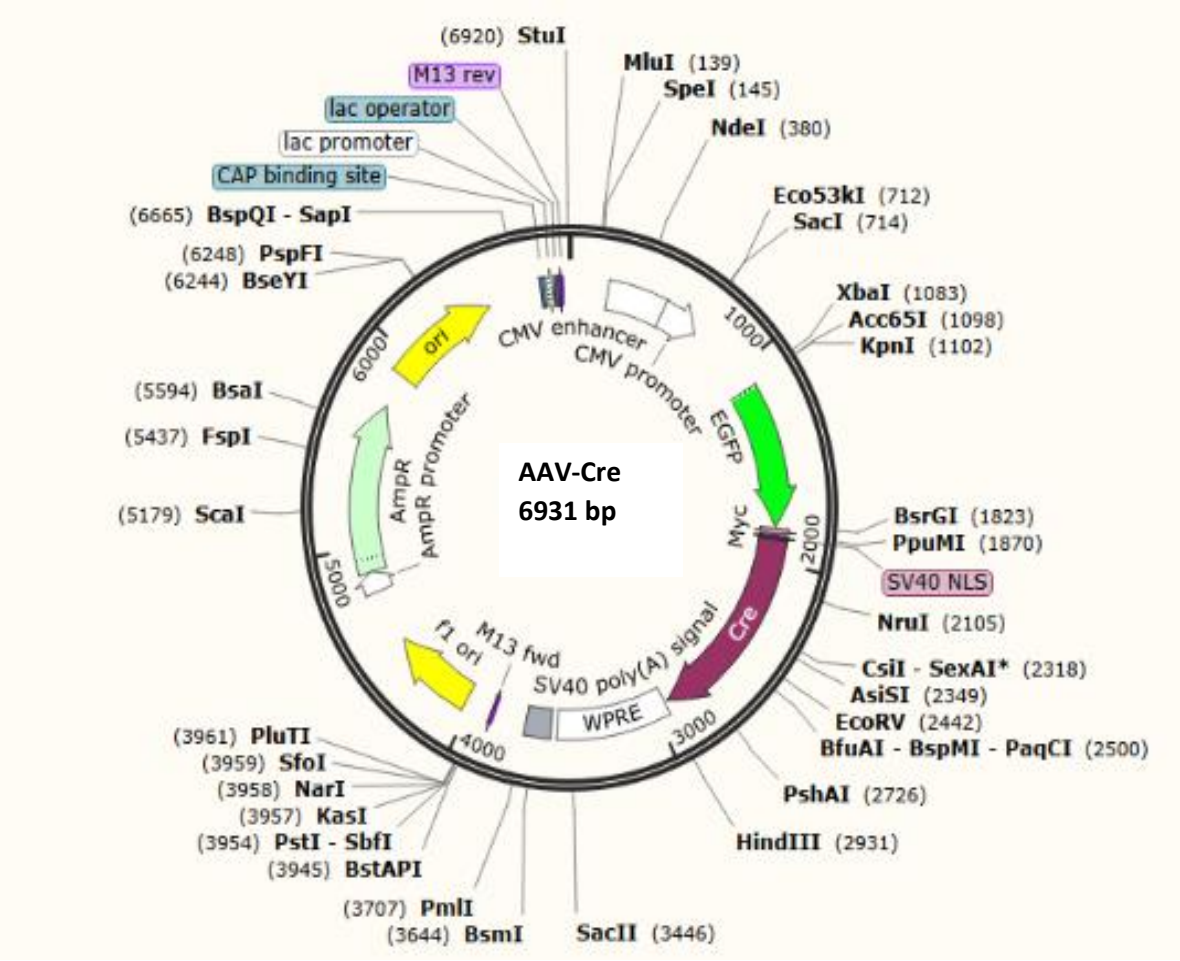
(6920) StuI
MluI (139)
SpeI (145)
NdeI (380)
Eco53kI (712)
SacI (714)
XbaI (1083)
Acc65I (1098)
KpnI (1102)
BsrGI (1823)
PpuMI (1870)
SV40 NLS
NruI (2105)
CsiI - SexAI* (2318)
AsiSI (2349)
EcoRV (2442)
BfuAI - BspMI - PaqCI (2500)
PshAI (2726)
HindIII (2931)
SacII (3446)
(3644) BsmI
(3707) PmlI
(3945) BstAPI
(3954) PstI - SbfI
(3957) KasI
(3958) NarI
(3959) SfoI
(3961) PluTI
(5179) ScaI
(5437) FspI
(5594) BsaI
(6244) BseYI
(6248) PspFI
(6665) BspQI - SapI
M13 rev
lac operator
lac promoter
CAP binding site
ori
CMV enhancer
CMV promoter
EGFP
Myc
Cre
SV40 poly(A) signal
WPRE
M13 fwd
f1 ori
AmpR
AmpR promoter
1000
2000
3000
4000
5000
6000
AAV-Cre
6931 bp

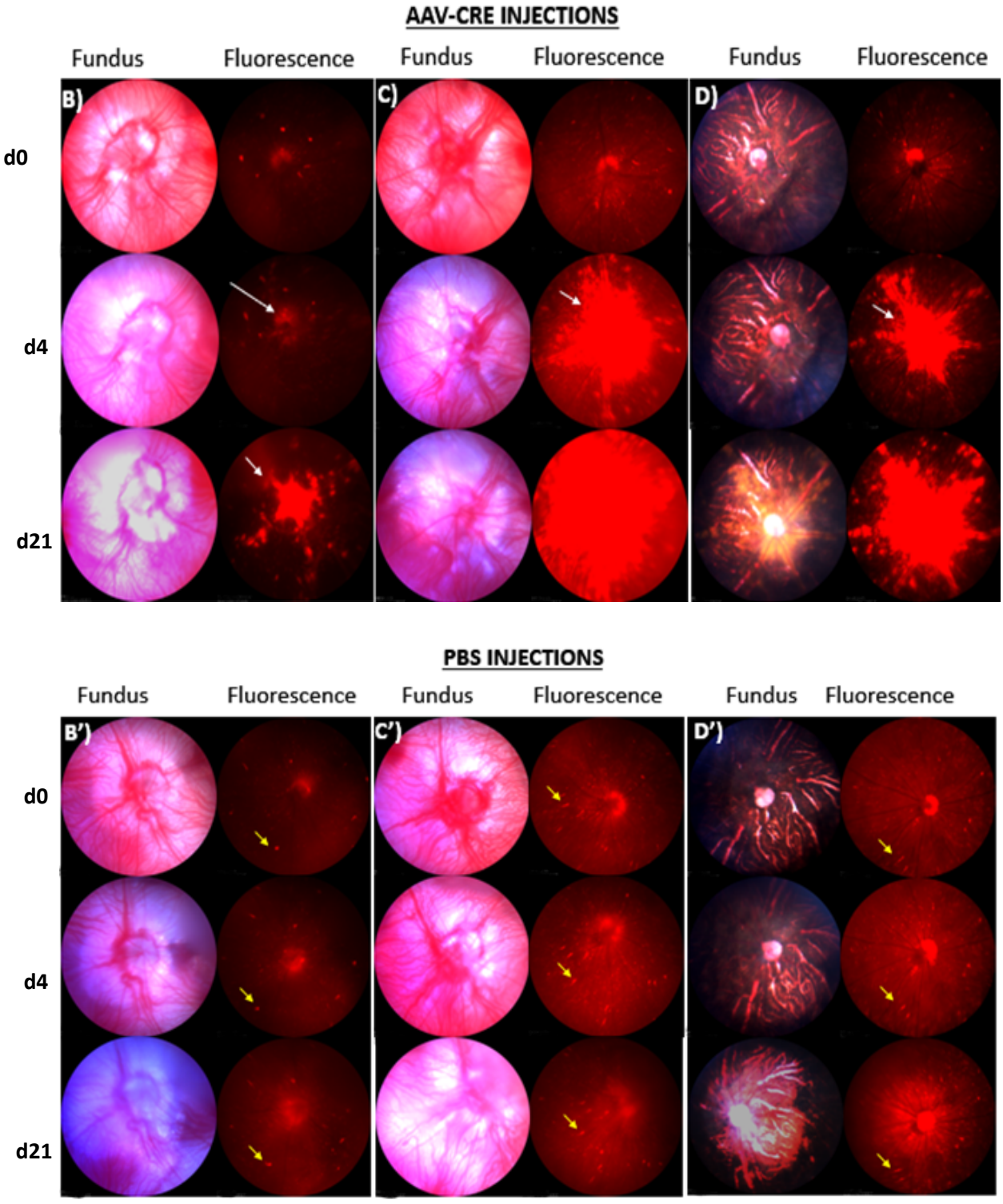
AAV-CRE INJECTIONS
Fundus
Fluorescence
Fundus
Fluorescence
Fundus
Fluorescence
B)
C)
D)
d0
d4
d21
PBS INJECTIONS
Fundus
Fluorescence
Fundus
Fluorescence
Fundus
Fluorescence
B')
C')
D')
d0
d4
d21

Figure 16: ***Activitaation of tdTomato*** **expression in rd1-tdTomato** ***mouse line using AAV that express Cre recombinase***.

Sequence map of the injected AAV-Cre plasmid ***(A)****. Left and right eyes of rd1-tdTomato animals were intravitraelly injected with AAV-Cre (****B****,* ***C*** *and* ***D****) and PBS (****B'****,* ***C'*** *and* ***D'****), respectively. AAV-Cre vector concentration was determined via ddPCR as 1.88364 x* 10^{12} *gc/ml. AAV-Cre injected retinas (****B****,* ***C*** *and* ***D****) expressed Cre recombinase as early as day 4 and activated tdTomato expression in transduced cells showing that it is feasible to label Cre-expressing cells upon induction. No additional tdTomato expression was observed in contralateral eye that is injected with PBS at day 4. Yellow arrows represent the reference points of the images. Since there was excessive expression of AAV-Cre in the week 4, fluorescent power was lowered to get better fundus fluorescence images.*

4.3. Establishing a Drug Testing Platform Using Tg(Rho-Cre);ROSA26-LSL-tdTomato Primary Müller Glial Cells

4.3.1. Strategy

In order to test the possible candidate drugs from the previously performed screen, an efficient platform was aimed to be established. This platform benefited from the primary Muller glia from the Tg(Rho-Cre);ROSA26-LSL-tdTomato mice **(Fig. 17)**. Retina dissociation of Tg(Rho-Cre);ROSA26-LSL-tdTomato mice were performed as mentioned in above protocols and 30 µl of the dissociated cell mixture was added onto fibronectin-coated plate with a total 200µl of the Muller glia selection media **(Fig. 17)**. As soon as selection procedure was completed, normal media was used to continue until the 80% of the well-coverage **(Fig. 17)**. In order to enhance the platform, rod induction protocol was used [106]. In this protocol, final concentration of 20µM Taurine, 5µM Retinoic Acid, 20ng/ml FGF2 and 100 ng/ml IGF-1 was used for induction **(Fig. 18)**. Overall induction protocol was successful in our reporter primary Muller glia. Previously identified Candidate drug I and candidate drug II (unpublished data / subject of patent application) also successfully induced rod fate in our novel drug testing protocol **(Fig. 18)**.

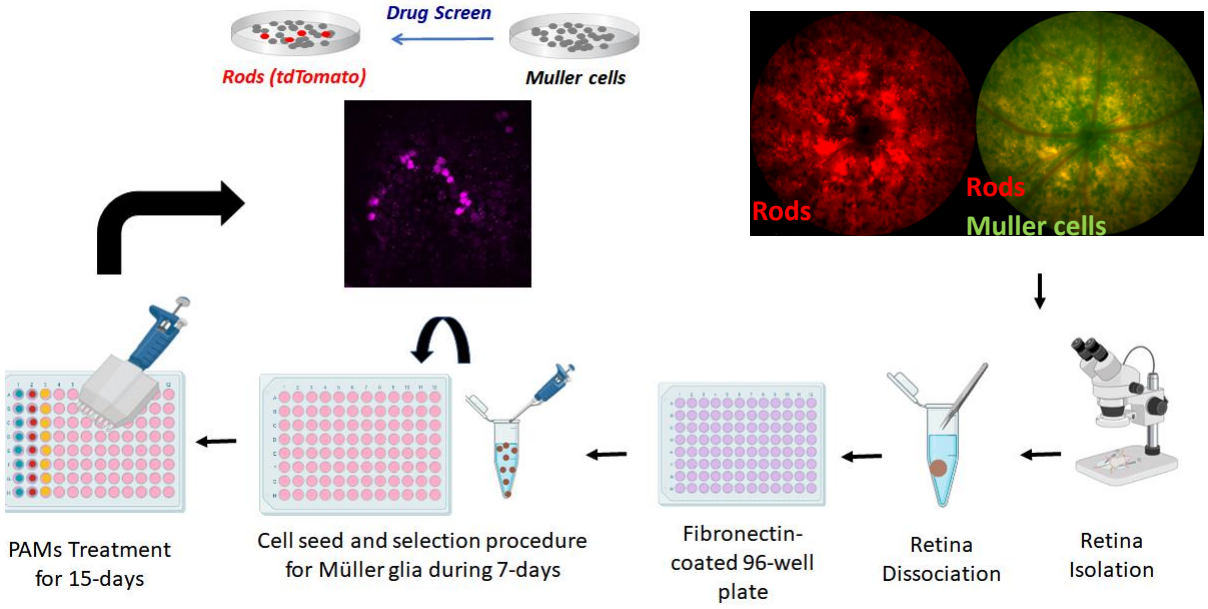

Figure 17. ***Screening Strategy for Selected Candidate Drugs.*** *After the genotyping of the mice (both micronIV and PCR), Tg(Rho-Cre);ROSA26-LSL-tdTomato mice were sacrificed and retina isolation was performed. Dissociated cells were seeded into the fibronectin coated 96-well and their selection procedure was completed within 7-days. After the selection and completion of their roughly 80% coverage of the wells, small molecules with or without retinoic acid induction were tested to evaluate the efficiency of the approach.*

4.3.2. Cell Culture Images

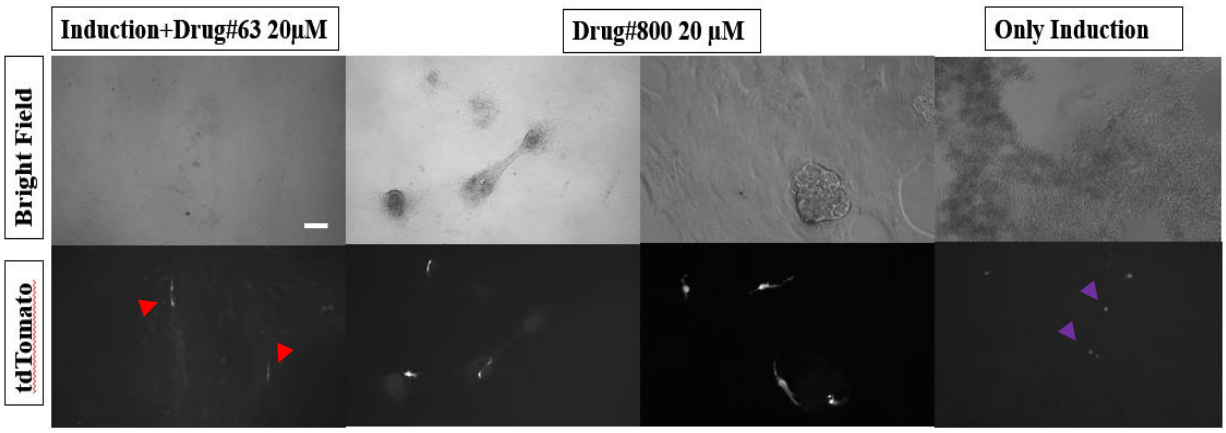

Figure 18. ***tdTomato Expression in the Presence of Rod Induction on Müller Glia Cells.*** *Purple arrows shows tdTomato expression after retinoic acid induction. Rod fate induction protocol successfully induced tdTomato expression as expected Combination of induction media and single candidate Drug#1 resulted in excess rhodopsin expressing cells both high (red arrows) and low tdTomoto expression is observed suggesting that the combination of induction protocol with small molecules enhances rod induction efficiency. In the treatment of the cells with candidate Drug#1, tdTomato expression were observed both inside of the neurospherical structures and Müller glia cells. These all images were captured with fluoresence microscope. (Scale bar: 100µm)*

Candidate small molecules coming from the previous PAMs screen suggested that induction of the rod fate by using single small molecules is feasible **(unpublished data).** We have establish a new method combining retinoic acid induction protocol with primary Muller glia with rod reporter function. This also allowed us to better mimic *in vivo* conditions since it was not necessary to eastablish stable cell lines. These results suggested our new protocol is suffucuently sensitive to further test novel drugs in the near future. Please note that candidate drugs I and II has been elucidated in another study and only used for testing purposes of the system that is generated.

4.4. Generation of ATFs for *Nrl, Oct4* and *Klf4*

4.4.1. gRNA Screen using dCas9-VP64-mCherry stable Muller glia cell line

In order to be able to establish ATFs that overexpress *Nrl, Oct4* and *Klf4,* it is crucial test several gRNAs in dCas9-VP64 expressing stable cell line. Performing the gRNA screen relies on dCas9-VP64 expression in a stable cell line, as well as a matching vector which encodes gRNA and an EGFP reporter. For that we have designed gRNAs against promoter regions of *Nrl, Oct4* and *Klf4*. using the Benchling software **(Fig. 19A).** One of the unspoken challenges of the usage of dCas9-based gene regulatory systems is to reach maximum efficiency of the system. Therefore, dCas9-VP64 and gRNA have to be expressed at high levels to elucidate the maximum output in terms of gene regulation. At this point, Muller cells` low transfection efficiency turn out to be a limitation step to be able use this system solely with one vector. In order to correctly characterize the maximum levels of gene upregulation from a given dCas9 and guide system. Dr. Agca recently generated a stable

Muller glia cell lines that have multiple copies of dCas9-VP64-P2A-mCherry **(Fig. 19B)**. This system works with similar logic but this time just by transfecting a small vector that expresses gRNA and an eGFP reporter. This allowed us to reduce the size of the vector by several kbs and increased the transfection efficiency of the vector that expresses gRNA. Since dCas9-VP64 is already available within the stable Muller cells, the efficiency of the system has been shown to increase tremendously. The cell lines which have 14 copies of dCas9-VP64-P2A-mCherry was used for evaluating gRNAs. Expression levels of dCas9 was also checked indirectly by mCherry levels. Flow cytometry was used to detect mCherry expression in stable Muller cells. Since the mRNA that is expressed from dCas9-VP64-P2A-mCherry is bicistronic, detection of mCherry also confirms the expression of dCas9-VP64 in stable Muller glial cell lines **(Fig. 19 C).**

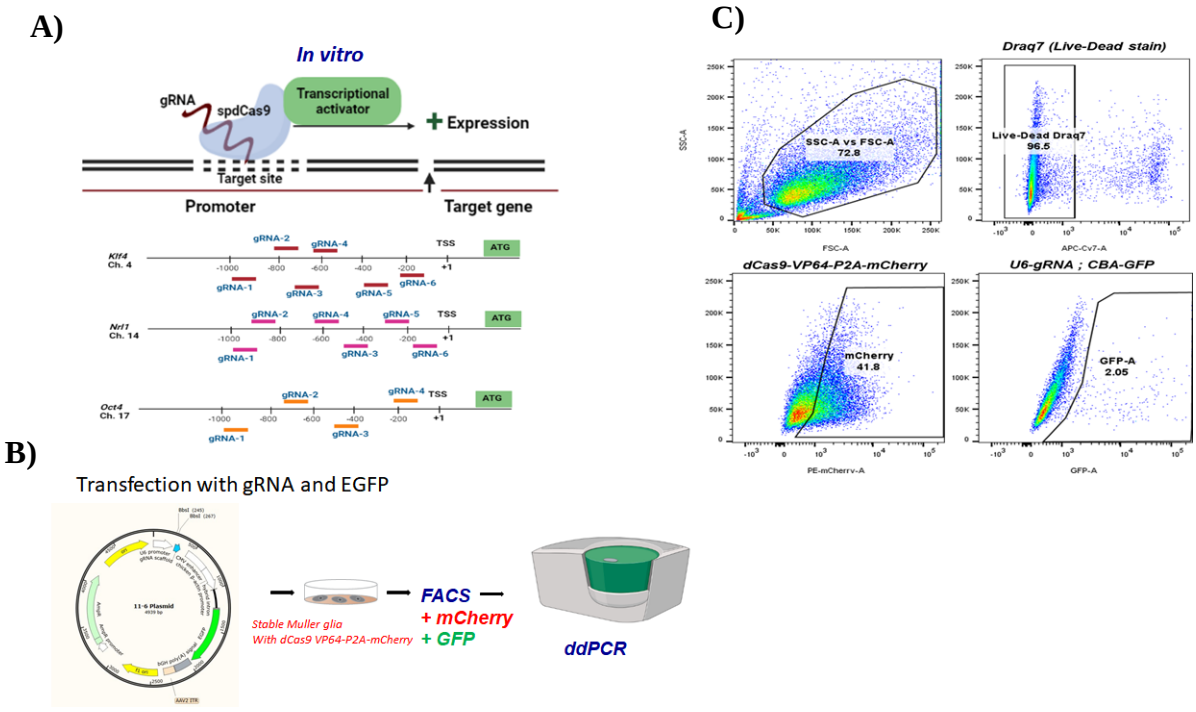

Figure 19. ***Gating Strategy for The Two Component in vitro ATF System.*** *gRNAs were generated for 3 different genes* ***(A)****. Gating strategy for the dCas9-VP64-P2A-mCherry Muller glia cells transfected with gRNA vectors. Draq7 was used to exclude dead cells from live dCas9-c7 population. mCherry positive dCas9-c7 positive cells were selected to assure*

for dCas9-VP64 expression. Among those mCherry positive cells, gRNA expressing cells were selected by expression of eGFP reporter ***(B,C)***.

In this strategy mCherry was employed as a reporter for the dCas9-VP64 expression and GFP reflected the gRNA vector transfected cell, sorting was done on cells which co-expresses GFP and mCherry **(Figure. 19B)**. Optimized and established gating strategy for our two component in vitro ATF system was used for the further ddPCR analysis for *Klf4*, *Nrl1* and *Oct4* genes **(Figure. 20 & 21)**.

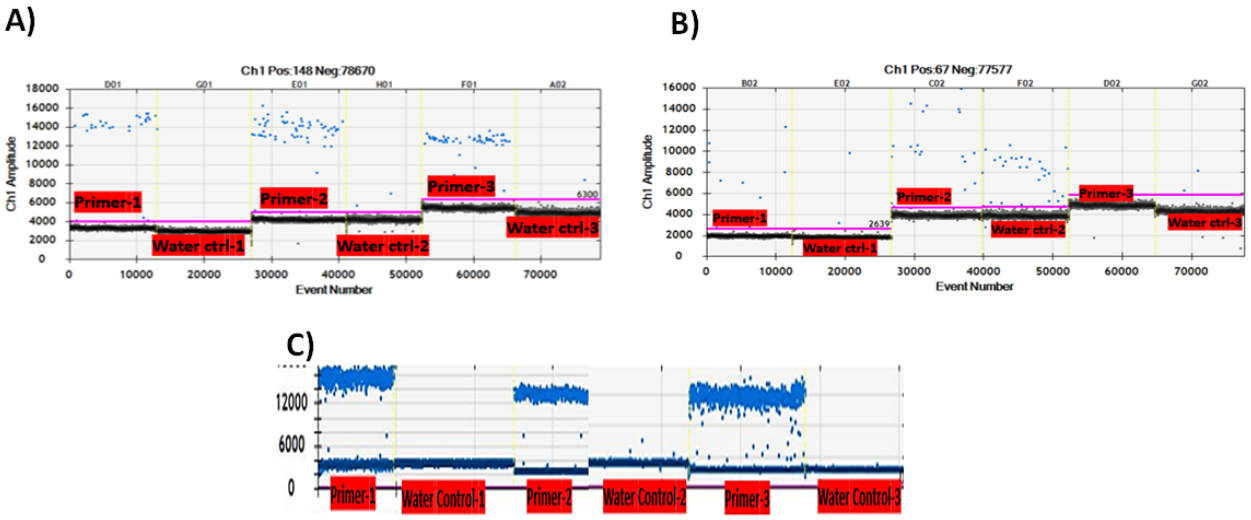

Figure 20. ***Primer Testing for Nrl1, Oct4 and Klf4 Genes by Using ddPCR.*** *Three different primer sets were used to identify which one is better for the evaluation of gRNAs. For the Klf4 gene* ***(A)*** *ddPCR results showed that second primer set was the best choice according to their water controls. These primers were tested on wild-type mouse retina cDNA generated from 0.5 ng total RNA. Secondly, according to the ddPCR results and comparison with their water controls of Oct4 gene, first primer set was chosen as it has less positive hits in water control. We were not able to find a strong control for Oct4 expression as it was weekly expressed in normal retina .* ***(B).*** *Nrl1 gene ddPCR results and their comparison with water controls suggested that third primer set is the best choice* ***(C).*** *All primer sets were tested with wild-type mouse retina cDNA generated from 0.5 ng total RNA.*

Evaluation of gRNA expressions was ready to be tested after establishment of appropriate gRNA primers for digital droplet PCR (ddPCR) **(Fig. 20)**. This system had allowed us to

detect even less amount of gene expression due to it's high sensitivity. To increase the sensitivity and better evaluation of gRNAs, 3 different primer sets were designed for each gene of interest. They were tested on wild-type mouse retina cDNA and second primer set for *Klf4*, first primer set for *Oct4*, and third primer set for *Nrl1* gene were selected as primer sets for further evaluations of gRNAs.

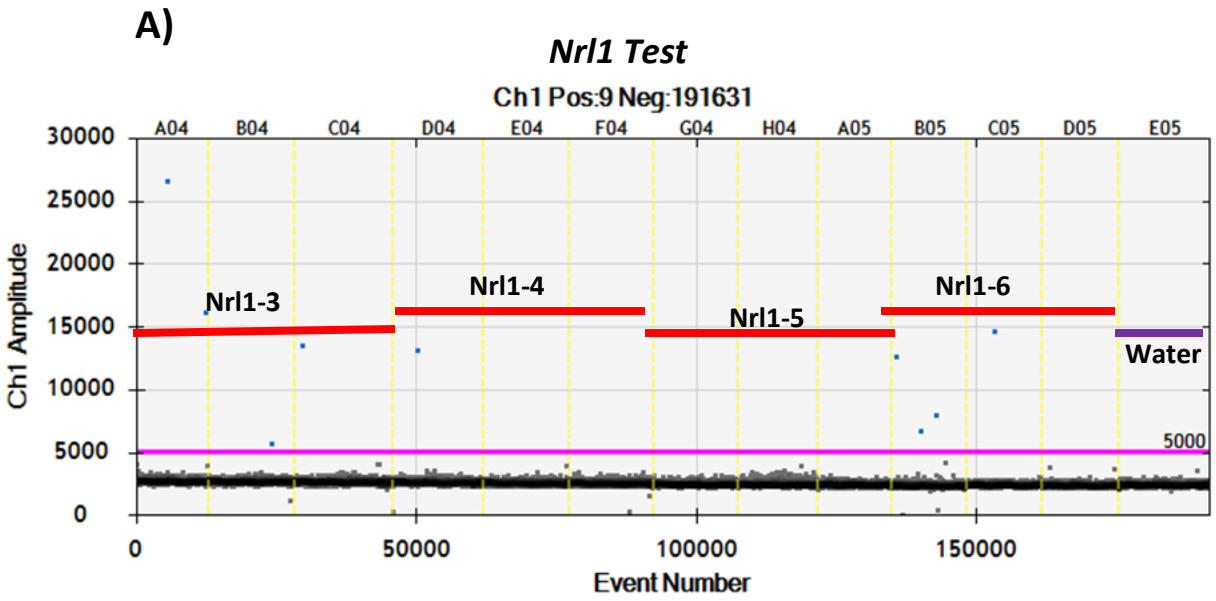

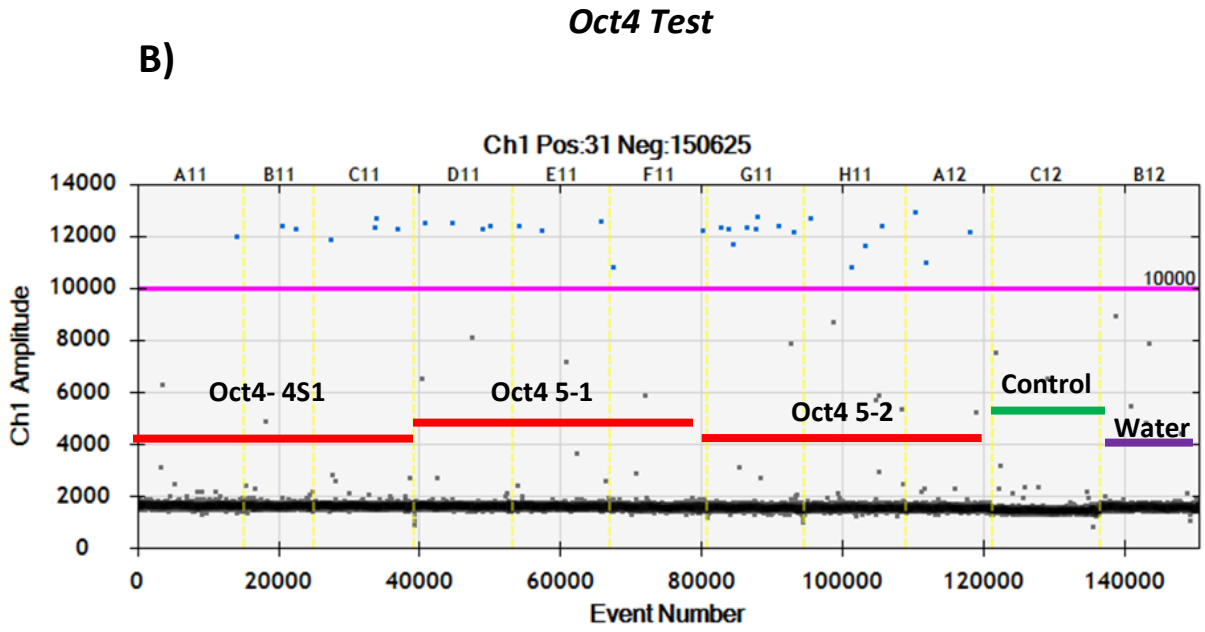

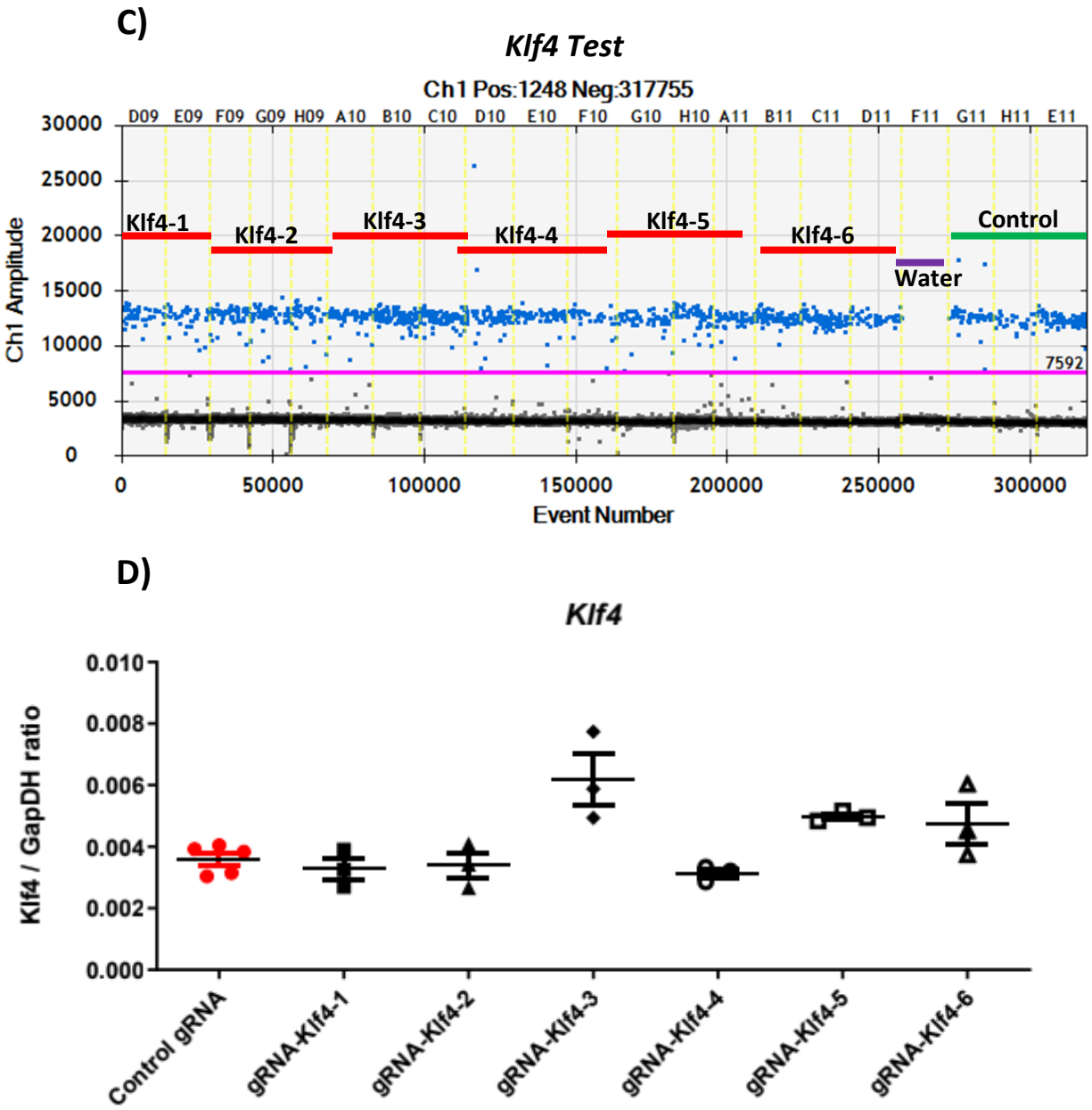

Figure 21. ***ddPCR Results for Nrl1, Oct4 and Klf4 ATFs in Stable*** dCas9-VP64 ***Müller Glia Cell Line.*** *Evaluation of the gRNAs were performed after transfection and FACS sorting of the cells. Nrl1* ***(A),*** *Oct4* ***(B)*** *and Klf4* ***(C)*** *data analyzed with QuantaSoft software. Four Nrl1 and three Oct4 gRNA were tested and there was no upregulation for Nrl1 and Oct4 gRNAs. Six Klf4 gRNA were tested for their effect on regulation of Klf4 expression by ddPCR analysis and Klf4-3 showed upregulation by 1.7 folds compared with the control* ***(D)****.*

dCas9-VP64 stable Muller glia cells transfected with *Nrl1, Oct4* and *Klf4* gRNAs to upregulate these gene in Muller glia cells. Two days after transfection cells were harvested and sorted by using FACS. Results showed that *Nrl1* and *Oct4* had no upregulation on dCas9-VP64 **(Fig. 21A-B)**. However, we found a gRNA that weakly upregulates *Klf4-3* approximately 1.7-fold compared to the no-guide control levels **(Fig. 21C)**. This suggested that VP64 as an activator is not sufficient to upregulate rod or stem cell specific genes in Muller glia as our system was successful targeting several neuroprotective factors and structural genes in other projects.

4.5. Generation of Double Transgenic dCas9-SPH; Tg(GFAP:Cre) Mouse Model and dCAS9-SPH stable Muller glia cell lines

4.5.1. Strategy

We initially wanted to establish a Muller glia specific dCas9-Activator mouse line. For that B6;D2-Gm33925<Tn(pb-CAG-cas9*-EGFP)1Yangh>/JdCas9 activator transgenic mouse line shortly called dCas9-SPH [107] from Jackson Laboratory was obtained. However, this line required a Cre expression which turns on the dCas9-SPH expression by removing the floxed-stop codon. For Muller glia specificity, we further obtained GFAP-Cre mouse line which express Cre-recombinase only in the activated Müller glia cells and resting microglial cells [108] **(Fig. 22)**.

4.5.2. Crossing and Genotyping

Tg(dCas9-SPH) and Tg (GFAP-Cre) were crossed to generate Tg(dCas9-SPH);Tg(GFAP-Cre) double transgenic mouse line and confirmed with both MicronIV and PCR genotyping **(Fig. 22 & 23)**. Since this double transgenic line has very low survival rate, it was very difficult to continue the line. Tg(dCas9-SPH); Tg(GFAP-Cre) had low GFP expression due to expression of Cre in resting microglia. However, Tg(dCas9-SPH) had very weak GFP expression which was later confirmed by flow cytometer. This was unexpected and most likely related to P2A activity **(Fig. 22B).**

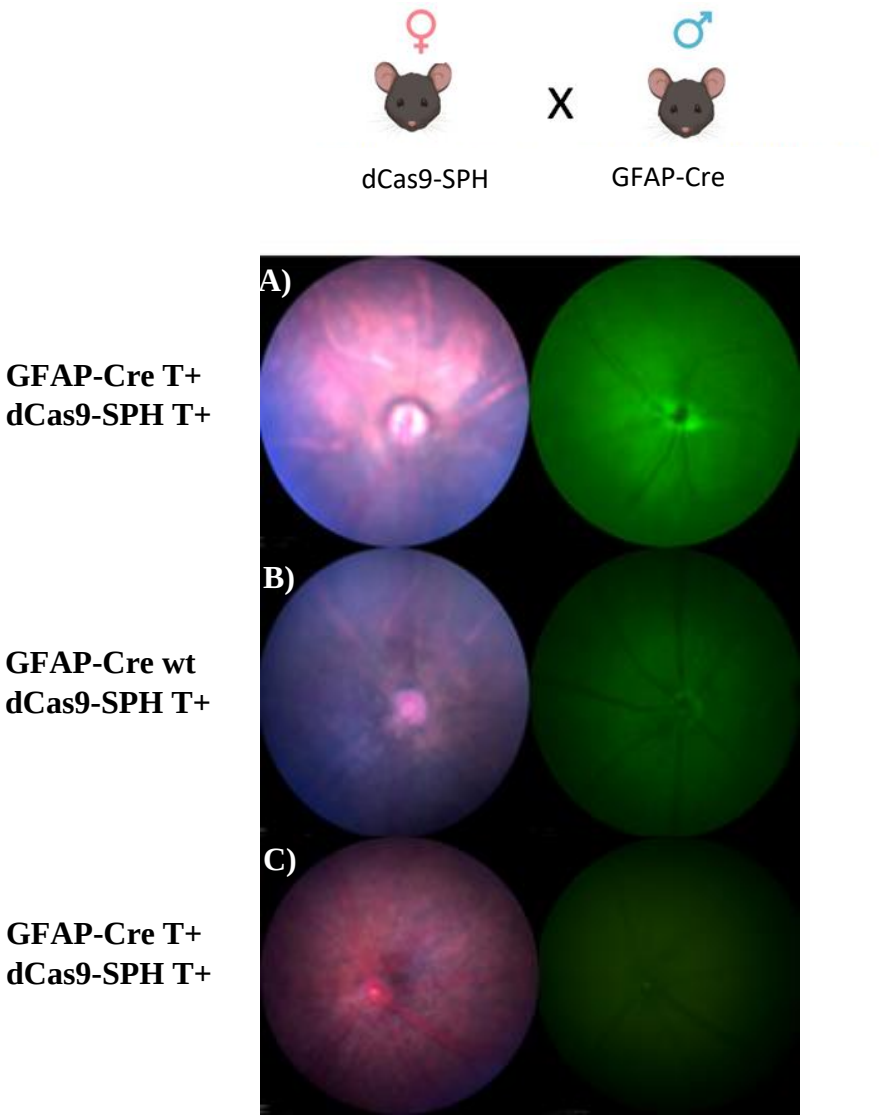

Figure 22. Generation of Double Transgenic dCas9-SPH; Tg (GFAP:Cre) Mouse Model. *Transgenic Tg(dCas9:SPH) and Tg(GFAP-Cre) mice were crossed to obtain double transgenic Tg(dCas9:SPH);Tg(GFAP-Cre) mouse line.* ***MicronIV*** *fundus images both bright field and GFP filter were captured to compare these two animals together with C57BL6/Control* ***(A-C)****. Despite there is no GFAP-Cre in* ***B)*** *and there is still weak GFP expression observed.*

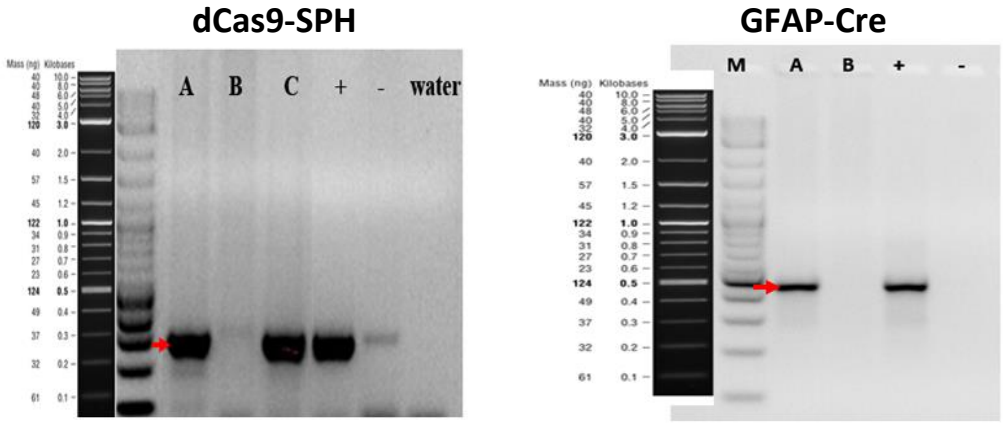

Figure 23. ***Representative dCas9-SPH and GFAP-Cre PCR Gel Images****. Representative dCas9-SPH PCR gel image shows that while* ***B*** *is dCas9-SPH negative,* ***A*** *and* ***C*** *samples are dCas9-SPH T+ in comparison with positive (+), negative (-) and water controls. Water control was used to determine whether contamination condition. Band sizes were determined by using 1kb marker (NEB, Cat#n3200). Red arrow represents the 264 bp. In the GFAP-Cre gel image it is represented that* ***A*** *is GFAP-Cre positive, and* ***B*** *is GFAP-Cre negative in comparison with positive (+) and negative (-) controls. Band sizes were determined by using 1kb marker (NEB, Cat#n3200). Red arrow represents the 450 bp.*

4.5.3 Generation of dCAS9-SPH stable Muller glia cell line

Since VP64 was not sufficient as an activator, we also wanted to establish another Muller glia cell line with a stronger activator. We have aimed here to get a mouse line containing SPH activator and generation of the primary cell line containing dCas9-SPH for the purpose of establishing a system for evaluation of gRNA by using another activator in addition to the dCas9-VP64. In this scenario, SPH activator was planned to use instead of VP64 for the gene expression profiling for *Oct4*, *Nrl* and *Klf4* genes. For that transgenic Tg(dCas9:SPH);Ai14 ki/ki which will express Cre and thus dCas9-SPH upon induction **(Fig. 24).** We successfully generated the dCas9-SPH stable Muller glial cell line for the in vitro evaluation of the gRNAs with a SPH activator by using co-transfection methodology **(Fig. 25).**

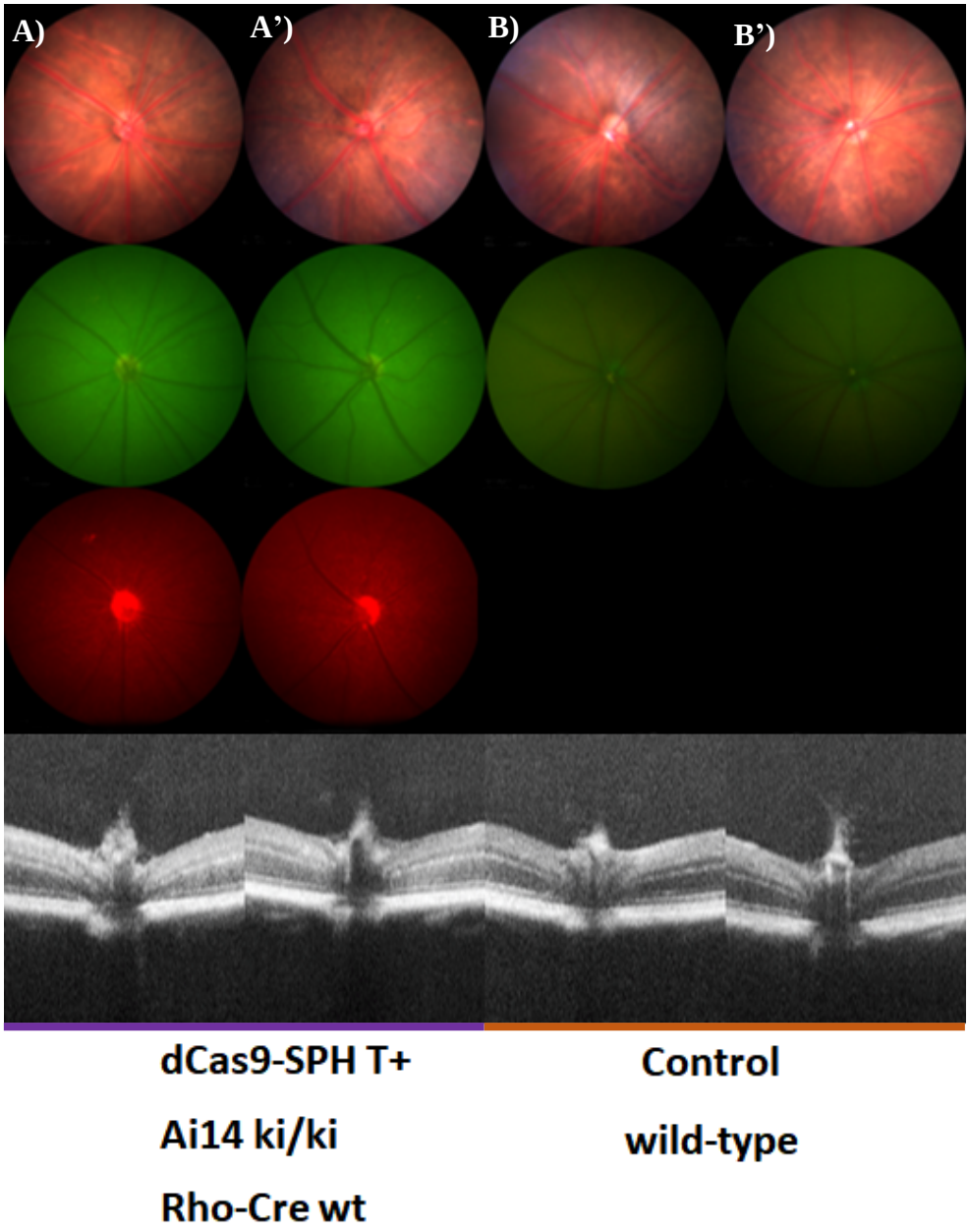

Figure 24. ***Generation of dCas9-SPH Muller glia stable cell line.***

Transgenic Tg(dCas9:SPH);Ai14 ki/ki mice shows weak GFP and tdTomato exprsssion compared to wild type controls. OCT images shows intact retina for Tg(dCas9:SPH);Ai14 ki/ki mice (bottom panel).

4.5.4. Testing of ATFs in dCas9-SPH Müller Glia Cell Line

Since activation of dCas9-SPH requires Cre activity in Muller glia, co-transfection methodology was performed with a plasmid which expresses Cre together with the appropriate artificial transcription factors (ATFs).

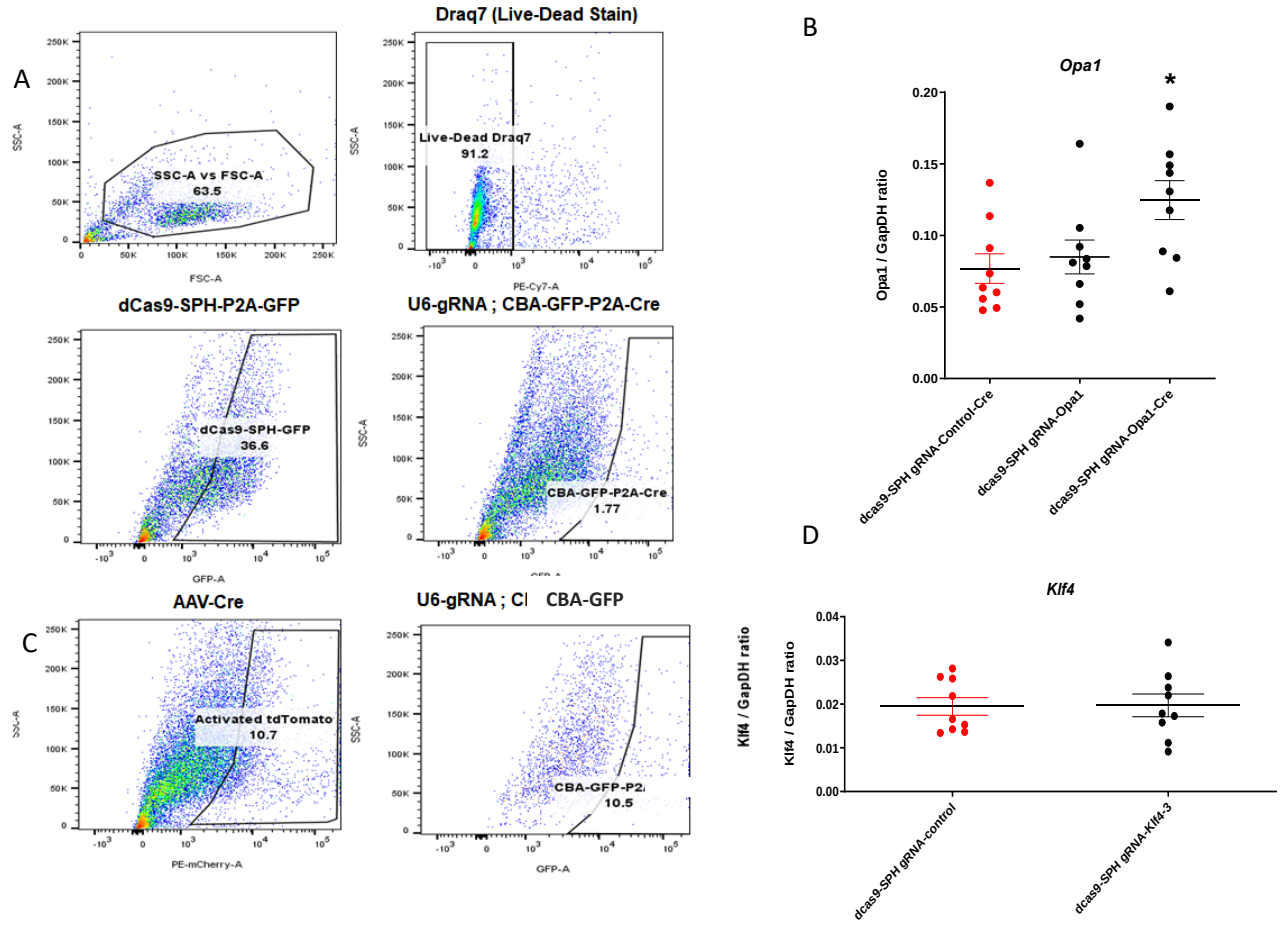

Figure 25. ***Gating Strategy For the dCas9-SPH in vitro ATF System.*** *Draq7 was used to exclude dead cells from live dCas9-SPH-P2A-GFP population* ***(A).*** *dCas9-SPH-P2A-GFP already leaks GFP. Transfection with gRNA vector with CBA-GFP-P2A-Cre expressed stronger GFP compared to leak GFP* ***(A)****. To test our system, OPA1 gene used as a proof-of-concept and showed significant upregulation* ***(B).*** *Sorted the cells both open up the tdTomato (activated tdTomato) and GFP-positive cells* ***C)*** *Klf4-3 gRNA and Cre co-transfection had no upregulation in comparison to its control* ***(D).*** *Statistical analysis were done Anova with Dunnet multiple comparison test for Opa1 gene and Student's t-test for Klf4 gene.*

In this gRNA testing strategy, SPH activator containing-Muller glia cells were used to upregulate gene of interests. FSC and SSC gating strategy was used for discrimination of cell size and granularity of the cells, respectively. Draq7 dye was used as a rapid staining dye for dead cells to separate them from main live population. Since there is a natural leakage of dCas9-SPH-P2A-GFP, it was not a problem for U6-gRNA upregulation system because they had more GFP expression than leaking GFP. So that, we have sorted cells expressing excess GFP **(Fig. 25 A).** However, since there is no Cre which opens up the dCas9-SPH promoter for the Klf4-3 gRNA, co-transfection for this gene upregulation was performed **(Fig. 25 C).** Unfortunately, there was no upregulation for Klf4-3 **(Fig. 25 D)**. As a proof-of-concept we have tested OPA1 gene which is already upregulated with dCas9-VP64 cell line, also upregulated on dCas9-SPH significantly **(Fig. 25 A).** Moreover several other neuroprotective factors had boost their upregulation confirming that the SPH is a stronger activator **(Data not shown).** These readouts suggest that our established cell line containg dCas9-SPH is a functional system for the evaluation of the gRNA upregulations.

4.6. Generation of rd1 -/- ; Tg(dCas9 SPH); Tg(Rho-Cre);ROSA-LSL-tdTomato Muller Glia Cell Line.

rd1-tdTomato model was generated as a fast degeneration model which was facilitated to detect Müller glia fate change into rod photoreceptors. Once the Müller glia dedifferentiates into rod fate, Rho-Cre is activated to turn on tdTomato expression. Since the rd1-tdTomato has already lost almost all rods, it will be an ideal platform to see dedifferentiating Müller glial cells in vivo. This model was also modified with Tg(dCas9-SPH) mouse model to test rod and stem cell-related transcription factors, *Nrl*, *Klf4* and *Oct4*. First, we crossed rd1-tdTomato with the dCas9-SPH ; Tg(Rho-Cre);ROSA26-LSL-tdTomato line which was previously generated as a separate reporter-activator line. Subsequent crossings of F1 generation with the rd1-tdTomato resulted in rd1 -/- ;Tg(dCas9 SPH); Tg(Rho-Cre);ROSA26-LSL-tdTomato (rd1-tdTomato-dCas9-SPH) transgenic line **(Fig. 26A) .**

A)

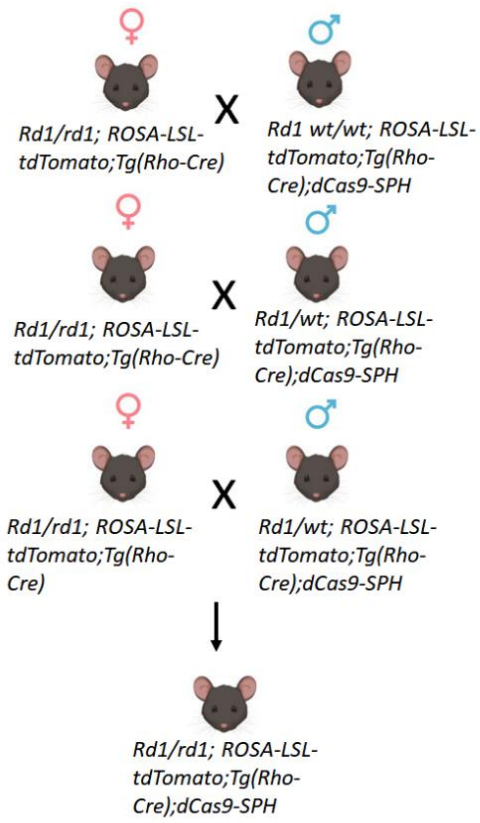

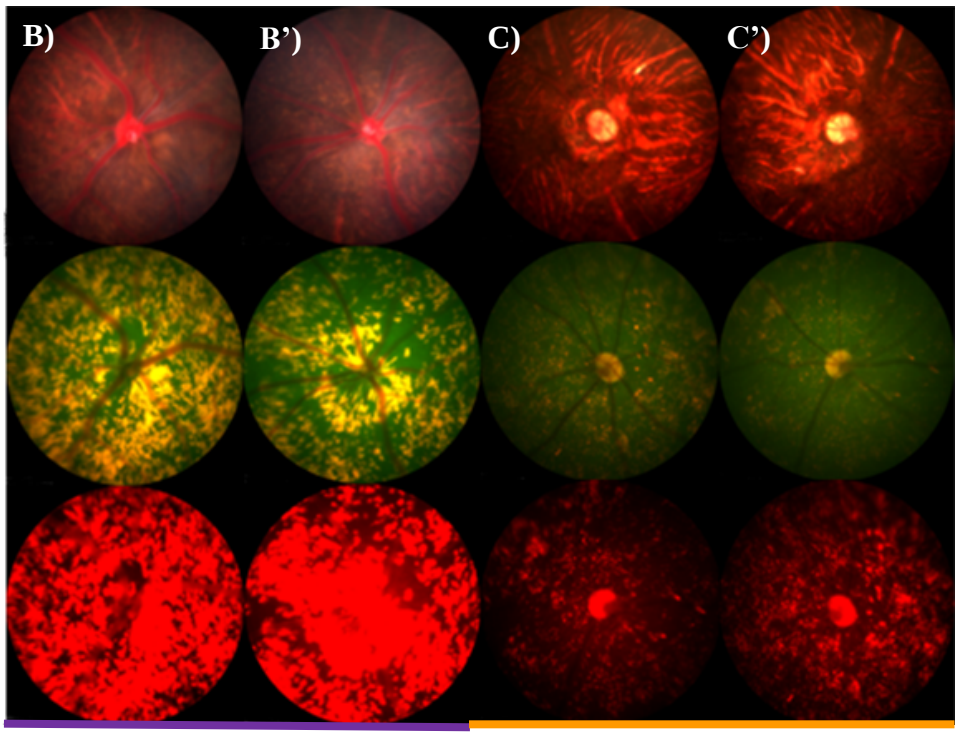

rd1/wt
dCas9-SPH
Ai14 ki/ki
Rho-Cre T+

rd1 -/-
dCas9-SPH
Ai14 ki/ki
Rho-Cre T+

Figure 26. ***Generation of rd1 -/- ;Tg(dCas9 SPH); Tg(Rho-Cre);ROSA-LSL-tdTomato Muller Mouse Line.*** *As a strategy, rd1-/- mice containing ROSA26-LSL-tdTomato and Cre recombinase, crossed with the rd1/wt mouse line expressing dCas9-SPH, ROSA26-LSL-tdTomato. Cre recombinase is planned to remove LSL stop codon to turn on tdTomato expression only in rods****(A).*** *MicronIV and OCT imaging of different mice with different genetic backgrounds of contralateral eyes were shown. Bright field fundus, GFP-fluorescence fundus and tdTomato-fluorescence fundus images were compared in addition to the OCT pictures, respectively.*

It is clearly observed that different phenotypes of the multiplex mouse model platform can be easily detected in the presence of even tiny amount of alteration with MicronIV imaging or OCT imaging. MicronIV images helped us to distinguish the tdTomato and GFP expressions of the reporters. We were surprised when we faced with a GFP leakage in the transgenic dCas9-SPH model. This was also shown in rd1-tdTomato-dCas9-SPH transgenic animals. In addition to that, cross-compared OCT images showed degenerated ONL due to the fast degeneration of photoreceptors in rd1-tdTomato-dCas9-SPH animals. Surprisingly, we observed excess tdTomato expression in this degenerated retina which requires further analysis. Overall, this animal model will be a novel tool for several regeneration studies regarding gene regulatory and gene therapy approaches.

5. DISCUSSION

One of the main achievements that we established in this thesis is the generation of rd1-reporter mouse model. This model combines our previous Tg(Rho-Cre);ROSA-LSL-tdTomato system with the RP disease model rd1. Combination of these features provided us a rod-free retina that has the potential to easily evaluate the outcome of any small molecule that has rod fate induction capacity. This was achieved by the using the rhodopsin promoter controlling the Cre expression. In this model, once rhodopsin promoter is activated, most likely due to rod fate induction and/or regeneration, Cre expression is initiated. This further removes the stop codon flanked in the tdTomato gene within flox sequences and express tdTomato. This system is one of the most efficient set up in order evaluate regenerative approaches. Our analysis of the model showed that it is feasible to do follow-ups analysis for even single rod photoreceptor degeneration and other even small alterations including rod cell digestion by macrophages using the MicronIV fluorescence imaging **(Fig.14)**. Further

testing of the model was done using AAV-Cre, that was generated in our AAV technology platform. This platform allows us to produce both high and low titer AAVs depending on the application. Instead of using the rhodopsin promoter based Cre expression, Cre expression is achieved by intravitreal injection AAV-Cre. Even in 4 days, Cre is expressed and turned on tdTomato expression **(Fig. 16).** In the following weeks, tdTomato expression covered almost all of the rod-free retina suggesting the Cre-based labeling is functional in our rd1-reporter mouse model. Therefore, rd1-reporter mouse model will be one of the most efficient and fast retinal regeneration models that has been established. This model also provides an extremely important feature, an appropriate niche for retinal regeneration, a rod-free retina available for a regenerative study.

We further improved our model for gene regulatory applications using the ATFs. For this purpose, we crossed the rd1-reporter mouse with the dCas9-SPH line. To achieve Muller cell specificity and to turn on dCas9-SPH expression by removing the stop codon, GFAP-Cre line that expresses Cre recombinase in activated Müller glia and resting microglia was also crossed to this complex transgenic line. However, this mouse line had shown some developmental impairment before reaching adolescence. It was previously reported that, this line had some severe disease-like conditions such as developmental retarding and bloody urinate [107]. As we move forward with the crossings, we were able to achieve rd1-reporter-dCas9-SPH mouse line. This model had the advantage to overexpress gene of express just by delivering a gRNA and Cre recombinase by AAV vectors. Cre opens up the dCas9-SPH and gRNA allows overexpression of target genes, in our case *Klf4, Oct4* and *Nrl1*. However, due to unspecific Cre expression, the rod fate reporter activity of the model is hampered. This will be due to parallel removal of the stop codon within tdTomato. Despite this disadvantage, upregulation of genes in a single or multiplex manner would be feasible. Although fluorescently labeled cells will not be solely dependent on rod fate induction, it would be feasible to follow up proliferative cells and expanding ONL by OCT imaging. These features of this model will also allow us to combine gene therapy and small molecule approaches within the same animal model.

We have designed and cloned several gRNA targeting *Klf4, Oct4* and *Nrl1* to establish ATFs for retinal regeneration studies. Since artificial transcription factors (ATFs) have the ability

to either increase or decrease gene expression, we used VP64 and SPH activators for the upregulation of gRNAs. While both of these ATFs upregulate the gene expression, SPH achieves best gene activation due to the breaking epigenetic block [107]. Despite we had tremendous success using dCas9-Vp64 system with several neuroprotective genes, VP64 activator solely was not successful to express *Nrl* or *Oct4* in Muller glia. We only had minor upregulation of *Klf4* with the dCas9-VP64 cell line. Therefore, we needed to have stronger activator to break the possible epigenetic block that did not allow us to express *Nrl* or *Oct4* in Muller glia. For that initial plan was to use dCas9-SPH; GFAP-Cre to establish a stable Muller glia line. However, as it was previously explained we had survival problems in this line. From the very few pups that survived, we tried to establish a Muller glia transgenic cell line that express dCas9-SPH: GFAP-Cre, however their proliferation capacity was quite weak and did not reach the sufficient confluency. Instead of waiting for the growth of these double transgenic animals, we had another plan to accelerate the ATF testing. We have generated another primary cell line solely from the dCas9-SPH. Since there is no Cre in the absence of GFAP-Cre, we have used the exogenous Cre and gRNA for co-transfection methodology to activate dCas9-SPH system in our primary cell line. All gRNAs together with Cre plasmid were tested on this dCas9-SPH cell line with the same gRNAs that previously tested on dCas9-VP64 cell line. The only difference between two primary cell lines was the type of the activator. SPH is known as a better activator than VP64 as it has been previously shown to upregulate *Oct4*, *Klf4* and other reprogramming genes [109]. gRNAs were tested on this two different cell lines and results were quite intriguing especially for neuroprotective factors (Data not shown) which was upregulated several folds compared to dCas9-VP64 activator. However, Klf4-3 gRNA was upregulated only 1.7-fold on dCas9-VP64 cell line, and unexpectedly there was no significant upregulation on dCas9-SPH cell line. To further test whether dCas9-SPH primary cell line is functional, we have used previously established *Opa1* gRNAs using dCas9-VP64 cell line. Together with several other neuroprotective genes, *Opa1* was also upregulated suggesting that the dCas9-SPH muller glia stable cell line is functional and SPH is mostly a more potent activator than the VP64 consistent with the previous findings. After the evaluation of gRNAs, we were sure that our recently generated dCas9-SPH primary cell line was working as foreseen. Since the in vitro part of the *Klf4*, *Oct4* and *Nrl1* gRNA cloning was completed in this thesis, we will later test

these gRNAs *in vitro* with dCas9-SPH Muller glia and later in vivo by using AAV-Cre delivery system as a vector with the combination of small molecules.

In a parallel to our animal experimentations to set up complex transgenic animals, we also tried to make a novel method to efficiently screen for small molecules that induce regeneration. We established a new strategy that involves direct seeding of dissociated retinal cells onto fibronectin-coated plates. This strategy also benefited from the rod reporter system that induces tdTomato expression. Double reporter mouse line that was already used for crossings and previous PAM screen had the Muller glia specific Rlbp1-GFP transgene. GFP reporter was initially planned to sort Muller glia in order to have a pure Muller glia population that could readily be labeled by tdTomato expression after rod fate induction. However, sorting had efficiency problems that reduced the survival rates of the cells. Moreover, previously established SV40 induced immortal double reporter Muller glia line had excess proliferation rate after certain passage numbers hampering the dedifferentiation capacity. We also had several difficulties setting up the system related to COVID-19 pandemic, such as delayed consumable deliveries as well as expired and low-quality products. All these problems forced us to set up a novel method that will benefit from direct seeding of retinal cells on fibronectin-coated plates as the Muller glia itself has extensive proliferation capacity unlike other retinal cell types in cell culture conditions. With the help of our collaborators, we have overcome these difficulties and established the methodology for the screen with extensive delays. Nevertheless, we tested the methodology with the candidate small molecules elucidated from the previously performed pharmacologically active molecules (PAMs) screen and had successful results after numerous attempts that failed due to aforementioned problems. We also enhanced the screen with a previously known protocol to induce rod fate. Rod induction was clearly shown using our novel screen method. This was primarily added to the screen method to enhance the rod inducing capacity of small molecules and elaborate their potential in a more repeatable and faster screen set up. Enhanced screen boosted the rod induction capacity of a candidate small molecules from the previous screen **(Fig. 18).** Furthermore, small molecules screen will be repeated using our novel screen method to elucidate more potent small molecules. This will eventually provide additional support and improve our *in vivo* regeneration studies together with the gene regulatory and gene therapy approaches.

6.BIBLIOGRAPHY

1. Bourne, R., et al., *Trends in prevalence of blindness and distance and near vision impairment over 30 years: an analysis for the Global Burden of Disease Study.* The Lancet global health, 2021. **9**(2): p. e130-e143.
2. Rein, D.B., et al., *The economic burden of vision loss and blindness in the United States.* Ophthalmology, 2022. **129**(4): p. 369-378.
3. Thomas, C.J., R.G. Mirza, and M.K. Gill, *Age-Related Macular Degeneration.* Medical Clinics, 2021. **105**(3): p. 473-491.
4. Kaplan, H.J., W. Wang, and D.C. Dean, *Restoration of cone photoreceptor function in retinitis pigmentosa.* Translational Vision Science & Technology, 2017. **6**(5): p. 5-5.
5. Meng, D., S.D. Ragi, and S.H. Tsang, *Therapy in rhodopsin-mediated autosomal dominant retinitis pigmentosa.* Molecular Therapy, 2020. **28**(10): p. 2139-2149.
6. Wang, W., et al., *Two-step reactivation of dormant cones in retinitis pigmentosa.* Cell reports, 2016. **15**(2): p. 372-385.
7. Malanson, K.M. and J. Lem, *Rhodopsin-Mediated Retinitis Pigmentosa.* Progress in molecular biology and translational science, 2009. **88**: p. 1-31.
8. Dias, M.F., et al., *Molecular genetics and emerging therapies for retinitis pigmentosa: basic research and clinical perspectives.* Progress in retinal and eye research, 2018. **63**: p. 107-131.
9. Hartong, D.T., E.L. Berson, and T.P. Dryja, *Retinitis pigmentosa.* The Lancet, 2006. **368**(9549): p. 1795-1809.
10. Bunker, C.H., et al., *Prevalence of retinitis pigmentosa in Maine.* American journal of ophthalmology, 1984. **97**(3): p. 357-365.
11. Grøndahl, J., *Estimation of prognosis and prevalence of retinitis pigmentosa and Usher syndrome in Norway.* Clinical genetics, 1987. **31**(4): p. 255-264.
12. Novak-Lauš, K., et al., *Primary tapetoretinal dystrophies as the cause of blindness and impaired vision in the republic of Croatia.* Acta Clinica Croatica, 2002. **41**(1): p. 23-25.
13. Dryja, T.P., et al., *Mutations within the rhodopsin gene in patients with autosomal dominant retinitis pigmentosa.* New England Journal of Medicine, 1990. **323**(19): p. 1302-1307.
14. Prado, D.A., M. Acosta-Acero, and R.S. Maldonado, *Gene therapy beyond luxturna: a new horizon of the treatment for inherited retinal disease.* Current opinion in ophthalmology, 2020. **31**(3): p. 147-154.
15. Maguire, A.M., et al., *Efficacy, safety, and durability of voretigene neparvovec-rzyl in RPE65 mutation–associated inherited retinal dystrophy: results of phase 1 and 3 trials.* Ophthalmology, 2019. **126**(9): p. 1273-1285.
16. de Hoz, R., et al., *Retinal macroglial responses in health and disease.* BioMed research international, 2016. **2016**.
17. Bringmann, A., et al., *Müller cells in the healthy and diseased retina.* Progress in retinal and eye research, 2006. **25**(4): p. 397-424.
18. Vecino, E., et al., *Glia–neuron interactions in the mammalian retina.* Progress in retinal and eye research, 2016. **51**: p. 1-40.

19. Rashid, K., I. Akhtar-Schaefer, and T. Langmann, *Microglia in Retinal Degeneration.* Front Immunol, 2019. **10**: p. 1975.
20. Bowmaker, J.K. and H. Dartnall, *Visual pigments of rods and cones in a human retina.* The Journal of physiology, 1980. **298**(1): p. 501-511.
21. Szél, Á., et al., *Distribution of cone photoreceptors in the mammalian retina.* Microscopy research and technique, 1996. **35**(6): p. 445-462.
22. Geisler, W.S., *Sequential ideal-observer analysis of visual discriminations.* Psychological review, 1989. **96**(2): p. 267.
23. Baylor, D.A., T. Lamb, and K.-W. Yau, *Responses of retinal rods to single photons.* The Journal of physiology, 1979. **288**(1): p. 613-634.
24. Surridge, A.K., D. Osorio, and N.I. Mundy, *Evolution and selection of trichromatic vision in primates.* Trends in Ecology & Evolution, 2003. **18**(4): p. 198-205.
25. Pugh Jr, E.N. and T.D. Lamb, *Phototransduction in vertebrate rods and cones: molecular mechanisms of amplification, recovery and light adaptation*, in *Handbook of biological physics*. 2000, Elsevier. p. 183-255.
26. Arshavsky, V.Y., T.D. Lamb, and E.N. Pugh, *G proteins and phototransduction.* Annual review of physiology, 2002. **64**(1): p. 153-187.
27. Yau, K.-W., *Phototransduction mechanism in retinal rods and cones. The Friedenwald Lecture.* Investigative ophthalmology & visual science, 1994. **35**(1): p. 9-32.
28. Ding, J.-D., R.Y. Salinas, and V.Y. Arshavsky, *Discs of mammalian rod photoreceptors form through the membrane evagination mechanism.* Journal of Cell Biology, 2015. **211**(3): p. 495-502.
29. Chabre, M. and P. Deterre, *Molecular mechanism of visual transduction.* EJB Reviews 1989, 1989: p. 1-12.
30. Pepperberg, D.R., *Bleaching desensitization: background and current challenges.* Vision Research, 2003. **43**(28): p. 3011-3019.
31. Wheeler, G.L. and M.W. Bitensky, *A light-activated GTPase in vertebrate photoreceptors: regulation of light-activated cyclic GMP phosphodiesterase.* Proceedings of the National Academy of Sciences, 1977. **74**(10): p. 4238-4242.
32. Farber, D.B., *From mice to men: the cyclic GMP phopshodiesterase gene in vision and disease: the proctor lecture.* Investigative ophthalmology & visual science, 1995. **36**(2): p. 263-275.
33. McLaughlin, M.E., et al., *Recessive mutations in the gene encoding the β–subunit of rod phosphodiesterase in patients with retinitis pigmentosa.* Nature genetics, 1993. **4**(2): p. 130-134.
34. Danciger, M., et al., *Mutations in the PDE6B gene in autosomal recessive retinitis pigmentosa.* Genomics, 1995. **30**(1): p. 1-7.
35. Bowes, C., et al., *Retinal degeneration in the rd mouse is caused by a defect in the β subunit of rod cGMP-phosphodiesterase.* Nature, 1990. **347**(6294): p. 677-680.
36. Farber, D. and R. Lolley, *Enzymic basis for cyclic GMP accumulation in degenerative photoreceptor cells of mouse retina.* Journal of cyclic nucleotide research, 1976. **2**(3): p. 139-148.
37. Farber, D.B. and R.N. Lolley, *Cyclic guanosine monophosphate: elevation in degenerating photoreceptor cells of the C3H mouse retina.* Science, 1974. **186**(4162): p. 449-451.

38. Chang, B., et al., *Retinal degeneration mutants in the mouse.* Vision research, 2002. **42**(4): p. 517-525.
39. Molday, R.S., *Photoreceptor membrane proteins, phototransduction, and retinal degenerative diseases: The Friedenwald Lecture.* Investigative ophthalmology & visual science, 1998. **39**(13): p. 2493-2513.
40. Mathenge, W., *Age-related macular degeneration.* Community eye health, 2014. **27**(87): p. 49.
41. Natarajan, S., *Retinitis pigmentosa: a brief overview.* Indian journal of ophthalmology, 2011. **59**(5): p. 343.
42. Daiger, S.P., S.J. Bowne, and L.S. Sullivan, *Perspective on genes and mutations causing retinitis pigmentosa.* Archives of ophthalmology, 2007. **125**(2): p. 151-158.
43. Sullivan, L.S., et al., *Prevalence of disease-causing mutations in families with autosomal dominant retinitis pigmentosa: a screen of known genes in 200 families.* Investigative ophthalmology & visual science, 2006. **47**(7): p. 3052-3064.
44. Pelletier, V., et al., *Comprehensive survey of mutations in RP2 and RPGR in patients affected with distinct retinal dystrophies: genotype–phenotype correlations and impact on genetic counseling.* Human mutation, 2007. **28**(1): p. 81-91.
45. Samiy, N., *Gene therapy for retinal diseases.* Journal of ophthalmic & vision research, 2014. **9**(4): p. 506.
46. Keeler, C.E., *The inheritance of a retinal abnormality in white mice.* Proceedings of the National Academy of Sciences, 1924. **10**(7): p. 329-333.
47. Keeler, C.E., *On the occurrence in the house mouse of mendelizing structural defect of the retina producing blindness.* Proceedings of the National Academy of Sciences, 1926. **12**(4): p. 255-258.
48. Sarra, G.-M., et al., *Gene replacement therapy in the retinal degeneration slow (rds) mouse: the effect on retinal degeneration following partial transduction of the retina.* Human molecular genetics, 2001. **10**(21): p. 2353-2361.
49. Chang, G.-Q., Y. Hao, and F. Wong, *Apoptosis: Final common pathway of photoreceptor death in rd, rds, and mutant mice.* Neuron, 1993. **11**(4): p. 595-605.
50. Portera-Cailliau, C., et al., *Apoptotic photoreceptor cell death in mouse models of retinitis pigmentosa.* Proceedings of the National Academy of Sciences, 1994. **91**(3): p. 974-978.
51. Wert, K.J., J.H. Lin, and S.H. Tsang, *General pathophysiology in retinal degeneration.* Cell-Based Therapy for Retinal Degenerative Disease, 2014. **53**: p. 33-43.
52. Gargini, C., et al., *Retinal organization in the retinal degeneration 10 (rd10) mutant mouse: a morphological and ERG study.* Journal of Comparative Neurology, 2007. **500**(2): p. 222-238.
53. Barhoum, R., et al., *Functional and structural modifications during retinal degeneration in the rd10 mouse.* Neuroscience, 2008. **155**(3): p. 698-713.
54. Sakami, S., et al., *Probing Mechanisms of Photoreceptor Degeneration in a New Mouse Model of the Common Form of Autosomal Dominant Retinitis Pigmentosa due to P23H Opsin Mutations**♦. Journal of Biological Chemistry, 2011. **286**(12): p. 10551-10567.
55. Suetsugu-Maki, R., et al., *Lens regeneration in axolotl: new evidence of developmental plasticity.* BMC biology, 2012. **10**(1): p. 1-8.

56. Angueyra, J.M. and K.S. Kindt, *Leveraging zebrafish to study retinal degenerations.* Frontiers in cell and developmental biology, 2018. **6**: p. 110.
57. Goldman, D., *Muller glial cell reprogramming and retina regeneration.* Nat Rev Neurosci, 2014. **15**(7): p. 431-42.
58. Thummel, R., et al., *Characterization of Müller glia and neuronal progenitors during adult zebrafish retinal regeneration.* Experimental eye research, 2008. **87**(5): p. 433-444.
59. Thomas, J.L., et al., *Reactive gliosis in the adult zebrafish retina.* Experimental Eye Research, 2016. **143**: p. 98-109.
60. Lenkowski, J.R. and P.A. Raymond, *Müller glia: Stem cells for generation and regeneration of retinal neurons in teleost fish.* Progress in retinal and eye research, 2014. **40**: p. 94-123.
61. Kassen, S.C., et al., *Time course analysis of gene expression during light-induced photoreceptor cell death and regeneration in albino zebrafish.* Developmental neurobiology, 2007. **67**(8): p. 1009-1031.
62. Fausett, B.V., J.D. Gumerson, and D. Goldman, *The proneural basic helix-loop-helix gene ascl1a is required for retina regeneration.* Journal of Neuroscience, 2008. **28**(5): p. 1109-1117.
63. Ramachandran, R., B.V. Fausett, and D. Goldman, *Ascl1a regulates Müller glia dedifferentiation and retinal regeneration through a Lin-28-dependent, let-7 microRNA signalling pathway.* Nature cell biology, 2010. **12**(11): p. 1101-1107.
64. Yu, J., et al., *Induced pluripotent stem cell lines derived from human somatic cells.* science, 2007. **318**(5858): p. 1917-1920.
65. Nelson, C.M., et al., *Stat3 defines three populations of Müller glia and is required for initiating maximal müller glia proliferation in the regenerating zebrafish retina.* Journal of Comparative Neurology, 2012. **520**(18): p. 4294-4311.
66. Sharma, P., et al., *Oct4 mediates Müller glia reprogramming and cell cycle exit during retina regeneration in zebrafish.* Life science alliance, 2019. **2**(5).
67. Ramachandran, R., X.-F. Zhao, and D. Goldman, *Ascl1a/Dkk/β-catenin signaling pathway is necessary and glycogen synthase kinase-3β inhibition is sufficient for zebrafish retina regeneration.* Proceedings of the National Academy of Sciences, 2011. **108**(38): p. 15858-15863.
68. Shyh-Chang, N., et al., *Lin28 enhances tissue repair by reprogramming cellular metabolism.* Cell, 2013. **155**(4): p. 778-792.
69. Melton, C., R.L. Judson, and R. Blelloch, *Opposing microRNA families regulate self-renewal in mouse embryonic stem cells.* Nature, 2010. **463**(7281): p. 621-626.
70. Todd, L., et al., *Microglia suppress Ascl1-induced retinal regeneration in mice.* Cell reports, 2020. **33**(11): p. 108507.
71. Mitra, S., et al., *Dual regulation of lin28a by Myc is necessary during zebrafish retina regeneration.* Journal of Cell Biology, 2019. **218**(2): p. 489-507.
72. Fischer, A.J., *Neural regeneration in the chick retina.* Progress in retinal and eye research, 2005. **24**(2): p. 161-182.
73. Bringmann, A., et al., *Cellular signaling and factors involved in Müller cell gliosis: neuroprotective and detrimental effects.* Progress in retinal and eye research, 2009. **28**(6): p. 423-451.
74. Xue, L., et al., *Nestin, a new marker, expressed in Müller cells following retinal injury.* Canadian journal of neurological sciences, 2010. **37**(5): p. 643-649.

75. Lewis, G.P. and S.K. Fisher, *Up-regulation of glial fibrillary acidic protein in response to retinal injury: its potential role in glial remodeling and a comparison to vimentin expression.* International review of cytology, 2003. **230**: p. 264-290.
76. Bringmann, A. and P. Wiedemann, *Müller glial cells in retinal disease.* Ophthalmologica, 2012. **227**(1): p. 1-19.
77. Ganesh, B.S. and S.K. Chintala, *Inhibition of reactive gliosis attenuates excitotoxicity-mediated death of retinal ganglion cells.* PloS one, 2011. **6**(3): p. e18305.
78. Zhang, Y., et al., *Neuronal integration in an abutting-retinas culture system.* Investigative ophthalmology & visual science, 2003. **44**(11): p. 4936-4946.
79. Lewis, G.P., et al., *The fate of Müller's glia following experimental retinal detachment: nuclear migration, cell division, and subretinal glial scar formation.* Molecular vision, 2010. **16**: p. 1361.
80. Dinet, V., et al., *Distinct effects of inflammation on gliosis, osmohomeostasis, and vascular integrity during amyloid beta-induced retinal degeneration.* Aging cell, 2012. **11**(4): p. 683-693.
81. Kim, K.-Y., W.-K. Ju, and A.H. Neufeld, *Neuronal susceptibility to damage: comparison of the retinas of young, old and old/caloric restricted rats before and after transient ischemia.* Neurobiology of aging, 2004. **25**(4): p. 491-500.
82. Ulbricht, E., et al., *Proliferative gliosis causes mislocation and inactivation of inwardly rectifying K+ (Kir) channels in rabbit retinal glial cells.* Experimental eye research, 2008. **86**(2): p. 305-313.
83. Sethi, C.S., et al., *Glial remodeling and neural plasticity in human retinal detachment with proliferative vitreoretinopathy.* Investigative ophthalmology & visual science, 2005. **46**(1): p. 329-342.
84. Jones, B.W., et al., *Retinal remodeling triggered by photoreceptor degenerations.* Journal of comparative neurology, 2003. **464**(1): p. 1-16.
85. Thummel, R., et al., *Inhibition of Müller glial cell division blocks regeneration of the light-damaged zebrafish retina.* Developmental neurobiology, 2008. **68**(3): p. 392-408.
86. Goldman, D., *Müller glial cell reprogramming and retina regeneration.* Nature Reviews Neuroscience, 2014. **15**(7): p. 431-442.
87. Iismaa, S.E., et al., *Comparative regenerative mechanisms across different mammalian tissues.* NPJ Regenerative medicine, 2018. **3**(1): p. 1-20.
88. García-García, D., M. Locker, and M. Perron, *Update on Müller glia regenerative potential for retinal repair.* Current opinion in genetics & development, 2020. **64**: p. 52-59.
89. Ansari, A.Z. and A.K. Mapp, *Modular design of artificial transcription factors.* Current opinion in chemical biology, 2002. **6**(6): p. 765-772.
90. Liu, X., et al., *Yamanaka factors critically regulate the developmental signaling network in mouse embryonic stem cells.* Cell research, 2008. **18**(12): p. 1177-1189.
91. Takahashi, K. and S. Yamanaka, *Induction of pluripotent stem cells from mouse embryonic and adult fibroblast cultures by defined factors.* cell, 2006. **126**(4): p. 663-676.
92. Huang, J., et al., *More synergetic cooperation of Yamanaka factors in induced pluripotent stem cells than in embryonic stem cells.* Cell research, 2009. **19**(10): p. 1127-1138.

93. Yao, K., et al., *Restoration of vision after de novo genesis of rod photoreceptors in mammalian retinas.* Nature, 2018. **560**(7719): p. 484-488.
94. Son, E.Y., et al., *Conversion of mouse and human fibroblasts into functional spinal motor neurons.* Cell stem cell, 2011. **9**(3): p. 205-218.
95. Vierbuchen, T., et al., *Direct conversion of fibroblasts to functional neurons by defined factors.* Nature, 2010. **463**(7284): p. 1035-1041.
96. Ieda, M., et al., *Direct reprogramming of fibroblasts into functional cardiomyocytes by defined factors.* Cell, 2010. **142**(3): p. 375-386.
97. Yang, N., et al., *Generation of oligodendroglial cells by direct lineage conversion.* Nature biotechnology, 2013. **31**(5): p. 434-439.
98. Najm, F.J., et al., *Transcription factor–mediated reprogramming of fibroblasts to expandable, myelinogenic oligodendrocyte progenitor cells.* Nature biotechnology, 2013. **31**(5): p. 426-433.
99. Du, Y., et al., *Human hepatocytes with drug metabolic function induced from fibroblasts by lineage reprogramming.* Cell stem cell, 2014. **14**(3): p. 394-403.
100. Hou, P., et al., *Pluripotent stem cells induced from mouse somatic cells by small-molecule compounds.* Science, 2013. **341**(6146): p. 651-654.
101. Lawrence, J., G. Tomaselli, and E. Marban, *Ion channels: structure and function.* Heart Disease And Stroke: A Journal For Primary Care Physicians, 1993. **2**(1): p. 75-80.
102. Brandstätter, J.H., P. Koulen, and H. Wässle, *Diversity of glutamate receptors in the mammalian retina.* Vision research, 1998. **38**(10): p. 1385-1397.
103. Schoenberger, S.D., et al., *Increased prostaglandin E2 (PGE2) levels in proliferative diabetic retinopathy, and correlation with VEGF and inflammatory cytokines.* Investigative ophthalmology & visual science, 2012. **53**(9): p. 5906-5911.
104. Miller, S.B. *Prostaglandins in health and disease: an overview*. in *Seminars in arthritis and rheumatism*. 2006. Elsevier.
105. Okan, I.C.T., et al., *Digital Droplet PCR Method for the Quantification of AAV Transduction Efficiency in Murine Retina.* JoVE (Journal of Visualized Experiments), 2021(178): p. e63038.
106. Jayaram, H., et al., *Transplantation of photoreceptors derived from human Muller glia restore rod function in the P23H rat.* Stem Cells Transl Med, 2014. **3**(3): p. 323-33.
107. Zhou, H., et al., *In vivo simultaneous transcriptional activation of multiple genes in the brain using CRISPR–dCas9-activator transgenic mice.* Nature neuroscience, 2018. **21**(3): p. 440-446.
108. Garcia, A.D.R., et al., *GFAP-expressing progenitors are the principal source of constitutive neurogenesis in adult mouse forebrain.* Nature neuroscience, 2004. **7**(11): p. 1233-1241.
109. Weltner, J., et al., *Human pluripotent reprogramming with CRISPR activators.* Nature communications, 2018. **9**(1): p. 1-12.

7. APPENDIX

A. *Nrl1, Klf4* and *Oct4* gRNAs and their locations in the genome

Klf4 Guides

***Klf4* 1-1**

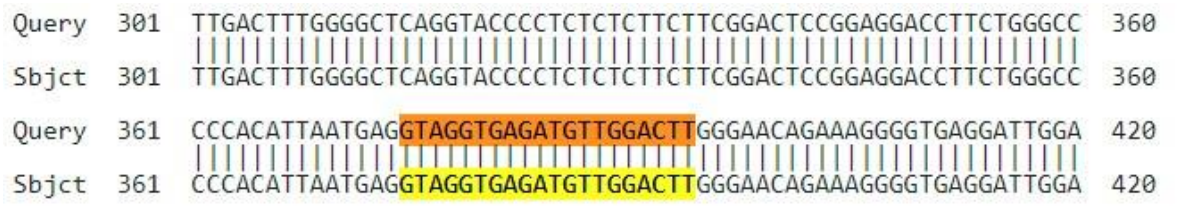

***Klf4* 2-1**

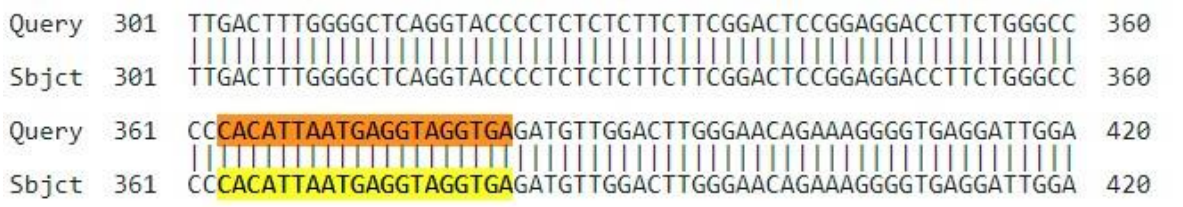

***Klf4* 3-1**

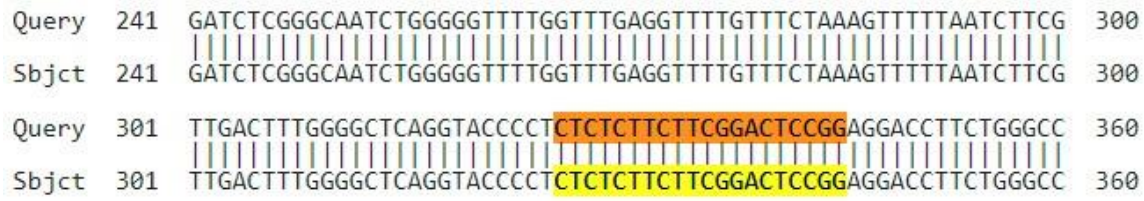

***Klf4* 4-1**

***Klf4* 5-1**

***Klf4* 6-1**

***Nrl* Guides**

***Nrl* 1-1**

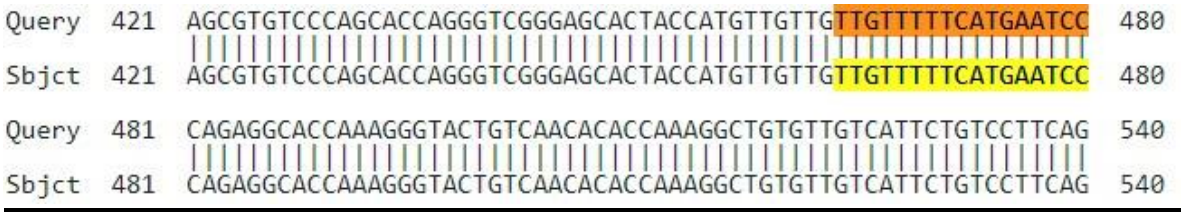

***Nrl* 3-1**

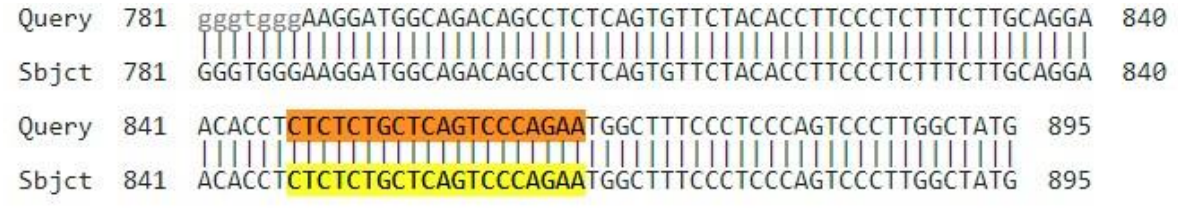

***Nrl* 4-1**

***Nrl* 5-1**

***Nr1* 6-1**

***Oct4* Guides**

***Oct4* 1S1**

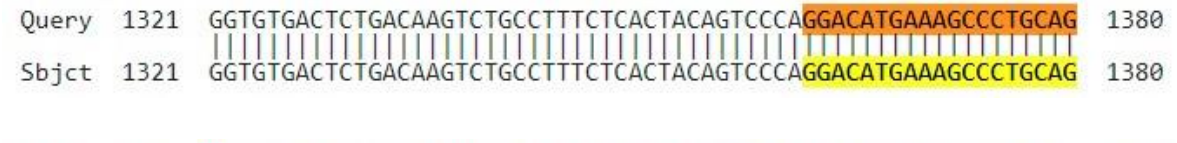

***Oct4* 3S1**

***Oct4* 4S1**

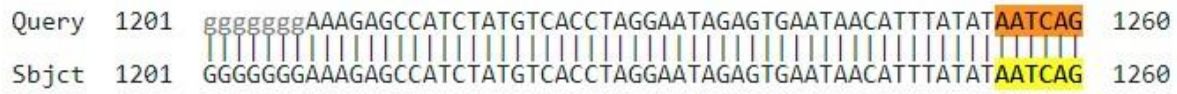

***Oct4* 5S1**

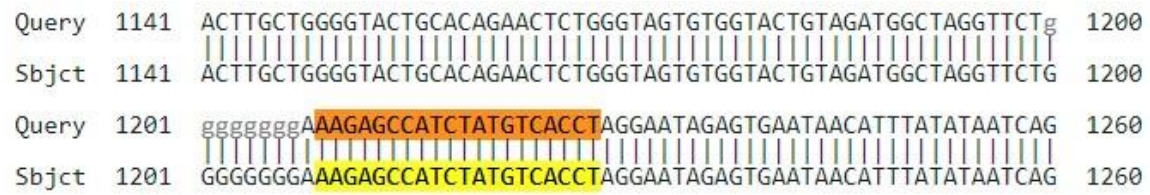

B. PCR Genotyping Primers

Rd1 Forward	CATCCCACCTGAGCTCACAGAAAG
Rd1 Reverse	GCCTACAACAGAGGAGCTTCTAGC
GFAP-Cre Forward	TCC ATA AAG GCC CTG ACA TC
GFAP-Cre Reverse	TGC GAA CCT CAT CAC TCG T
Ai14 td Forward	CTGTTCCTGTACGGCATGG
Ai14 td Reverse	GGCATTAAAGCAGCGTATCC
Ai14 wild-type Forward	AAGGGAGCTGCAGTGGAGTA
Ai14 wild-type Reverse	CCGAAAATCTGTGGGAAGTC